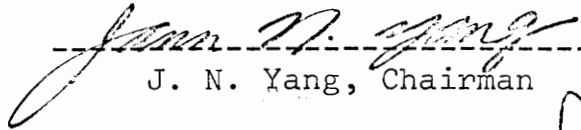DYNAMIC ANALYSIS AND ACTIVE CONTROL OF

TWO CABLE-STAYED BRIDGE
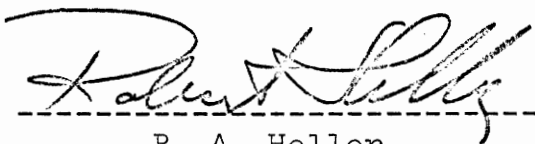
by

Fanis Giannopoulos

Dissertation submitted to the Graduate Faculty of the

Virginia Polytechnic Institute and State University

in partial fulfillment of the requirements for the degree of

DOCTOR OF PHILOSOPHY

in

Engineering Mechanics

APPROVED:

J. N. Yang, Chairman

D. Frederick, Dept. Head

D. P. Telionis

R. A. Heller

H. F. Vanlandingham

April 1978

Blacksburg, Virginia

ACKNOWLEDGMENTS

TABLE OF CONTENTS

LIST OF SYMBOLS

A_i^*, A_i	aerodynamic coefficients corresponding to torsional bridge motion
A_0	cross-sectional area of suspension cables
a	distance from piers to anchorages of suspension cables
B	bridge deck width
C_b, C_t	viscous damping coefficients in bending and torsion, respectively
$E[\cdot]$	expectation operator
EI	bending rigidity of bridge deck
E_0	modulus of elasticity of suspension cables
F_{s-e}, F_b	self-excited and buffeting loads, respectively
$\underset{\sim}{F}_n$, $\underset{\sim}{F}$	generalized buffeting loads for the nth and first modes, respectively
f_n, f	generalized normal coordinates in torsion for the nth and first modes, respectively
GJ	torsional rigidity of bridge deck
g_n, g	generalized normal coordinates in bending for the nth and first modes, respectively
$\underline{H}(\omega)$	frequency response matrix for the coupled flexural and torsional motion
H_i^*, H_i	aerodynamic coefficients corresponding to vertical bridge motion
h_n, h	generalized normal coordinates associated with control displacement for the nth and first modes, respectively
I_n, I	generalized moment of inertia for the nth and first modes, respectively

I_s — moment of inertia per unit length

J_{f_n}, J_f — generalized damping ratios in torsion for the nth and first modes, respectively

J_{g_n}, J_g — generalized damping ratios in bending for the nth and first modes, respectively

k — reduced frequency

$L_i[\cdot]$ — linear operator associated with the input sensor

ℓ — bridge length

ℓ_0 — length of suspension cables

$M_{\sim n}$, $M_{\sim}$ — generalized buffeting moments for the nth and first modes, respectively

M_{s-e}, M_b — self-excited and buffeting moments, respectively

m — mass per unit length of bridge deck

P — restoring force from each suspension cable

P_i — transducer constant associated with the input sensor

Q — restoring moment from suspension cables

q_n, q — generalized normal coordinates associated with control rotation for the nth and first modes, respectively

R — feedback gain of the hydraulic servomechanism

R_1 — loop gain of the feedback control system

R_{0i} — feedback gain of the feedback control system

$R(x_1,x_2;\omega)$ — cross-correlation coefficient for buffeting loads

S — control elongation of suspension cables

$\underline{S}(\omega)$ — power spectral density matrix of response

$\underline{S}_b(\omega)$ — power spectral density matrix of buffeting loads

$\tilde{S}_F^+(\omega)$, $\tilde{S}_M^+(\omega)$ one-sided reference spectral densities of buffeting force and moment, respectively

$S_{FF}(\omega)$, $S_{MM}(\omega)$ spectral densities of generalized buffeting force and moment, respectively

$S_{gg}(\omega)$, $S_{ff}(\omega)$ spectral densities of generalized normal coordinates in bending and torsion, respectively

$S_u^+(\omega)$, $S_w^+(\omega)$ one-sided spectral densities of longitudinal and vertical wind velocity fluctuations, respectively

$S_{Z_1 Z_1}(x,\omega)$,

$S_{Z_2 Z_2}(x,\omega)$ spectral densities of the combined motion at each side of bridge deck

s Laplace transform variable

T, ΔT tension in suspension cables, and change in tension due to the motion of bridge deck

T_0 initial tension in suspension cables due to dead weight

t time

U restoring force from suspension cables

u control displacement

$\bar{u}$ mean wind velocity

$\bar{u}_f$ critical wind velocity (flutter speed)

v control rotation

W flexural displacement of bridge deck

X_n, Y_n normal modes in bending and torsion

Z_0 initial elongation of suspension cables due to dead weight

ΔZ elongation of suspension cables due to bridge motion and control action

Z_1, Z_2 — combined motion at each side of bridge deck

γ_i — feedback voltage from input sensor

$|\gamma_i(\omega)|$ — aerodynamic admittances

$\delta(\cdot)$ — Dirac delta function

δ_{kn} — Kronecker delta

ε — nondimensional loop gain

θ — rotation of bridge deck

ν — vertical displacement at anchorages due to combined flexural and torsional motion of bridge deck

ρ — air density

σ_z — standard deviation of the combined flexural and torsional motion

τ — nondimensional feedback gain

$\overline{\Phi}$ — average power requirement for control devices

ϕ — angle between suspension cables and bridge deck

ω — frequency

ω_{g_n}, ω_g — flexural natural frequencies for the nth and first modes, respectively

ω_{f_n}, ω_f — torsional natural frequencies for the nth and first modes, respectively

ω_f^* — flutter frequency

LIST OF ILLUSTRATIONS

I. INTRODUCTION

It has been the practice in the structural design field to control excessive structural responses, e.g., deflections and accelerations, by the use of passive damping devices, such as damping treatments, rubber mountings, hanging chain dampers, etc. Recently, more advanced mechanisms, such as tuned vibration absorbers, have also been frequently used to excellent advantage.

The advancement in the development of high strength materials and in the techniques for structural analysis and design has resulted in a trend towards the construction of more flexible structures in the future [e.g., Refs. 1-7]. Due to the excessive flexibility, however, such structures may experience large deflections and accelerations under stochastic dynamic loads, such as wind buffeting and earthquake, thus introducing the problems of safety and comfort [e.g., Refs. 2,8].

A typical example of flexible structure is the suspension bridge which is particularly vulnerable to wind gusts. The dramatic collapse of the Tacoma Narrows bridge near Seattle, Washington, in 1940 has triggered extensive research effort. An excellent literature review on suspension bridges can be found in Reference 9.

Under the excitation of strong wind gusts, a flexible suspension bridge may exhibit vibrations with large amplitudes, and it may become unstable (flutter) when the mean wind velocity reaches a critical level, referred to as the flutter speed.

Wind loads have been modeled as stationary Gaussian random processes [e.g., Refs. 10,11-14,15,16], and the buffeting of wind sensitive structures, such as bridges, has been investigated by many researchers [e.g., Refs. 10, 11-14, 17,18].

The mechanism of flutter is attributed to "vortex type" excitations, which, coupled with the bridge motion, generate motion-dependent (self-excited) aerodynamic forces. If the resulting aerodynamic forces reinforce the motion associated with them, a self-excited oscillation (flutter) may develop [e.g., Refs. 9,10,19-26].

The most noticeable advancement in suspension bridge aerodynamics is the development of analytical and experimental techniques pertinent to the stability problem. Early work in gust stabilization of bridges has been performed by Steinman [e.g., Refs. 27-31]. Wind tunnel tests which revealed the inadequacy of early bridge specifications have been conducted at Virginia Polytechnic Institute by Maher [e.g., Refs. 32-34]. More recent work by Scanlan, utilizing wind tunnel tests on section models, provided valuable information on the aeroelastic behavior of many

types of bridge decks [e.g., Refs. 9,21-26,35,36]. Recently, Béliveau et al. combined the problems of buffeting and flutter of suspension bridges in a unified approach [e.g., Ref. 10].

The traditional methods to reduce excessive responses and to increase reliability and safety of flexible structures, such as suspension bridges, usually yield a conservative and expensive design. An alternative approach to circumvent these problems is the use of active control devices. As a result, feasibility studies of applying active control theory to reduce the vibrational levels of structures have recently attracted increasing attentions [e.g., Refs. 1-5,8,37-44].

Unlike the conventional dissipative damping mechanisms, the active control devices rely for their performance on the availability of an external energy supply. As such, the active control is more effective and advantageous than the passive control. Active control devices generally consist of a feedback control system that is designed to sense structural motions so as to generate the necessary corrective actions.

The application of active control theory to civil engineering structures has been discussed by several investigators [e.g., Refs. 1-5,8,41-45]. Feasibility studies in applying active tendon control to slender structures have been performed. In these both modal analysis and

transfer matrix techniques have been used [e.g., Refs. 2,45].

In practical applications, the principle of active control has been applied to certain civil engineering structures, such as a communication antenna at Northwest Cape, Australia and the John Hancock Center in Chicago, Illinois [e.g., Refs. 7,8].

It is the purpose of this thesis to present a feasibility study on the application of active control to a particular type of suspension bridge, referred to as the two cable-stayed bridge [see figure 1, appendix 3]. The effect of active control on the flutter speed and the bridge response under severe storm gusts as well as the power requirement for the active control devices have been investigated.

Cable-stayed bridges are ideal for implementing the active control devices [Ref. 46]. The existing four suspension cables, which are designed to carry the dead weight, are used as active tendons to which the active feedback control systems (hydraulic servomechanisms) are attached. One sensor is installed at the anchorage of each suspension cable in order to sense the motion of each anchorage of the bridge deck. The sensed motions are transmitted as signals to serve as input information to the feedback control system. The feedback signal is then used to regulate motions of hydraulic rams in the servomechanisms, thus

generating the necessary restoring forces in the suspension cables to counter the motion of the bridge. The control mechanism is activated only under severe wind storms to ensure the safety and integrity of the bridge.

Under the excitations of wind gusts, the bridge deck experiences both buffeting and self-excited loads which are assumed to be separable [e.g., Ref. 10]. The buffeting loads, which are independent of the bridge motion, are stochastic processes expressed in terms of the horizontal and vertical components of the wind turbulence [e.g., Refs. 10-15]. In the quasi-steady formulation, self-excited loads are expressed in terms of current motions through the aerodynamic coefficients [e.g., Refs. 9,10,21-26,47,48].

Under the actions of buffeting and self-excited loads as well as the active control forces, the resulting coupled differential equations of bridge motions have been solved using the modal analysis. The stability condition and the statistics of steady-state bridge responses have been obtained. The results for bridges with and without active control have been compared. Finally, the analytical expressions for the power requirement of the feedback active control servomechanisms have been derived.

It is shown in this study that the active control not only raises the flutter speed up to any desirable level but also reduces significantly the statistical variations

of the bridge response, whereas the power requirement for the control devices is very small. From the physical standpoint, these results are not surprising. When the rotation of the bridge deck increases in the clockwise direction, the left suspension cable will release its initial, dead weight tension, whereas the right suspension cable will increase its tension thus producing a counter reaction to the bridge rotation. The regulation by the control devices to release (or increase) the tension in the suspension cables does not require large power.

II. STATEMENT OF THE PROBLEM

1. Equations of Motion

A typical two cable-stayed bridge as shown in figures 1 and 2a [see appendix 3] is considered. The motion of the bridge deck consists of a flexural displacement $W(x,t)$ and a rotation $\theta(x,t)$ of the midplane about the center of gravity, see figure 2b [appendix 3]. The horizontal displacement due to drag force is neglected. With the assumption of "strip theory" aerodynamics, the equations of motion for the bridge deck are [e.g., Refs. 9,10,21,22,24, 25,47,49,50]:[1]

$$EI \frac{\partial^4}{\partial x^4}W(x,t)+m\ddot{W}(x,t)+C_b\dot{W}(x,t) = F_b(x,t)+F_{s-e}(x,t)+U(x,t) \tag{1}$$

$$GJ \frac{\partial^2}{\partial x^2}\theta(x,t)+I_s\ddot{\theta}(x,t)+C_t\dot{\theta}(x,t) = M_b(x,t)+M_{s-e}(x,t)+Q(x,t) \tag{2}$$

in which:

$\quad$ B = bridge deck width

$\quad$ EI = bending rigidity of bridge deck

$\quad$ GJ = torsional rigidity of bridge deck

$\quad$ m = mass per unit length

$\quad$ I_s = moment of inertia per unit length

---

[1]The equations of motion (1) and (2) without the control terms are applicable to the newly designed Sitka Harbor Bridge in Alaska [e.g., Ref. 35].

7

C_b = damping coefficient in bending

C_t = damping coefficient in torsion

$F_b(x,t)$ = lift force due to buffeting loads

$M_b(x,t)$ = pitching moment due to buffeting loads

$F_{s-e}(x,t)$ = self-excited force

$M_{s-e}(x,t)$ = self-excited moment

$U(x,t)$ = restoring force from suspension cables

$Q(x,t)$ = restoring moment from suspension cables

Three types of external forces have been considered on the right hand side of equations 1 and 2. The buffeting loads, $F_b(x,t)$ and $M_b(x,t)$, resulting from the wind turbulence are independent of the bridge motion. The self-excited aerodynamic loads, $F_{s-e}(x,t)$ and $M_{s-e}(x,t)$, are functions of the bridge motions, and for small angles of attack are assumed to be separable from the buffeting loads [e.g., Ref. 10]. The restoring forces, $U(x,t)$ and $Q(x,t)$, from suspension cables depend on both the motion of the bridge and the control devices as will be discussed later.

2. Self-excited and Buffeting Loads

The self-excited loads are related to the oscillatory instability-flutter of bluff structures. They exhibit self-excited characteristics and have a memory of hysterysis effect [e.g., Ref. 51]. Because of the self-excited characteristics, the motion of the structure may become

unstable. Analytical expressions for the self-excited loads have been developed for a classical airfoil [e.g., Refs. 48,51,52]. These results, however, may not be applicable to the bridge decks because of the geometrical difference between the airfoil and the bridge sections [e.g., Refs. 23,26,53]. As a result, semi-empirical methods have been developed in which the results from wind-tunnel tests on the suspension bridge model are used and extrapolated to the prototype under similarity considerations. Two methods have been widely used in the literature for the representation of the self-excited loads;

(a) The indicial function approach: This method corresponds to the classical flutter approach and is applicable to both unsteady and quasi-steady aerodynamics [e.g., Refs. 48,52]. The self-excited loads are expressed in a Duhamel integral form, and the critical wind speed at which the motion becomes unstable is determined by the classical Theodorsen method [e.g., Refs. 23,47,48,51,52,53].

(b) The aerodynamic coefficient approach: The self-excited loads are approximated by those terms involving the current motion only. Hence this method is a quasi-steady aerodynamic approach [e.g., Ref. 26]. In this approach, the critical velocity can be determined by use of classical stability criteria [e.g., Refs. 9,10,47].

In the present analysis, the second approach will be used to express the self-excited loads, because of simplicity [e.g., Ref. 10]. In terms of the aerodynamic coefficients, the self-excited force $F_{s-e}(x,t)$ and moment $M_{s-e}(x,t)$ can be expressed as functions of the mean wind velocity $\bar{u}$, as well as the displacement $W(x,t)$ and the rotation $\theta(x,t)$ of the bridge deck as follows [e.g., Refs. 9, 26,35]:

$$F_{s-e}(x,t) = \frac{1}{2}\rho\bar{u}^2(2B)\left\{ KH_1^*\left(\frac{2\pi}{K}\right)\frac{\dot{W}(x,t)}{\bar{u}} + KH_2^*\left(\frac{2\pi}{K}\right)B\,\frac{\dot{\theta}(x,t)}{\bar{u}} \right.$$

$$\left. + K^2H_3^*\left(\frac{2\pi}{K}\right)\theta(x,t)\right\} \tag{3}$$

$$M_{s-e}(x,t) = \frac{1}{2}\rho\bar{u}^2(2B^2)\left\{ KA_1^*\left(\frac{2\pi}{K}\right)\frac{\dot{W}(x,t)}{\bar{u}} + KA_2^*\left(\frac{2\pi}{K}\right)B\,\frac{\dot{\theta}(x,t)}{\bar{u}} \right.$$

$$\left. + K^2A_3^*\left(\frac{2\pi}{K}\right)\theta(x,t)\right\} \tag{4}$$

in which ρ is the air density, $\bar{u}$ is the mean wind velocity, and K is the reduced frequency given by

$$K = \frac{B\omega_f^*}{\bar{u}} \tag{5}$$

where ω_f^* is the flutter frequency at which the oscillatory motion of the structure occurs with all degrees of freedom coupled at this single frequency. ω_f^* will be determined later. In equations 3 and 4, the quantities $H_1^*(2\pi/K)$, $H_2^*(2\pi/K)$, $H_3^*(2\pi/K)$, $A_1^*(2\pi/K)$, $A_2^*(2\pi/K)$, $A_3^*(2\pi/K)$ are aerodynamic coefficients being functions of the reduced velocity $2\pi/K$. They are experimentally determined for each type of bridge

deck over a range of reduced velocities [e.g., Ref. 26].

The buffeting loads are related to the vertical and horizontal components of the wind turbulence. They are stochastic processes defined by their power spectral densities [e.g., Refs. 10,11,13-15,54] as will be discussed later.

3. Restoring Forces from Suspension Cables

For the two cable-stayed bridge shown in figure 1, appendix 3, the restoring forces $U(x,t)$ and moments $Q(x,t)$ acting on the bridge from the suspension cables are point loadings.

$$U(x,t) = U(a,t) \delta(x-a) + U(\ell-a,t) \delta(x-\ell+a) \tag{6}$$

$$Q(x,t) = Q(a,t) \delta(x-a) + Q(\ell-a,t) \delta(x-\ell+a) \tag{7}$$

in which ℓ and a are shown in figure 2a [appendix 3]. The restoring forces and moments consist of two terms [see appendix 1],

$$U(a,t) = - \frac{2E_0 A_0}{\ell_0}[W(a,t)\sin\phi + u(a,t)]\sin\phi \tag{8}$$

$$Q(a,t) = - \frac{B^2}{2} \frac{E_0 A_0}{\ell_0}[\theta(a,t)\sin\phi + v(a,t)]\sin\phi \tag{9}$$

in which E_0, A_0 and ℓ_0 are the modulus of elasticity, the cross-sectional area, and the length of the suspension cables, respectively, and ϕ is the angle between the suspension cables and the bridge deck. The quantities

$U(\ell-a,t)$ and $Q(\ell-a,t)$ appearing in equations 6 and 7 are given by equations 8 and 9 with the argument "a" replaced by "$\ell-a$".

On the right hand sides of equations 8 and 9, the first term is due to the stiffness of the suspension cables. The second terms, $u(a,t)$ and $v(a,t)$, come from the active control devices as will be discussed in the following.

The existing suspension cables are used as active tendons. The devices for the active tendon control considered herein are identical to those discussed in Refs. 2 and 45. The four suspension cables are connected to electrohydraulic servomechanisms that will generate the necessary control displacements for each cable, thus exerting control forces to the bridge deck at the points of anchorage [see figure 3, appendix 3]. One transducer is installed at the anchorage of each cable, to sense the motion at that point. The sensed motion in the form of electric voltage is used to regulate the motion of the hydraulic ram connected to the other end of the cable, thus generating the required control forces [see figure 4, appendix 3, and appendix 1 for discussion of this control scheme].

Note that the simultaneous application of the control forces with different magnitudes in four cables at the locations x=a and x=ℓ-a, respectively, yield the resulting

control forces and moments with respect to the center of
the cross-section at these locations. For instance, let
the vertical forces exerted on the bridge at the location
x=a by the cables on the left and right sides be denoted
by $P_\ell(a,t)$ and $P_r(a,t)$, respectively. Then, the resulting
total vertical control force is $P_\ell(a,t)+P_r(a,t)$ and the
total control moment is $\frac{B}{2}[P_\ell(a,t)-P_r(a,t)]$. The feedback
voltage, $\gamma_i(t)$, from the sensor is proportional to either
the sensed displacement, velocity, or acceleration [e.g.,
Refs. 2,44,45], for instance,

$$\gamma_i(t) = P_i L_i[v(t)] \tag{10}$$

in which $v(t)$ is the sensed displacement of the bridge
deck at the anchorage, and $L_i[\cdot]$ is a linear operator,
denoting the displacement sensor $L_1[\cdot]$, the velocity
sensor $L_2[\cdot]$, and the acceleration sensor $L_3[\cdot]$ as follows:

$$L_1[\cdot] = 1, \; L_2[\cdot] = \frac{d}{dt}, \; L_3[\cdot] = \frac{d^2}{dt^2} \tag{11}$$

In equation 10, P_i is the proportionality constant
associated with each sensor. The displacement $S(t)$ of the
hydraulic ram, which is equal to the additional elongation
of the suspension cable due to active control, is related
to the feedback voltage γ_i through the first order differ-
ential equation [e.g., Refs. 2,45,55,56],

$$\dot{S}(t)+R_1 S(t) = (R_1/R)\gamma_i(t) \tag{12}$$

in which R_1 is the loop gain, and R is the feedback gain of
the servomechanism.

When such active control devices are used, the
restoring forces and moments from the suspension cables are
given by equations 8 and 9, in which the control displace-
ment u(a,t) and the control rotation v(a,t) are given by
[see appendix 1 for derivation]:

$$\dot{u}(a,t) + R_1 u(a,t) = R_1 R_{0i} L_i [w(a,t)] \tag{13}$$

$$\dot{v}(a,t) + R_1 v(a,t) = R_1 R_{0i} L_i [\theta(a,t)] \tag{14}$$

where

$$R_{0i} = \frac{P_i}{R} \tag{15}$$

It is obvious from equations 8-9 and equations 13-14 that
the control forces, U(a,t), and moments, Q(a,t), depend
on the displacement, W(a,t) and the rotation $\theta(a,t)$ of the
cross-section at which the suspension cables are attached.

III. MODAL EXPANSION

To solve the equations of motion given by equations 1 and 2, the deflection $W(x,t)$ and the rotation $\theta(x,t)$ are expanded in terms of normal modes

$$W(x,t) = \sum_K g_K(t)X_K(x)$$

$$\theta(x,t) = \sum_K f_K(t)Y_K(x) \quad\quad (16)$$

in which $X_K(x)$ and $Y_K(x)$ are the normal modes in bending and torsion, and $g_K(t)$ and $f_K(t)$ are the associated normal coordinates. The control displacements and rotations are also expanded in terms of the normal modes [see appendix 2].

$$u(a,t) = \sum_K h_K(t)X_K(a)$$

$$u(\ell-a,t) = \sum_K h_K(t)X_K(\ell-a)$$

$$v(a,t) = \sum_K q_K(t)Y_K(a) \quad\quad (17)$$

$$v(\ell-a,t) = \sum_K q_K(t)Y_K(\ell-a)$$

Substituting equations 16-17 into equations 13 and 14, and using the fact that normal modes are mutually orthogonal and linearly independent, one can show that [see appendix 2],

$$\dot{h}_K(t)+R_1 h_K(t) = R_1 R_{0i} L_i[g_K(t)] \quad\quad (18)$$

15

$$\dot{q}_K(t) + R_1 q_K(t) = R_1 R_{0i} L_i [f_K(t)] \tag{19}$$

Equations 18 and 19 relate the control normal coordinates, $h_K(t)$ and $q_K(t)$, to the normal coordinates, $g_K(t)$ and $f_K(t)$, of the displacement and rotation of the bridge deck.

The following equations of motion for the bridge deck in normal coordinates, $g_n(t)$ and $f_n(t)$, are obtained by (i) substituting equations 3, 4, 6-9, 16, 17 into equations 1 and 2, (ii) multiplying the resulting equations by $X_n(x)$ and $Y_n(x)$, respectively, and integrating over the range of x, (iii) using the orthogonality conditions for normal modes [see appendix 2],

$$M_n \left\{ \ddot{g}_n(t) + 2 J_{g_n} \omega_{g_n} \dot{g}_n(t) + \omega_{g_n}^2 g_n(t) \right\}$$

$$+ \frac{2 E_0 A_0}{\ell_0} \sin^2\phi \sum_{K \neq n} g_K(t) [X_K(a) X_n(a)$$

$$+ X_K(\ell-a) X_n(\ell-a)] + \frac{2 E_0 A_0}{\ell_0} \sin\phi \sum_K h_K(t) \cdot [X_K(a) X_n(a)$$

$$+ X_K(\ell-a) X_n(\ell-a)] - \rho B^2 \omega_{\tilde{f}}^* H_1^* V_{g_n} \dot{g}_n(t)$$

$$- \rho B \sum_K [B^2 \omega_{\tilde{f}}^* H_{\tilde{f}}^* \dot{f}_K(t) + B^2 \omega_{\tilde{f}}^{*2} H_3^* f_K(t)] G_{Kn} = \underset{\sim}{F}_n(t)$$

$$\tag{20}$$

$$I_n \left\{ \ddot{f}_n(t) + 2J_{f_n} \omega_{f_n} \dot{f}_n(t) + \omega_{f_n}^2 f_n(t) \right\}$$

$$+ \frac{B^2}{2} \frac{E_0 A_0}{\ell_0} \sin^2\phi \sum_{k \neq n} f_K [Y_K(a) Y_n(a)$$

$$+ Y_K(\ell-a) Y_n(\ell-a)] + \frac{B^2 E_0 A_0}{2} \frac{1}{\ell_0} \sin\phi \sum_k q_K(t) [Y_K(a) Y_n(a)$$

$$+ Y_K(\ell-a) Y_n(\ell-a)] - \rho B^4 \omega_f^* [A_2^* \ddot{f}_n(t)$$

$$+ \omega_f^* A_3^* f_n(t)] V_{f_n} - \rho B^2 \sum_K B \omega_f^* A_1^* \dot{g}_K(t) G_{nK} = \underset{\sim}{M}_n(t)$$

$$(21)$$

in which

$$V_{gn} = \left[\int_0^\ell X_K(x) X_n(x) dx \right] \delta_{kn}$$

$$(22)$$

$$V_{f_n} = \left[\int_0^\ell Y_K(x) Y_n(x) dx \right] \delta_{kn}$$

$$G_{Kn} = \int_0^\ell Y_K(x) X_n(x) dx$$

$$(23)$$

$$G_{nk} = \int_0^\ell X_K(x) Y_n(x) dx$$

$$\underset{\sim}{F}_n(t) = \int_0^\ell F_b(x,t) X_n(x) dx$$

$$(24)$$

$$\underset{\sim}{M}_n(t) = \int_0^\ell M_b(x,t) Y_n(x) dx$$

$$M_n = m \, V_{g_n} \tag{25}$$

$$I_n = I_s V_{f_n} .$$

$$C_{bn} = C_b V_{g_n} \tag{26}$$

$$C_{tn} = C_t V_{f_n}$$

$$\omega_{g_n}^2 = \bar{\omega}_{g_n}^2 + \frac{2E_0 A_0}{M_n \ell_0} \sin^2\phi \; [X_n^2(a) + X_n^2(\ell-a)]$$

$$\tag{27}$$

$$\omega_{f_n}^2 = \bar{\omega}_{f_n}^2 + \frac{B^2 E_0 A_0}{2I_n \ell_0} \sin^2\phi \; [Y_n^2(a) + Y_n^2(\ell-a)]$$

$$J_{g_n} = \frac{C_{bn}}{2M_n \omega_{g_n}}$$

$$\tag{28}$$

$$J_{f_n} = \frac{C_{tn}}{2I_n \omega_{f_n}}$$

where δ_{Kn} is the Kronecker delta. Both $\bar{\omega}_{g_n}$ and $\bar{\omega}_{f_n}$ are the natural frequencies in bending and torsion of the bridge deck without suspension cables and they satisfy the following equations:

$$EI \frac{\partial^4}{\partial x^4} X_n(x) = m \bar{\omega}_{g_n}^2 X_n(x)$$

(29)

$$GJ \frac{\partial^2}{\partial x^2} Y_n(x) = I_s \bar{\omega}_{f_n}^2 Y_n(x)$$

Both ω_{g_n} and ω_{f_n} given in equations 27 are the natural frequencies in bending and torsion of the two cable-stayed bridge. The difference between $(\bar{\omega}_{g_n}, \bar{\omega}_{f_n})$ and $(\omega_{g_n}, \omega_{f_n})$ is that the latter, equation 27, incorporates the stiffness provided by the suspension cables.

Equations 20 and 21 are coupled not only between the normal coordinates $g_K(t)$ and $f_K(t)$, but also between the normal modes of the same type of locations x-a and x=ℓ-a. The first coupling comes from the aerodynamic coefficients H_2^*, H_3^* and A_1^*, whereas the second coupling stems from the active control devices.

For the cable-stayed bridge considered herein, the normal modes $X_K(x)$ and $Y_K(x)$ are approximately identical and they are assumed to have the following form [e.g., Refs. 10,57]

$$X_K(x) = Y_K(x) = \sin \frac{K\pi x}{\ell}$$

(30)

Furthermore, the positions of the anchorage for the suspension cables are chosen at

$$a = \ell/3$$

which is exactly the case of the newly designed Sitka

Harbor Bridge in Alaska.

By virtue of the approximation given in equation 30

and the particular choice for "a" in equation 31, equations

20-29 can be simplified considerably as follows [see

appendix 2]:

$$\ddot{g}_n(t) + [2J_{g_n}\omega_{g_n} - H_1]\dot{g}_n(t) + \omega_{g_n}^2 g_n(t) + \frac{4E_0A_0}{M_n\ell_0}\sin\phi\sin^2\frac{n\pi}{3}h_n(t)$$

$$- H_2\dot{f}_n(t) - H_3f_n(t) = \frac{\underset{\sim}{F}_n(t)}{M_n} \tag{32}$$

$$\ddot{f}_n(t) + [2J_{f_n}\omega_{f_n} - A_2]\dot{f}_n(t) + [\omega_{f_n}^2 - A_3]f_n(t)$$

$$+ \frac{B^2E_0A_0}{I_n\ell_0}\sin\phi\sin^2\frac{n\pi}{3}q_n(t) - A_1\dot{g}_n(t) = \frac{\underset{\sim}{M}_n(t)}{I_n} \tag{33}$$

In which

$$M = M_n = \frac{m\ell}{2}, \quad I = I_n = \frac{I_s\ell}{2} \tag{34}$$

$$H_1 = \frac{\rho B^2\omega_f^* H_1^*}{m}, \quad H_2 = \frac{\rho B^3\omega_f^* H_2^*}{m}, \quad H_3 = \frac{\rho B^3\omega_f^{*2}}{m}H_3^*$$

$$\tag{35}$$

$$A_1 = \frac{\rho B^3\omega_f^* A_1^*}{I_s}, \quad A_2 = \frac{\rho B^4\omega_f^*}{I_s}A_2^*, \quad A_3 = \frac{\rho B^4\omega_f^{*2}}{I_s}A_3^*$$

It is observed that equations 32 and 33 are still

coupled because of the aerodynamic coefficients. It is

important to notice, however, that $g_n(t)$ coordinate is

coupled only with the $f_n(t)$ coordinate and vice versa,

i.e., $g_n(t)$ is not coupled with $f_k(t)$ for n≠k. This is due to the assumption that the normal modes in bending and torsion are identical [equation 30]. As a result, each set of equations of motion for the nth bending and torsional modes, i.e., $g_n(t)$ and $f_n(t)$, can be investigated separately. Moreover, it is interesting to observe that for n=3, we have sin $\frac{3\pi}{3}$=0 and hence the set of equations corresponding to the third flexural and torsional modes becomes uncontrolled [see equations 32 and 33 with n=3]. This comes from the fact that the control forces and moments are applied at the nodal points of the third mode, i.e., a=ℓ/3. It should be mentioned that the form of the equations of motion, given by equations 30 and 31, for n=1 is identical to that for n=2. In order to demonstrate the analysis approach presented herein, we shall investigate the first set of equations for n=1 only, i.e., the first mode vibration, realizing that the solution for the second mode vibration is of the same form. Hence, we shall drop the subscript n in the following discussions of the first mode vibration.

IV. FLUTTER ANALYSIS

One of the important problems in the dynamic analysis of the cable-stayed bridges or the conventional suspension bridges is the determination of the flutter speed; i.e., the wind speed at which the bridge becomes aerodynamically unstable. This problem will be investigated in the Laplace transform domain for the two cable-stayed bridge under both active control and no control.

Taking Laplace transform on both sides of equations 32 and 33 and assuming zero initial conditions for the normal coordinates [e.g., Ref. 45], one obtains,

$$[s^2+(2J_g\omega_g-H_1)s+\omega_g^2]\bar{g}(s)+\frac{4E_0A_0}{M\ell_0}\sin\phi\sin^2\frac{\pi}{3}\bar{h}(s)$$

$$- [H_2s+H_3]\bar{f}(s) = \underset{\sim}{\bar{F}}(s)/M \tag{36}$$

$$[s^2+(2J_f\omega_f-A_2)s+(\omega_f^2-A_3)]\bar{f}(s)+\frac{B^2E_0A_0}{I\ell_0}\sin\phi\sin^2\frac{\pi}{3}\bar{q}(s)$$

$$- A_1s\bar{g}(s) = \underset{\sim}{\bar{M}}(s)/I \tag{37}$$

in which s is the Laplace transform parameter and the quantities with a bar represent the Laplace transforms of the corresponding quantities in the time domain (without a bar).

The Laplace transforms $\bar{h}(s)$ and $\bar{q}(s)$ appearing in equations 36 and 37 can be obtained in terms of $\bar{g}(s)$ and $\bar{f}(s)$ by taking the Laplace transforms on equations 18 and 19; with the results,

$$\bar{h}(s) = \frac{R_1 R_{0i} \bar{L}_i(s)}{R_1 + S} \bar{g}(s)$$

$$\bar{q}(s) = \frac{R_1 R_{0i} \bar{L}_i(s)}{R_1 + s} \bar{f}(s)$$

(38)

Equations 36 and 37 can be written in a matrix form after substitution of equation 38 into them,

$$\begin{bmatrix} \bar{Q}_{11}(s) & \bar{Q}_{12}(s) \\ \bar{Q}_{21}(s) & \bar{Q}_{22}(s) \end{bmatrix} \begin{Bmatrix} \bar{g}(s) \\ \bar{f}(s) \end{Bmatrix} = \begin{Bmatrix} \tilde{F}(s)/M \\ \tilde{M}(s)/I \end{Bmatrix}$$

(39)

in which:

$$\bar{Q}_{11}(s) = s^2 + (2J_g \omega_g - H_1)s + \omega_g^2 + \Gamma_g \frac{R_1 R_{0i} \bar{L}_i(s)}{R_1 + s}$$

$$\bar{Q}_{12}(s) = -(H_2 s + H_3)$$

(40)

$$\bar{Q}_{21}(s) = -A_1 s$$

$$\bar{Q}_{22}(s) = s^2 + (2J_f \omega_f - A_2)s + (\omega_f^2 - A_3) + \Gamma_f \frac{R_1 R_{0i} \bar{L}_i(s)}{R_1 + s}$$

$$\Gamma_g = \frac{4}{M} \frac{E_0 A_0}{\ell_0} \sin\phi \sin^2 \frac{\pi}{3} \tag{41}$$

$$\Gamma_f = \frac{B^2}{I} \frac{E_0 A_0}{\ell_0} \sin\phi \sin^2 \frac{\pi}{3}$$

and $\overline{L}_i(s)$ follows from equation 11 as:

$$\overline{L}_1(s) = 1 \quad \text{for displacement sensor}$$

$$\overline{L}_2(s) = s \quad \text{for velocity sensor} \tag{42}$$

$$\overline{L}_3(s) = s^2 \text{ for acceleration sensor}$$

A block diagram for the closed loop control system represented by equations 39-41 is shown in figure 5 (appendix 3). Equation 39 can readily be solved as follows:

$$\overline{g}(s) = \left\{ [\overline{Q}_{22}(s)\underset{\sim}{\overline{F}}(s)/M] - [\overline{Q}_{12}(s)\underset{\sim}{\overline{M}}(s)/I] \right\} / \overline{D}(s)$$

$$\overline{f}(s) = -\left\{ [\overline{Q}_{21}(s)\underset{\sim}{\overline{F}}(s)/M] - [\overline{Q}_{11}(s)\underset{\sim}{\overline{M}}(s)/I] \right\} / \overline{D}(s) \tag{43}$$

where

$$\overline{D}(s) = \overline{Q}_{11}(s)\overline{Q}_{22}(s) - \overline{Q}_{12}(s)\overline{Q}_{21}(s) \tag{44}$$

A linear control system, such as the one given by equation 43, is stable if and only if the responses $\overline{g}(s)$ and $\overline{f}(s)$ are bounded for every bounded inputs $\underset{\sim}{\overline{F}}(s)$ and $\underset{\sim}{\overline{M}}(s)$. Since, however, the buffeting loads $\underset{\sim}{\overline{F}}(s)$ and $\underset{\sim}{\overline{M}}(s)$ are assumed to be bounded, the boundness of the responses will be determined by the poles of the transfer functions $\overline{Q}_{11}(s)/\overline{D}(s)$, $\overline{Q}_{12}(s)/\overline{D}(s)$, $\overline{Q}_{21}(s)/\overline{D}(s)$, $\overline{Q}_{22}(s)/\overline{D}(s)$. A careful examination of these transfer functions indicates that the poles can be determined by the characteristic

equation:

$$\overline{D}(s) = 0 \tag{45}$$

in which D(s) is given by equation 44.

Therefore, the actively controlled two cable-stayed bridge considered herein is stable if and only if all the roots of the characteristic equation have negative real parts [e.g., Ref. 58].

1. Bridges with Active Control

By substitution of equations 40 and 44 into equation 45, the characteristic polynomial for the bridge under active control is obtained as:

$$\overline{D}(s) = s^6 + a_1 s^5 + a_2 s^4 + a_3 s^3 + a_4 s^2 + a_5 s + a_6 = 0 \tag{46}$$

in which a_i (i=1,2,3,4,5,6) depend on the structural characteristics, control parameters, and the type of sensor as described in equations 42,

(a) For acceleration sensor

$$
\begin{aligned}
a_1 &= \rho_1 + 2R_1 + D_{13} \\
a_2 &= \rho_2 + R_1(2\rho_1 + R_1 + D_{13}) + D_{23} + D_{43} \\
a_3 &= \rho_3 + R_1(2\rho_2 + R_1\rho_1 + D_{23}) + D_{33} \\
a_4 &= \rho_4 + R_1(2\rho_3 + R_1\rho_2 + D_{33}) \\
a_5 &= R_1(2\rho_4 + R_1\rho_3) \\
a_6 &= R_1^2 \rho_4
\end{aligned}
\tag{47}
$$

(b) For velocity sensor

$$a_1 = \rho_1 + 2R_1$$

$$a_2 = \rho_2 + D_{12} + R_1(2\rho_1 + R_1)$$

$$a_3 = \rho_3 + D_{22} + R_1(2\rho_2 + R_1\rho_1 + D_{12})$$

$$a_4 = \rho_4 + D_{32} + D_{42} + R_1(2\rho_3 + R_1\rho_2 + D_{22})$$

$$a_5 = R_1(2\rho_4 + R_1\rho_3 + D_{32})$$

$$a_6 = R_1^2 \rho_4$$

(48)

(c) For displacement sensor

$$a_1 = \rho_1 + 2R_1$$

$$a_2 = \rho_2 + R_1(2\rho_1 + R_1)$$

$$a_3 = \rho_3 + D_{11} + R_1(2\rho_2 + R_1\rho_1)$$

$$a_4 = \rho_4 + D_{21} + R_1(2\rho_3 + R_1\rho_2 + D_{11})$$

$$a_5 = D_{31} + R_1(2\rho_4 + R_1\rho_3 + D_{21})$$

$$a_6 = D_{41} + R_1(R_1\rho_4 + D_{31})$$

(49)

where ρ_i (i=1,2,3,4) are structural characteristics,

$$\rho_1 = 2J_f\omega_f - A_2 + 2J_g\omega_g - H_1$$

$$\rho_2 = \omega_f^2 - A_3 + \omega_g^2 + (2J_g\omega_g - H_1)(2J_f\omega_f - A_2) - A_1H_2$$

$$\rho_3 = (2J_g\omega_g - H_1)(\omega_f^2 - A_3) + (2J_f\omega_f - A_2)\omega_g^2 - A_1H_3$$

$$\rho_4 = \omega_g^2(\omega_f^2 - A_3)$$

(50)

and D_{ji} (j=1,2,3,4; i=1,2,3) depend on both the structural characteristics and the control parameters

$$D_{1i} = (\Gamma_g + \Gamma_f) R_1 R_{0i}$$

$$D_{2i} = [\Gamma_g(2J_f\omega_f - A_2) + \Gamma_f(2J_g\omega_g - H_1)]R_1 R_{0i}$$

$$D_{3i} = [\Gamma_g(\omega_f^2 - A_3) + \Gamma_f\omega_g^2]R_1 R_{0i}$$

$$D_{4i} = \Gamma_g\Gamma_f R_1^2 R_{0i}^2$$

(51)

The stability conditions can be established from the characteristic polynomial of equation 46 using the Routh-Hurwitz criteria [e.g., Refs. 59,60]. By virtue of the Routh-Hurwitz criteria, the necessary and sufficient conditions for the roots of equation 46 to have negative real parts are that (i) each coefficient of the polynomial be positive

$$a_i > 0 \text{ for } i = 1, 2, \ldots 6$$

(52)

and (ii) the determinants (test functions), T_i, be positive for $i = 1, 2, \ldots 5$ i.e.

$$T_i > 0 \text{ for } i = 1, 2, \ldots 5$$

(53)

where

$$T_1 = a_1 \qquad T_2 = \begin{vmatrix} a_1 & 1 \\ a_3 & a_2 \end{vmatrix} \qquad T_3 = \begin{vmatrix} a_1 & 1 & 0 \\ a_3 & a_2 & a_1 \\ a_5 & a_4 & a_3 \end{vmatrix}$$

(54)

$$T_4 = \begin{vmatrix} a_1 & 1 & 0 & 0 \\ a_3 & a_2 & a_1 & 1 \\ a_5 & a_4 & a_3 & a_2 \\ 0 & a_6 & a_5 & a_4 \end{vmatrix} \qquad T_5 = \begin{vmatrix} a_1 & 1 & 0 & 0 & 0 \\ a_3 & a_2 & a_1 & 1 & 0 \\ a_5 & a_4 & a_3 & a_2 & a_1 \\ 0 & a_6 & a_5 & a_4 & a_3 \\ 0 & 0 & 0 & a_6 & a_5 \end{vmatrix}$$

For the active control devices considered in this report it is found that the conditions given in equation 52

as well as the conditions that $T_i > 0$ for $i=1,2,3,4$ are
satisfied. Thus, the conditions for stability are deter-
mined from the test function T_5. In flutter analyses, the
transitory motion, where the structure moves from stable
oscillation into unstable oscillation, is usually of con-
cern. Such a transitory situation takes place whenever the
test function T_5 vanishes, i.e.

$$T_5(\overline{u}=\overline{u}_f) = 0 \tag{55}$$

indicating that there exists at least one purely imaginary
double root $i\omega_f^*$. As a result, the flutter speed $\overline{u}_f$ is
obtained from equation 55. In determining the flutter
speed $\overline{u}_f$ from equation 55, however, several important
features should be pointed out in the following:

(1) The aerodynamic coefficients H_i^* and A_i^*, which
are responsible for instability in an otherwise stable
bridge, are functions of the bridge geometry, structural
properties, and the oncoming wind velocity $\overline{u}$. These aero-
dynamic coefficients are usually expressed in terms of the
reduced wind velocity

$$\frac{2\pi\overline{u}}{\omega_f^* B} \tag{56}$$

(2) The aerodynamic coefficients, expressed in
terms of $2\pi\overline{u}/\omega_f^* B$ are determined experimentally from the
wind tunnel tests on a scale model. Then the nondimen-
sional experimental parameters are extended and applied to

the actual full-scale bridge. A detailed discussion of this approach is given, e.g., in Refs. 9,21, and 26.

(3) It is obvious from equations 47-56 that the instability condition of equation 55 involves both the flutter frequency ω_f^* and the flutter speed $\bar{u}_f$ which are unknown. In some of the literature, the flutter frequency ω_f^* is approximated by the fundamental frequency of either the torsional or the flexural motion, or is determined experimentally on a scale model [e.g., Refs. 10,21]. In the present analysis, however, both the flutter speed $\bar{u}_f$ and the flutter frequency ω_f^* will be determined exactly using an iterative procedure as follows:

(i) A flutter frequency $\omega_{f_1}^*$ between the fundamental frequencies of both the flexural and torsional modes is assumed [e.g., Ref. 31]

(ii) The corresponding flutter speed $\bar{u}_{f_1}$ is then determined from the instability condition, Eq. 55, given $\omega_{f_1}^*$

(iii) From the coefficients of the characteristic polynomial corresponding to the flutter state at $\bar{u}_{f_1}$, a new flutter frequency $\omega_{f_2}^*$ is determined

(iv) The iterative procedure is continued until both $\bar{u}_f$ and ω_f^* converge.

It must be noted here that the iterative procedure described above is very efficient, and both $\bar{u}_f$ and ω_f^* converge after 4 to 5 iterations.

2. Bridges without Control

When the active control devices are not implemented, the characteristic polynomial for the bridge can be obtained from equations 40, 44, and 45 as

$$\overline{D}(s) = s^4 + \rho_1 s^3 + \rho_2 s^2 + \rho_3 s + \rho_4 = 0 \tag{57}$$

in which the coefficients ρ_1, ρ_2, ρ_3 and ρ_4 are given by equation 50. Unlike equation 46 which is a sixth degree polynomial, equation 57 is a polynomial of fourth degree. Again, by virtue of the Routh-Hurwitz criteria, the necessary and sufficient conditions for the bridge to be stable are

$$\rho_i > 0 \quad \text{for } i=1,2,3,4 \tag{58}$$

$$T_i > 0 \quad \text{for } i=1,2,3 \tag{59}$$

It has been examined in Ref. 9 that the conditions $\rho_i > 0$ for $i=1,2,3,4$ and $T_i > 0$ for $i=1,2$ are normally satisfied for bridge decks. Consequently, the stability condition is determined by

$$T_3 = \begin{vmatrix} \rho_1 & 1 & 0 \\ \rho_3 & \rho_2 & \rho_1 \\ 0 & \rho_4 & \rho_3 \end{vmatrix} = 0 \tag{60}$$

It should be mentioned that T_i given in equation 59 can be obtained from equation 54 by setting all the control parameters to be zero. Therefore, the stability condition for the uncontrolled bridge is a special case of

the bridge under active control, and the corresponding flutter speed $\bar{u}_f$ and flutter frequency ω_f^* can be obtained easily following the iterative procedure mentioned above.

V. STATISTICS OF BRIDGE RESPONSE

Another important problem in the dynamic analysis of cable-stayed bridges is the determination of bridge responses under stochastic wind gusts. Cable-stayed bridges may fail not only because of instability, but also because of excessively large responses, such as displacements or stresses. Even if the bridge response is moderate, fatigue failure may occur owing to repeated applications of gust loads.

The buffeting loads resulting from the gust winds are statistical in nature. These loads have been modeled as stationary Gaussian random processes with zero mean and a finite duration [e.g., Ref. 12]. Consequently, the bridge responses, $W(x,t)$ and $\theta(x,t)$, are also stationary Gaussian random processes with zero mean and a finite duration. In this chapter, the statistics of bridge responses, such as the standard deviation, at the critical locations will be determined.

1. Power Spectral Density Matrix of Response

Traditionally, the buffering loads have been specified by their power spectral densities [e.g., Refs. 10,11,13-15,54]. It is more convenient in the present analysis to

carry out the computation of the response statistics in the frequency domain. Hence, the frequency response matrix of the bridge will be determined first.

The equations of motion for the normal coordinates, $g(t)$ and $f(t)$, in the frequency domain can be obtained from the Laplace transform domain, equations 39, by replacing s by $j\omega$ as follows:

$$
\begin{bmatrix} MQ_{11}(j\omega) & MQ_{12}(j\omega) \\ IQ_{21}(j\omega) & IQ_{22}(j\omega) \end{bmatrix} \begin{Bmatrix} g(j\omega) \\ f(j\omega) \end{Bmatrix} = \begin{Bmatrix} \underset{\sim}{F}(j\omega) \\ \underset{\sim}{M}(j\omega) \end{Bmatrix} \tag{61}
$$

in which the quantities with the argument $j\omega$ represent the Fourier transforms of the corresponding quantities with the argument t. In particular,

$$
\underset{\sim}{F}(j\omega) = \int_{-\infty}^{\infty} \underset{\sim}{F}(t) e^{-j\omega t} d\omega
$$

$$
\underset{\sim}{M}(j\omega) = \int_{-\infty}^{\infty} \underset{\sim}{M}(t) e^{-j\omega t} d\omega
$$

\begin{equation} \tag{62} \end{equation}

where $\underset{\sim}{F}(t)$ and $\underset{\sim}{M}(t)$ are given by equation 24, and

$$
Q_{11}(j\omega) = -\omega^2 + (2J_g \omega_g - H_1) j\omega + \omega_g^2 + \Gamma_g \frac{R_1 R_{0i}}{R_1 + j\omega} L_i(j\omega)
$$

$$
Q_{12}(j\omega) = -j\omega H_2 - H_3
$$

$$
Q_{21}(j\omega) = -j\omega A_1 \tag{63}
$$

$$
Q_{22}(j\omega) = -\omega^2 + (2J_f \omega_f - A_2) j\omega + (\omega_f^2 - A_3) + \Gamma_f \frac{R_1 R_{0i}}{R_1 + j\omega} L_i(j\omega)
$$

$$L_1(j\omega) = 1, \quad L_2(j\omega) = j\omega, \quad L_3(j\omega) = -\omega^2 \tag{64}$$

It should be mentioned that the subscript n for $g_n(j\omega)$, $f_n(j\omega)$, and the other quantities, has been dropped, since we are investigating the first mode vibration (both torsional and flexural), i.e., n=1. Furthermore, the equations of motion for the second modes (both torsional and flexural), i.e., n=2, have exactly the same form as those of the first mode vibration.

The frequency response matrix for the normal coordinates g(t) and f(t) follows from equation 61 as:

$$\underline{H}(j\omega) = \begin{bmatrix} H_{11}(j\omega) & H_{12}(j\omega) \\ H_{21}(j\omega) & H_{22}(j\omega) \end{bmatrix} = \begin{bmatrix} MQ_{11}(j\omega) & MQ_{12}(j\omega) \\ IQ_{21}(j\omega) & IQ_{22}(j\omega) \end{bmatrix}^{-1} \tag{65}$$

where

$$H_{11}(j\omega) = \frac{Q_{22}(j\omega)}{M\Delta(j\omega)} \qquad H_{12}(j\omega) = -\frac{Q_{12}(j\omega)}{I\Delta(j\omega)}$$

$$H_{21}(j\omega) = -\frac{Q_{21}(j\omega)}{M\Delta(j\omega)} \qquad H_{22}(j\omega) = \frac{Q_{11}(j\omega)}{I\Delta(j\omega)} \tag{66}$$

and

$$\Delta(j\omega) = Q_{11}(j\omega)Q_{22}(j\omega) - Q_{12}(j\omega)Q_{21}(j\omega) \tag{67}$$

It is obvious from equations 65-67 that each element, $H_{ij}(j\omega)$, of the frequency response matrix is complex. In order to facilitate the numerical computations and to simplify the solutions the real and the imaginary parts of these elements will be separated using the following

notations:

$$Q_{11}(j\omega) = a_1(\omega) + j a_2(\omega) \tag{68}$$

$$Q_{22}(j\omega) = \beta_1(\omega) + j \beta_2(\omega)$$

in which $a_1(\omega)$, $a_2(\omega)$, $\beta_1(\omega)$ and $\beta_2(\omega)$ are real,

$$a_1(\omega) = \xi_1(\omega) + \Gamma_g n_1(\omega)$$

$$a_2(\omega) = \xi_2(\omega) + \Gamma_g n_2(\omega) \tag{69}$$

$$\beta_1(\omega) = \Omega_1(\omega) + \Gamma_f n_1(\omega)$$

$$\beta_2(\omega) = \Omega_2(\omega) + \Gamma_f n_2(\omega)$$

By comparison of equations 63, 64, 68, and 69, it is obvious that the elements $\xi_1(\omega)$, $\xi_2(\omega)$, $\Omega_1(\omega)$ and $\Omega_2(\omega)$ are not functions of control parameters,

$$\xi_1(\omega) = \omega_g^2 - \omega^2 \qquad \xi_2(\omega) = (2J_g\omega_g - H_1)\omega \tag{70}$$

$$\Omega_1(\omega) = \omega_f^2 - \omega^2 - A_3 \qquad \Omega_2(\omega) = (2J_f\omega_f - A_2)\omega$$

while $n_1(\omega)$ and $n_2(\omega)$ are functions of active control parameters depending on the particular type of sensor given by equation 64,

$$\left. \begin{array}{l} n_1(\omega) = -\dfrac{R_{03}R_1^2\omega^2}{R_1^2 + \omega^2} \\[4mm] n_2(\omega) = \dfrac{R_{03}R_1\omega^3}{R_1^2 + \omega^2} \end{array} \right\} \quad \text{for acceleration sensor} \tag{71}$$

$$n_1(\omega) = -\frac{R_{02}R_1\omega^2}{R_1^2+\omega^2}$$

$$n_2(\omega) = \frac{R_{02}R_1^2\omega}{R_1^2+\omega^2}$$

for velocity sensor (72)

$$n_1(\omega) = \frac{R_{01}R_1^2}{R_1^2+\omega^2}$$

$$n_2(\omega) = \frac{R_{01}R_1\omega}{R_1^2+\omega^2}$$

for displacement sensor (73)

It should be emphasized that the separation of the functions $n_1(\omega)$ and $n_2(\omega)$, which are functions of active control parameters, from those functions, such as $\xi_i(\omega)$ and $\Omega_i(\omega)$, which are independent of the control devices, enables one to examine easily the effect of active control on the bridge responses.

By virtue of equations 63, 69-70, $\Delta(j\omega)$ appearing in equation 67 can be written as

$$\Delta(j\omega) = D_1(\omega)+jD_2(\omega) \tag{74}$$

in which

$$D_1(\omega) = a_1(\omega)\beta_1(\omega)-a_2(\omega)\beta_2(\omega)+A_1H_2\omega^2$$

$$D_2(\omega) = a_1(\omega)\beta_2(\omega)-a_2(\omega)\beta_1(\omega)-A_1H_3\omega \tag{75}$$

Finally the elements $H_{ij}(j\omega)$ appearing in equation 66 can be separated into real and imaginary parts as follows:

$$H_{11}(j\omega) = \frac{\beta_1(\omega)D_1(\omega)+\beta_2(\omega)D_2(\omega)}{M|\Delta(j\omega)|^2} + j\frac{\beta_2(\omega)D_1(\omega)-\beta_1(\omega)D_2(\omega)}{M|\Delta(j\omega)|^2}$$

$$\tag{76}$$

$$H_{12}(j\omega) = \frac{H_3 D_1(\omega)+\omega H_2 D_2(\omega)}{I|\Delta(j\omega)|^2} + j\frac{\omega H_2 D_1(\omega)-H_3 D_2(\omega)}{I|\Delta(j\omega)|^2}$$

$$H_{21}(j\omega) = \frac{\omega A_1 D_2(\omega)}{M|\Delta(j\omega)|^2} + j\frac{A_1 D_1(\omega)\omega}{M|\Delta(j\omega)|^2}$$

$$H_{22}(j\omega) = \frac{a_1(\omega)D_1(\omega)+a_2(\omega)D_2(\omega)}{I|\Delta(j\omega)|^2} + j\frac{a_2(\omega)D_1(\omega)-a_1(\omega)D_2(\omega)}{I|\Delta(j\omega)|^2}$$

Let $\underline{S}(j\omega)$ be the power spectral density matrix of the normal coordinates $[g(t),\ f(t)]$, i.e.,

$$\underline{S}(j\omega) = \begin{bmatrix} S_{gg}(\omega) & S_{gf}(j\omega) \\ S_{fg}(j\omega) & S_{ff}(\omega) \end{bmatrix} \tag{77}$$

Then, it follows from equation 61 that $\underline{S}(j\omega)$ is related to the power spectral density matrix $\underline{S}_b(j\omega)$ of the generalized buffeting loads, $\underset{\sim}{F}(t)$ and $\underset{\sim}{M}(t)$ associated with the first torsional and flexural modes as follows [e.g., Refs. 61,62];

$$\underline{S}(j\omega) = \underline{H}(j\omega)\underline{S}_b(j\omega)\underline{H}^{*T}(j\omega) \tag{78}$$

in which the star denotes the complex conjugate and the superscript T denotes the transpose of the matrix, and

$$\underline{S}_b(i\omega) = \begin{bmatrix} S_{FF}(\omega) & S_{FM}(j\omega) \\ S_{MF}(j\omega) & S_{MM}(\omega) \end{bmatrix} \tag{79}$$

2. Buffeting Loads

As mentioned previously, the buffeting loads are defined by the power spectral density matrix in equation 79, in which the cross-spectral densities between the lifting force and the moment are assumed to be zero [e.g., Ref. 10], i.e.,

$$S_{FM}(j\omega) = 0$$
$$S_{MF}(j\omega) = 0 \tag{80}$$

The power spectral densities $S_{FF}(\omega)$ and $S_{MM}(\omega)$ are by definition

$$S_{FF}(\omega) = \lim_{T\to\infty} \frac{1}{2\pi T} E[\underset{\sim}{F}(j\omega)\underset{\sim}{F^*}(j\omega)]$$

$$S_{MM}(\omega) = \lim_{T\to\infty} \frac{1}{2\pi T} E[\underset{\sim}{M}(j\omega)\underset{\sim}{M^*}(j\omega)] \tag{81}$$

in which E[ ] represents the ensemble average and T denotes the length of time [e.g., Refs. 63,64].

Substituting equations 24 and 30 for n=1 into equation 62 and then into equation 81, one obtains

$$S_{FF}(\omega) = \int_0^\ell \int_0^\ell S_F(x_1,x_2;\omega)\sin\frac{\pi x_1}{\ell}\sin\frac{\pi x_2}{\ell} \, dx_1 dx_2 \tag{82}$$

$$S_{MM}(\omega) = \int_0^\ell \int_0^\ell S_M(x_1,x_2;\omega)\sin\frac{\pi x_1}{\ell}\sin\frac{\pi x_2}{\ell} \, dx_1 dx_2$$

in which $S_F(x_1,x_2;\omega)$ and $S_M(x_1,x_2;\omega)$ are, respectively, the cross power spectral densities of the lifting force and the pitching moment at two points x_1 and x_2.

According to Refs. 10 and 11, the cross power spectral density $S_F(x_1,x_2;\omega)$ [or $S_M(x_1,x_2;\omega)$] can be decomposed into the product of a cross-correlation coefficient $R(x_1,x_2;\omega)$ between the buffeting loads at two points x_1 and x_2 and a power spectral density $\tilde{S}_F(\omega)$ [or $\tilde{S}_M(\omega)$] of the buffeting loads at a reference point,

$$S_F(x_1,x_2;\omega) = \tilde{S}_F(\omega)R(x_1,x_2;\omega)$$
$$S_M(x_1,x_2;\omega) = \tilde{S}_M(\omega)R(x_1,x_2;\omega)$$

(83)

where the buffeting loads are assumed to be homogeneous in space.

The cross-correlation coefficient, $R(x_1,x_2;\omega)$, can reasonably be expressed in the following form [e.g., Refs. 10,11,13]

$$R(x_1,x_2;\omega) = \exp\left[-\frac{K_1\omega}{2\pi\bar{u}}|x_1-x_2|\right]$$

(84)

in which K_1 is used to define the scale of turbulence and is assumed to be $K_1=7$.

By substitution of equations 83 and 84 into equation 82, the double integrations can be carried out; with the results,

$$S_{FF}(\omega) = \tilde{S}_F(\omega)|J(\omega)|^2$$
$$S_{MM}(\omega) = \tilde{S}_M(\omega)|J(\omega)|^2$$

(85)

in which

$$|J(\omega)|^2 = \frac{1}{\lambda^2+\left(\frac{\pi}{\ell}\right)^2}\left\{\lambda\ell + \frac{2\left(\frac{\pi}{\ell}\right)^2}{\lambda^2+\left(\frac{\pi}{\ell}\right)^2}\cdot[1+e^{-\lambda\ell}]\right\}$$

(86)

where

$$\lambda = \frac{K_1 \omega}{2\pi \bar{u}} \tag{87}$$

The power spectral densities of the buffeting loads at a point, $\tilde{S}_F(\omega)$ and $\tilde{S}_M(\omega)$, are one-half of their corresponding one-sided power spectral densities, $\tilde{S}_F^+(\omega)$ and $\tilde{S}_M^+(\omega)$,

$$\tilde{S}_F(\omega) = \frac{1}{2} \tilde{S}_F^+(\omega) \quad ; \quad \tilde{S}_M(\omega) = \frac{1}{2} \tilde{S}_M^+(\omega) \tag{88}$$

where $\tilde{S}_F(\omega)$ and $\tilde{S}_M(\omega)$ are symmetrical with respect to $\omega=0$.

Both the one-sided power spectral densities, $\tilde{S}_F^+(\omega)$ and $\tilde{S}_M^+(\omega)$, of the buffeting loads can be expressed in terms of the horizontal and vertical turbulent wind velocity fluctuations [e.g., Refs. 10,11,13-15,54],

$$\tilde{S}_F^+(\omega) = 4\bar{L}^2 |\gamma_2(\omega)|^2 \frac{\tilde{S}_u^+(\omega)}{\bar{u}^2} + \left(\frac{dL}{d\psi}\right)^2 |\gamma_3(\omega)|^2 \frac{\tilde{S}_w^+(\omega)}{\bar{u}^2} \tag{89}$$

$$\tilde{S}_M^+(\omega) = 4\bar{M}^2 |\gamma_4(\omega)|^2 \frac{\tilde{S}_u^+(\omega)}{\bar{u}^2} + \left(\frac{dM}{d\psi}\right)^2 |\gamma_5(\omega)|^2 \frac{\tilde{S}_w^+(\omega)}{\bar{u}^2}$$

in which $\bar{L}$ and $\bar{M}$ are the static lift and the static moment, respectively, and $\frac{d\bar{L}}{d\psi}$ and $\frac{d\bar{M}}{d\psi}$ are the corresponding slopes. These quantities are functions of the mean wind velocity $\bar{u}$ and the angle of attack ψ, and they can be expressed as [e.g., Refs. 10,52]:

$$\bar{L} = \frac{1}{2} \rho\bar{u}^2(2B)[L_0 + \frac{\partial C_L}{\partial\psi} \psi] \tag{90}$$

$$\bar{M} = \frac{1}{2} \rho\bar{u}^2(2B^2)[M_0 + \frac{\partial C_M}{\partial\psi} \psi]$$

where L_0 and M_0 are the static unbalance lift and moment, respectively, and $\dfrac{\partial C_L}{\partial \psi}$ and $\dfrac{\partial C_M}{\partial \psi}$ are the respective slopes. These quantities correspond to zero mean angle of attack, and they are determined experimentally for each particular bridge cross-section.

The aerodynamic admittances, $|\gamma_2(\omega)|$ through $|\gamma_5(\omega)|$, given in equation 89 are essentially the measures of the ratios of the aerodynamic forces in fluctuating flows to their corresponding quasi-static values. These aerodynamic admittances are assumed to be equal with the form [e.g., Refs. 10,11],

$$|\gamma_i(\omega)|^2 = |\gamma(\omega)|^2 = \frac{2[\lambda B - 1 + e^{-\lambda B}]}{(\lambda B)^2} \quad \text{for } i = 2,3,4,5 \qquad (91)$$

Finally, the one-sided spectra, $S_u^+(\omega)$ and $S_W^+(\omega)$, appearing in equations 89 are expressed as [e.g., Refs. 10, 13,15,54]:

$$S_u^+(\omega) = \frac{6 K_1 K \overline{u}_1^2}{2\pi\beta \left\{ 1 + \left(\dfrac{\omega}{2\pi\beta}\right)^2 \right\}^{5/6}}$$

$$\hspace{8cm} (92)$$

$$S_W^+(\omega) = \frac{6 K \overline{u}_1 Z^*}{2\pi \left(1 + \dfrac{2\omega Z^*}{\pi \overline{u}_1} \right)^2}$$

in which

$$\beta = K_2 (K\bar{u}_1^2)^{-3/2} \bar{u}_1^{-4} (p \frac{K}{Z_1^*}) (\frac{Z^*}{Z_1^*})^{(4p-1)}$$

where $K_1 = 0.4751$, $K_2 = 1.169 \times 10^{-2}$ and K is the surface drag coefficient depending on the topographical conditions.

In equation 92, $\bar{u}_1$ is the reference wind velocity at a height of $Z_1^* = 10$ meters, and it is related to the mean wind velocity at a height Z^* through the power law formula [e.g., Ref. 13]

$$\bar{u}(z) = \bar{u}_1 (\frac{Z^*}{Z_1^*})^p \tag{93}$$

where p is a constant depending also on the topographic conditions.

3. Statistics of Response

The elements of the power spectral density matrix, $\underline{S}(j\omega)$, are obtained from equations 65, 77-79, and 80 as follows:

$$S_{gg}(\omega) = |H_{11}(j\omega)|^2 S_{FF}(\omega) + |H_{12}(j\omega)|^2 S_{MM}(\omega)$$
$$S_{gf}(j\omega) = H_{11}(j\omega) H_{21}^*(j\omega) S_{FF}(\omega) + H_{12}(j\omega) H_{22}^*(j\omega) S_{MM}(\omega)$$
$$S_{fg}(j\omega) = S_{gf}^*(j\omega)$$
$$S_{ff}(\omega) = |H_{21}(j\omega)|^2 S_{FF}(\omega) + |H_{22}(j\omega)|^2 S_{MM}(\omega)$$

$$\tag{94}$$

in which $S_{gg}(\omega)$ and $S_{ff}(\omega)$ are real, whereas $S_{gf}(j\omega)$ and $S_{fg}(j\omega)$ are complex.

The spectra of the flexural displacement, $W(x,t)$, and the rotation, $\theta(x,t)$, denoted by $S_{WW}(x,\omega)$ and $S_{\theta\theta}(x,\omega)$, respectively, can be obtained from equations 16 and 30 as

$$S_{WW}(x,\omega) = S_{gg}(\omega)\sin^2(\pi x/\ell)$$
$$S_{\theta\theta}(x,\omega) = S_{ff}(\omega)\sin^2(\pi x/\ell) \tag{95}$$

in which only the fundamental modes have been considered.

Since $S_{gg}(\omega)$ and $S_{ff}(\omega)$ are real and symmetric with respect to $\omega = 0$, the variances of $W(x,t)$ and $\theta(x,t)$ are, respectively, given by

$$\sigma_w^2(x) = \sin^2(\pi X/\ell)\int_0^\infty 2S_{gg}(\omega)\,d\omega$$
$$\sigma_\theta^2(x) = \sin^2(\pi X/\ell)\int_0^\infty 2S_{ff}(\omega)\,d\omega \tag{96}$$

In addition to the variances of the flexural and torsional motion at the center of the bridge deck given by equation 96, the variances of the motion at each side of the bridge deck can be determined as follows:

Let $Z_1(x,t)$ be the total displacement at one side of the bridge deck, i.e.,

$$Z_1(x,t) = W(x,t) + \frac{B}{2}\,\theta(x,t) \tag{97}$$

Then, expressing $Z_1(x,t)$ in terms of the normal modes and retaining the first modes only, one obtains

$$Z_1(x,t) = \left[g(t) + \frac{B}{2}\,f(t)\right]\sin\left(\frac{\pi x}{\ell}\right) \tag{98}$$

The power spectral density of $Z_1(x,t)$ is by definition,

$$S_{Z_1Z_1}(x,\omega) = \lim_{T\to\infty} \frac{1}{2\pi T} E\left[Z_1(x,j\omega)Z_1^*(x,j\omega)\right] \tag{99}$$

Taking Fourier transform on equation 98 and substituting the result into equation 99, one can express the power spectral density, $S_{Z_1Z_1}(x,\omega)$, in terms of the power spectral densities of the normal coordinates as follows:

$$S_{Z_1Z_1}(x,\omega) = \left[S_{gg}(\omega)+(B^2/4)S_{ff}(\omega)+B\mathrm{Re}\left\{S_{gf}(j\omega)\right\}\right]\sin^2(\pi X/\ell) \tag{100}$$

in which $\mathrm{Re}\left\{S_{gf}(j\omega)\right\}$ is the real part of $S_{gf}(j\omega)$.

The variance of the displacement $Z_1(x,t)$ is therefore,

$$\sigma_{Z_1}^2 = \int_0^\infty 2S_{Z_1Z_1}(x,\omega)d\omega = 2\sin^2(\pi X/\ell)\int_0^\infty\left[S_{gg}(\omega)+(B^2/4)S_{ff}(\omega)\right.$$

$$\left.+ B\mathrm{Re}\left\{S_{gf}(j\omega)\right\}\right]d\omega \tag{101}$$

The displacement, $Z_2(x,t)$, at the other side of the bridge deck is

$$Z_2(x,t) = W(x,t)-\frac{B}{2}\theta(x,t) \tag{102}$$

In a similar manner, the variance of $Z_2(x,t)$ can be obtained as

$$\sigma_{Z_2}^2(x) = 2\sin^2(\pi x/\ell)\int_0^\infty\left[S_{gg}(\omega)+(B^2/4)S_{ff}(\omega)\right.$$

$$\left.- B\mathrm{Re}\left\{S_{gf}(j\omega)\right\}\right]d\omega \tag{103}$$

VI.   POWER REQUIREMENT FOR
ACTIVE CONTROL DEVICES

As mentioned previously, the purpose of this study
is to investigate the feasibility of applying active control
devices to raise the flutter speed and to reduce the struc-
tural responses in order to improve the safety of the
bridge.   The additional costs due to the installation of
control devices as well as the energy consumption should be
balanced economically by the safety improvement and a less
conservative design for the bridge.   It is important to
determine whether or not the power requirement for a sub-
stantial reduction of bridge motion and a significant in-
crease in flutter speed is within the capability of avail-
able control devices, such as the hydroservomechanism.   An
active control for cable-stayed bridges will not be feasible
if the power requirement exceeds the limit of the practical
control devices.   In this chapter, the power requirement of
the control devices will be estimated analytically.

The instantaneous power associated with the motion
of the hydraulic ram connected to one of the suspension
cables is given by:

$$\Phi(t) = -T(t)\dot{S}(t) \tag{104}$$

in which $\dot{S}(t)$ is the velocity of the ram, and $T(t)$ is the

tension in the suspension cable to which the hydraulic ram is subjected.[2] The tension in the cable T(t) consists of the tension T_0 due to the dead weight of the bridge and the fluctuation $\Delta T(t)$ due to the bridge motions [see appendix 1, equations 1-1 to 1-3],

$$T(t) = T_0 + \Delta T(t) \tag{105}$$

in which

$$\Delta T(t) = \frac{E_0 A_0}{\ell_0} [v(t)\sin\phi + S(t)] \tag{106}$$

where $v(t)$ is the vertical displacement at the anchorage [see appendix 1, equation 1-4].

By substitution of equations 105 and 106 into equation 104, the instantaneous power $\Phi(t)$ can be expressed as

$$\Phi(t) = -T_0 \dot{S}(t) - \frac{E_0 A_0}{\ell_0} [v(t)\dot{S}(t)\sin\phi + S(t)\dot{S}(t)] \tag{107}$$

Expressing $v(t)$, $S(t)$ and $\dot{S}(t)$ in terms of their Fourier transforms,

$$v(t) = \frac{1}{2\pi} \int_{-\infty}^{\infty} v(j\omega) e^{j\omega t} d\omega$$

$$S(t) = \frac{1}{2\pi} \int_{-\infty}^{\infty} S(j\omega) e^{j\omega t} d\omega$$

$$\dot{S}(t) = \frac{1}{2\pi} \int_{-\infty}^{\infty} j\omega S(j\omega) e^{j\omega t} d\omega$$

---

[2]The minus sign here means that the tension acts against the velocity.

one obtains from equation 107

$$\Phi(t) = -\frac{T_0}{2\pi}\int_{-\infty}^{\infty} j\ \omega\ S(j\omega)e^{j\omega t}d\omega$$

$$+ \frac{E_0 A_0}{\ell_0}\left\{\frac{\sin\phi}{(2\pi)^2}\int_{-\infty}^{\infty}\int_{-\infty}^{\infty} j\omega_1 \nu(j\omega)S*(j\omega_1)e^{-j(\omega_1-\omega)t}d\omega_1 d\omega\right.$$

$$\left.+ \frac{1}{(2\pi)^2}\int_{-\infty}^{\infty}\int_{-\infty}^{\infty} j\omega_1 S(j\omega)S*(j\omega_1)e^{-j(\omega_1-\omega)}d\omega_1 d\omega\right\}$$

$$\tag{108}$$

The average instantaneous power can be estimated from equation 108 by taking the ensemble average as,

$$\overline{\Phi}(t) = \frac{T_0}{2\pi}\int_{-\infty}^{\infty} j\omega E[S(j\omega)]e^{j\omega t}d\omega$$

$$+ \frac{E_0 A_0}{\ell_0}\left\{\frac{\sin\phi}{(2\pi)^2}\int_{-\infty}^{\infty}\int_{-\infty}^{\infty} j\omega_1 E[\nu(j\omega)S*(j\omega_1)]e^{-j(\omega_1-\omega)t}d\omega_1 d\omega\right.$$

$$+ \frac{1}{(2\pi)^2}\int_{-\infty}^{\infty}\int_{-\infty}^{\infty} j\omega_1 E[S(j\omega)S*(j\omega_1)]e^{-j(\omega_1-\omega)}d\omega_1 d\omega\left.\right\} \tag{109}$$

Since the buffeting loads are assumed to be stationary Gaussian random processes with zero mean, the bridge responses $W(x,t)$ and $\theta(x,t)$ are also stationary Gaussian random processes with zero mean. Furthermore, $S(t)$ is related to $W(x,t)$ and $\theta(x,t)$ through a linear differential equation [see appendix 1, equations 1-11, 1-12], and hence $S(t)$ is a stationary Gaussian random process with zero mean,

$$E[S(j\omega)] = 0 \tag{110}$$

The average power can then be calculated by averaging equation 109 over a long period of time as follows;

$$\overline{\Phi} = \lim_{T \to \infty} \frac{1}{T} \int_{-T/2}^{T/2} \overline{\Phi}(t)dt$$

$$= \frac{E_0 A_0}{\ell_0} \left\{ \lim_{T \to \infty} \frac{\sin\phi}{(2\pi)^2 T} \int_{-T/2}^{T/2} \int_{-\infty}^{\infty} \int_{-\infty}^{\infty} j\omega_1 E[v(j\omega)S^*(j\omega_1)] \cdot \right.$$

$$e^{-j(\omega_1-\omega)t} d\omega_1 d\omega dt + \lim_{T \to \infty} \frac{1}{(2\pi)^2 T} \int_{-T/2}^{T/2} \int_{-\infty}^{\infty} \int_{-\infty}^{\infty} j\omega_1 E[S(j\omega)S^*(j\omega_1)] \cdot$$

$$\left. e^{-j(\omega_1-\omega)t} d\omega_1 d\omega dt \right\} \tag{111}$$

where equation 110 has been incorporated.

Interchanging the order of integration in equation 111 and carrying out the integration with respect to time, one obtains

$$\overline{\Phi} = \frac{E_0 A_0}{\ell_0} \left\{ \lim_{T \to \infty} \frac{\sin\phi}{2\pi T} \int_{-\infty}^{\infty} \int_{-\infty}^{\infty} j\omega_1 E[v(j\omega)S^*(j\omega_1)] \delta(\omega_1-\omega) d\omega_1 d\omega \right.$$

$$\left. + \lim_{T \to \infty} \frac{\sin\phi}{2\pi T} \int_{-\infty}^{\infty} \int_{-\infty}^{\infty} j\omega_1 E[S(j\omega)S^*(j\omega_1)] \delta(\omega_1-\omega) d\omega_1 d\omega \right\} \tag{112}$$

in which the relationship

$$\int_{-\infty}^{\infty} e^{-i(\omega_1-\omega)t} dt = 2\pi\delta(\omega_1-\omega)$$

has been used.

Finally, integration of equation 112 with respect to ω_1 yields:

$$\bar{\Phi} = \frac{E_0 A_0}{\ell_0} \left\{ \lim_{T \to \infty} \frac{1}{2\pi T} \int_{-\infty}^{\infty} j\omega E[\nu(j\omega)S^*(j\omega)]d\omega \right.$$

$$\left. + \lim_{T \to \infty} \frac{1}{2\pi T} \int_{-\infty}^{\infty} j\omega E[S(j\omega)S^*(j\omega)]d\omega \right\} \tag{113}$$

The power spectral density $S_{SS}(\omega)$ of the random process $S(t)$ (displacement of hydraulic ram) is by definition,

$$S_{SS}(\omega) = \lim_{T \to \infty} \frac{1}{2\pi T} E[S(j\omega)S^*(j\omega)] \tag{114}$$

and $S_{SS}(\omega)$ is an even function of ω so that

$$\int_{-\infty}^{\infty} j\omega S_{SS}(\omega)d\omega = 0 \tag{115}$$

By virtue of equations 114 and 115, equation 113 becomes

$$\bar{\Phi} = \frac{E_0 A_0}{\ell_0} \sin\phi \lim_{T \to \infty} \frac{1}{2\pi T} \int_{-\infty}^{\infty} j\omega E[\nu(j\omega)S^*(j\omega)]d\omega \tag{116}$$

The average power requirement derived in equation 116 is for the control device connected to one suspension cable without specifying a particular one. Let $\bar{\Phi}_\ell(a)$, $\bar{\Phi}_r(a)$, $\bar{\Phi}_\ell(\ell-a)$, and $\bar{\Phi}_r(\ell-a)$ be the average powers for the control devices associated with the left and the right suspension cables, respectively, at $x=a$ and $x=\ell-a$. Then, in a similar manner, it can be shown that

$$\bar{\Phi}_\ell(a) = \frac{E_0 A_0}{\ell_0} \sin\phi \lim_{T \to \infty} \frac{1}{2\pi T} \int_{-\infty}^{\infty} j\omega E[\nu_\ell(a,j\omega)S_\ell^*(a,j\omega)]d\omega \tag{117}$$

$$\overline{\Phi}_r(a) = \frac{E_0 A_0}{\ell_0} \sin\phi \lim_{T\to\infty} \frac{1}{2\pi T} \int_{-\infty}^{\infty} j\omega E[\nu_r(a,j\omega)S_r^*(a,j\omega)]d\omega \quad (118)$$

$$\overline{\Phi}_\ell(\ell-a) = \frac{E_0 A_0}{\ell_0} \sin\phi \lim_{T\to\infty} \frac{1}{2\pi T} \int_{-\infty}^{\infty} j\omega E[\nu_\ell(\ell-a,j\omega)S_\ell^*(\ell-a,j\omega)]d\omega$$

$$(119)$$

$$\overline{\Phi}_r(\ell-a) = \frac{E_0 A_0}{\ell_0} \sin\phi \lim_{T\to\infty} \frac{1}{2\pi T} \int_{-\infty}^{\infty} j\omega E[\nu_r(\ell-a,j\omega)S_r^*(\ell-a,j\omega)]d\omega$$

$$(120)$$

The integrands of equations 117-120 can be expressed in terms of the expected values of $W(a,j\omega)$, $\theta(a,j\omega)$, $u(a,j\omega)$, $v(a,j\omega)$, etc., by use of equations 1-12 and 1-13 of appendix 1 as follows;

$$E[\nu_\ell(a,j\omega)S_\ell^*(a,j\omega)] = E[W(a,j\omega)u^*(a,j\omega)+\frac{B}{2}W(a,j\omega)v^*(a,j\omega)$$
$$+ \frac{B}{2}\theta(a,j\omega)u^*(a,j\omega)$$
$$+ \frac{B^2}{4}\theta(a,j\omega)v^*(a,j\omega)] \quad (121)$$

$$E[\nu_r(a,j\omega)S_r^*(a,j\omega)] = E[W(a,j\omega)u^*(a,j\omega)-\frac{B}{2}W(a,j\omega)v^*(a,j\omega)$$
$$- \frac{B}{2}\theta(a,j\omega)u^*(a,j\omega)$$
$$+ \frac{B^2}{4}\theta(a,j\omega)v^*(a,j\omega)] \quad (122)$$

$$E[\nu_\ell(\ell-a,j\omega)S_\ell^*(\ell-a,j\omega)] = E[W(\ell-a,j\omega)u^*(\ell-a,j\omega)$$
$$+ \frac{B}{2}W(\ell-a,j\omega)v^*(\ell-a,j\omega)$$
$$+ \frac{B}{2}\theta(\ell-a,j\omega)u^*(\ell-a,j\omega)$$
$$+ \frac{B^2}{4}\theta(\ell-a,j\omega)v^*(\ell-a,j\omega)] \quad (123)$$

$$E[v_r(\ell-a,j\omega)S_r^*(\ell-a,j\omega)] = E[W(\ell-a,j\omega)u^*(\ell-a,j\omega)$$
$$- \frac{B}{2} W(\ell-a,j\omega)v^*(\ell-a,j\omega)$$
$$- \frac{B}{2} \theta(\ell-a,j\omega)u^*(\ell-a,j\omega)$$
$$+ \frac{B^2}{4} \theta(\ell-a,j\omega)v^*(\ell-a,j\omega)] \qquad (124)$$

Summing equations 117 to 120 and using equations 121-124, one obtains the total average power as follows:

$$\bar{\Phi} = \frac{2E_0A_0}{\ell_0} \sin\phi \lim_{T\to\infty} \frac{1}{2\pi T} \int_{-\infty}^{\infty} j\omega E[W(a,j\omega)u^*(a,j\omega)$$
$$+ W(\ell-a,j\omega)u^*(\ell-a,j\omega) + \frac{B^2}{4} \theta(a,j\omega)v^*(a,j\omega)$$
$$+ \frac{B^2}{4} \theta(\ell-a,j\omega)v^*(\ell-a,j\omega)]d\omega \qquad (125)$$

The quantities $W(a,t)$, $\theta(a,t)$, $u(a,t)$, $v(a,t)$, etc., have been expanded in terms of the normal modes in equations 16 and 17. Taking the Fourier transforms of equations 16 and 17, and substituting the resulting equations into equation 125, one obtains

$$\bar{\Phi} = \frac{4E_0A_0}{\ell_0} \sin\phi \sum_n \sin^2 \frac{n\pi}{3} \left\{ \lim_{T\to\infty} \frac{1}{2\pi T} \int_{-\infty}^{\infty} j\omega E[g_n(j\omega)h_n^*(j\omega) \right.$$
$$\left. + \frac{B^2}{4} f_n(j\omega)q_n^*(j\omega)]d\omega \right\} \qquad (126)$$

in which the relations $X_k(x) = Y_k(x) = \sin k\pi x/\ell$ and $a = \ell/3$ [Equations 30 and 31] have been used. In equation 126, $g_n(j\omega)$, $f_n(j\omega)$, $h_n(j\omega)$, $q_n(j\omega)$ are the Fourier transforms of $g_n(t)$, $f_n(t)$, $h_n(t)$, and $g_n(t)$, respectively.

If only the first mode of the flexural and torsional vibration is considered, the summation and subscript of

equation 126 can be dropped to yield

$$\bar{\Phi} = \frac{4E_0A_0}{\ell_0} \sin\phi\sin^2 \frac{\pi}{3} \lim_{T\to\infty} \frac{1}{2\pi T} \int_{-\infty}^{\infty} j\omega E[g(j\omega)h*(j\omega)$$

$$+ \frac{B^2}{4} f(j\omega)q*(j\omega)]d\omega \tag{127}$$

The Fourier transforms $h(j\omega)$ and $g(j\omega)$ can be obtained in terms of the Fourier transforms $g(j\omega)$ and $f(j\omega)$ by substituting $s=i\omega$ in equations 38; with the results,

$$h(j\omega) = \frac{R_1R_{0i}L_i[j\omega]}{R_1+j\omega} g(j\omega)$$

$$\tag{128}$$

$$q(j\omega) = \frac{R_1R_{0i}L_i[j\omega]}{R_1+j\omega} f(j\omega)$$

The quantity $R_1R_{0i}L_i[j\omega]/(R_1+j\omega)$ appearing in equation 128 can be separated into the real and imaginary parts

$$\frac{R_1R_{0i}L_i[j\omega]}{R_1+j\omega} = n_1(\omega)+jn_2(\omega) \tag{129}$$

in which the real functions $n_1(\omega)$ and $n_2(\omega)$ have been defined in equations 71-73 for different sensors.

Substituting equations 128 and 129 into equation 127, and using the quantities given in equation 41, one obtains

$$\overline{\Phi} = M\Gamma_g \left\{ \lim_{T\to\infty} \frac{1}{2\pi T} \int_{-\infty}^{\infty} j\omega[n_1(\omega)-jn_2(\omega)]E[g(j\omega)g^*(j\omega)]d\omega \right\}$$

$$+ I\Gamma_f \left\{ \lim_{T\to\infty} \frac{1}{2\pi T} \int_{-\infty}^{\infty} j\omega[n_1(\omega)-jn_2(\omega)]E[f(j\omega)f^*(j\omega)] \right\} d\omega$$

$$= \int_{-\infty}^{\infty} j\omega[n_1(\omega)-jn_2(\omega)] \cdot \left\{ M\Gamma_g S_{gg}(\omega)+I\Gamma_f S_{ff}(\omega) \right\} d\omega \qquad (130)$$

in which $S_{gg}(\omega)$ and $S_{ff}(\omega)$ are the power spectral densities of the normal coordinates $g(t)$ and $f(t)$ [see equation 77]

$$S_{gg}(\omega) = \lim_{T\to\infty} \frac{1}{2\pi T} E[g(j\omega)g^*(j\omega)]$$

$$\qquad (131)$$

$$S_{ff}(\omega) = \lim_{T\to\infty} \frac{1}{2\pi T} E[f(j\omega)f^*(j\omega)]$$

It can be observed from equations 71-73 that $n_1(\omega)$ is an even function whereas $n_2(\omega)$ is an odd function of ω. Since both $S_{gg}(\omega)$ and $S_{ff}(\omega)$ are even functions of ω, the integration for each term associated with $n_1(\omega)$ in equation 130 is zero. As a result, equation 130 reduces to the following;

$$\overline{\Phi} = 2M\Gamma_g \int_0^{\infty} \omega n_2(\omega)S_{gg}(\omega)d\omega + 2I\Gamma_f \int_0^{\infty} \omega n_2(\omega)S_{ff}(\omega)d\omega \qquad (132)$$

VII. NUMERICAL EXAMPLES

1. Bridge Properties and Input Data

In order to demonstrate the feasibility of applying active tendon control devices to the cable-stayed bridges, the Sitka Harbor Bridge, Sitka, Alaska, is considered herein, referred to as Bridge 1. The stiffness of the same bridge is then theoretically reduced to represent a less conservative design, referred to as Bridge 2. The analysis results of both bridges are compared to illustrate the effect of active control on the bridge design.

(i) Bridge 1: Design information on the Sitka Harbor Bridge has been provided by the Fairbank Highway Research Station, Department of Transportation, McLean, Virginia, as follows: $m = 6.859 \times 10^3$ kg/m(143.3 slugs/ft), $I_s = 12.4517 \times 10^4$ kg·m^2/m(2.8×10^4 slugs ft^2/ft), $\ell = 137.16$m (450 ft), $B = 11.43$m(37.75 ft), $\omega_g = 5.083$ rad/sec, $\omega_f = 8.589$ rad/sec, $J_g = 0.01$, $J_f = 0.01$, $a = \ell/3$, $\phi = 0.54\pi$, $\ell_0 = 106.32$m(348.8 ft), $E_0 = 1.586 \times 10^{11}$N/m^2($23 \times 10^6$psi), $A_0 = 1.045 \times 10^{-2}$m^2(16.2 in^2), $Z^* = 15.85$m(52 ft), $\rho = 1.25$ kg/m^3(0.002425 slugs/ft^3).

The experimental data on buffeting loads used in Ref. 10 have been used herein for approximation; $K = 0.003$,

55

$p = 1/7$, $L_0 = 0.0$, $M_0 = 0.05$, $\frac{\partial C_L}{\partial \psi} = 1.5$, $\frac{\partial C_M}{\partial \psi} = 0.93$, $\psi = 0°$.

Furthermore, the aerodynamic coefficients used in the present example are plotted in figure 6. These coefficients were experimentally determined from wind tunnel tests on a model of the Sitka Harbor Bridge for $\psi = 0°$ and they have been presented in Ref. 35. The aerodynamic coefficients, H_2^*, H_3^*, A_1^* and A_3^*, were found to be negligible.

(ii) Bridge 2: The input data described above for Bridge 1 have been maintained, except that the stiffness of the bridge has been reduced by reducing both the flexural and torsional natural frequencies. The reduced fundamental natural frequencies in bending and torsion are given as follows:

$\omega_g = 3.3653$ rad/sec, $\omega_f = 5.6863$ rad/sec.

It is mentioned that the ratio ω_g/ω_f was kept identical for both bridges, i.e., $\omega_g/\omega_f = 1.69$.

2. Stability of Bridges

(i) Bridges without active control: Using the aerodynamic coefficients presented in figure 6 along with the fact that H_2^*, H_3^*, A_1^*, and A_3^* are zero, one can show from the stability conditions of equations 58 and 59 that instability occurs when

$$2J_f\omega_f - A_2 \leq 0 \tag{133}$$

indicating that the instability is due to torsional vibration. The flutter state corresponds to the equality sign in equation 133.

By substitution of $s = i\omega_f^*$ and the flutter condition given by equation 133 into equation 57, it can be shown that the flutter frequency ω_f^* is equal to the fundamental torsional frequency,

$$\omega_f^* = \omega_f$$

Then, the critical wind velocity $\bar{u}_f$ at which the torsional vibration becomes unstable is determined from the flutter condition, equation 133. As a result, the iterative procedures discussed in chapter 4 are not necessary in the present situation (bridges without active control).

The results for the two bridges are as follows: $\bar{u}_f = 69.52$ m/sec (155.52 mph), $\omega_f^* = \omega_f = 8.589$ rad/sec for Bridge 1, whereas $\bar{u}_f = 46.02$ m/sec (102.9 mph) $\omega_f^* = \omega_f$ $= 5.6863$ rad/sec for Bridge 2.

(ii) Bridges with active control: When the control devices are implemented, the flutter speed, $\bar{u}_f$, and flutter frequency, ω_f^*, become functions of the control parameters R_1 and $R_{0i}(i=1,2,3)$ as can be observed from equations 47 through 49. For simplicity, both R_1 and R_{0i} are non-dimensionalized by the torsional frequency ω_f as follows:

$$\varepsilon = R_1/\omega_f \quad ; \quad \tau = R_{0i}\omega_f^2 \tag{134}$$

The critical wind velocities, $\bar{u}_f$, have been calculated using the stability conditions, equations 52 and 53, for the acceleration sensor (equations 49), the velocity sensor (equations 50), and the displacement sensor (equations 51), respectively. The corresponding flutter frequencies, ω_f^*, have also been evaluated numerically using the iterative procedure described in chapter 4.

The results for Bridge 1 are plotted in figures 7-10 [appendix 3] for various values of ε and τ (equation 134). It will be discussed later that the displacement sensor is not efficient as compared to the acceleration and velocity sensors. Consequently, the results associated with the displacement sensor will not be presented. It should be mentioned that the case $\varepsilon = 0$ corresponds to the stability condition without active control.

The aerodynamic coefficients are available only over certain range of the reduced velocity $2\pi\bar{u}/B\omega_f^*$ as observed from figure 6 [appendix 3] [e.g., Refs. 26 and 35], i.e.,

$$\frac{2\pi\bar{u}}{B\omega_f^*} \leq 10.$$

Such a limitation restricts the range over which the flutter speed, $\bar{u}_f$, and flutter frequency, ω_f^*, can be calculated. This is the reason why some curves in figures 9 and 10 [appendix 3] are not plotted over the full range of τ.

The results on the flutter speed, $\bar{u}_f$, and the flutter frequency, ω_f^*, for Bridge 2 are plotted in figures 11-14 [appendix 3] for various values of ε and τ.

It is found from numerical computations that both bridges are stable only if the following conditions for the control parameters are satisfied.

$$\varepsilon \geq 0 \ , \qquad \tau \geq 0 \ \text{for acceleration sensor}$$

$$\varepsilon \geq 0 \ , \qquad \tau \geq 0 \ \text{for velocity sensor} \qquad (135)$$

$$\varepsilon \geq 0 \ , \qquad \tau \leq 0 \ \text{for displacement sensor}$$

It can be observed from figures 7, 8, 11 and 12 [appendix 3] that the flutter speed $\bar{u}_f$ increased as the values of the control parameters ε and τ increase, and in some regions the flutter speed is raised more than 100%. In fact, the flutter speed $\bar{u}_f$ increases drastically and approaches infinity (the curve becomes vertical) when certain values of ε and τ are chosen as shown in these figures, e.g., $\varepsilon=0.6$, $\tau=0.25$, or $\varepsilon=0.5$, $\tau=0.29$, for acceleration sensor in Bridge 1 [see figure 7, appendix 3]. As a result, by use of the active control devices with appropriate control parameters, the flutter speed can be raised to any desirable level for both conservatively (Bridge 1) and less conservatively (Bridge 2) designed cable-stayed bridges.

Comparison of figures 7 and 8 with figures 11 and 12 [appendix 3] indicates that for the same percentage of increment in flutter speed, Bridge 2 requires smaller

values of control parameter ε than Bridge 1. Accordingly, it follows from equations 134 that the loop gain and the capacity of the required servomechanism is much smaller for Bridge 2 than Bridge 1. As a result, the active control is more efficient in raising the flutter speed for less stiff and less conservatively designed cable-stayed bridges. This conclusion is of practical importance and should be emphasized, since the payoff in implementing the active control is much higher for a less conservatively designed bridge.

For the case of acceleration sensor, it can be observed from figures 9 and 13 [appendix 3] that the flutter frequency ω_f^* decreases from the fundamental torsional frequency ω_f as the values of the control parameters ε and τ increase. However, the shift in the flutter frequency ω_f^* from ω_f is very small indicating that the approximation of the flutter frequency ω_f^* by the fundamental torsional frequency ω_f is reasonable, when the acceleration is used as the feedback sensor. For the case of the velocity sensor, on the other hand, ω_f^* increases from ω_f as ε and τ increase [see figures 10 and 14, appendix 3], and the shift of ω_f^* from ω_f is not small for large values of ε and τ.

When a value of the aerodynamic coefficient A_2^* [see figure 6, appendix 3] satisfies the stability condition, equation 55, a higher flutter frequency ω_f^* results in a higher flutter speed $\bar{u}_f$ as can be observed from equation

56. Consequently, the velocity sensor seems to be slightly
more favorable than the acceleration sensor as far as the
stability problem is concerned.

3. Bridge Response and
   Power Requirement

In contrast to the flutter speed $\bar{u}_f$ and frequency ω_f^*
the statistics of the bridge motion depend not only on the
control parameters ε and τ but also on the mean wind veloc-
ity $\bar{u}$. This is because the aerodynamic coefficients H_1 and
A_2 are functions of the mean wind velocity $\bar{u}$.

The frequency response matrix of the bridge motion
with active control is computed using equations 69-76,
whereas the frequency response matrix of the bridge motion
without active control is obtained from the same equations
by setting $\varepsilon=\tau=0$. Since A_1, H_2 and H_3 are all zero, it is
obvious from equation 76 that

$$H_{12}(j\omega) = H_{21}(j\omega) = 0 \tag{136}$$

Therefore, the cross-power spectral densities of the
response $S_{gf}(j\omega)$ and $S_{fg}(j\omega)$ are zero [see equation 94],
i.e.,

$$S_{gf}(j\omega) = S_{fg}(j\omega) = 0 \tag{137}$$

The power spectral densities for the fundamental
modes of the flexural and torsional vibrations, $S_{gg}(\omega)$ and
$S_{ff}(\omega)$, are computed from equation 94. By virtue of
equation 137, it is obvious from equations 101 and 103 that

the variances of the vertical displacements at both sides

of a bridge station X are identical, denoted by $\sigma_Z^2(x)$, i.e.,

$$\sigma_{Z_1}^2(x) = \sigma_{Z_2}^2(x) = \sigma_Z^2(x) \tag{138}$$

The variance $\sigma_Z^2(\ell/2)$ of the vertical displacement

at the center span $x = \ell/2$ is computed using equation 101

along with a numerical integration procedure. Furthermore,

the average power $\bar{\Phi}$ required for the active control devices

is computed from equation 132 together with a numerical

integration procedure.

Numerical results on standard deviations, $\sigma_Z(\ell/2)$,

of the vertical displacement at the center span $x = \ell/2$, and

the average power requirement $\bar{\Phi}$ for certain particular

values of the control parameters ϵ and τ are plotted as

functions of the mean wind velocity $\bar{u}$, in figures 15 and 16

[appendix 3] for Bridge 1, and in figures 17 and 18

[appendix 3] for Bridge 2, for the various sensors. In

figures 15 and 17 [appendix 3], the standard deviations of

the bridge response without active control are also dis-

played for the purpose of comparison.

It is clearly demonstrated in figures 15 and 17

[appendix 3] that a substantial reduction in bridge response

can be achieved by the active control devices, in particu-

lar, in the region where the mean wind velocity exceeds

the flutter speed of the uncontrolled bridge. It can be

easily observed that the displacement sensor is not as

efficient as the velocity and acceleration sensors.

It is further observed from figures 16 and 18 [appendix 3] that the average power requirement for active control is small, and it is within the range of practicality (smaller than 10^3 horsepower) even at the extremely high wind velocities.

The fact that the active control devices can significantly suppress the bridge response using only such a small average power is another important conclusion obtained in the present study. From the physical standpoint, this is not surprising at all. As described previously, the suspension cables are initially subjected to large tension T_0 due to the dead weight of the bridge deck. When the rotation $\theta(x,t)$ of the bridge deck at x=a or ℓ-a occurs in the clockwise direction, all the control devices have to do is to release part of the initial tension T_0 in the left suspension cable and to increase the additional tension in the right suspension cable to effectively produce the counter reaction (or restoring moment) to the rotation $\theta(x,t)$. A similar situation applies to the vertical motion $W(x,t)$. To release part of the initial tension in the suspension cables requires only a very small amount of power. This is a major advantage of implementing the active control devices to cable-stayed bridges.

For demonstrative purpose, a particular value of mean wind velocity $\bar{u}$ = 45 m/sec (100.7 mph) has been chosen,

which is close to the flutter speed of Bridge 2 but far away from the flutter speed of Bridge 1. The uncontrolled standard deviation of the displacement at the center span position of Bridge 2 is $\sigma_{Z_0}(\ell/2) = 0.18$ m, that is approximately 8 times larger than that of Bridge 1, $\sigma_{Z_0}(\ell/2) = 0.0274$ m. The ratios, $\sigma_Z(\ell/2)/\sigma_{Z_0}(\ell/2)$ between the controlled standard deviation of the bridge displacement at $x=\ell/2$ and the uncontrolled one together with the corresponding average power requirements are plotted for both bridges in figures 19-26 [appendix 3] for various values of the control parameters ε and τ.

For Bridge 1 it is observed from figures 19-22 [appendix 3] that the standard deviation of the bridge response can be reduced as much as 50% to 40% ($\varepsilon > 0.1$ in figures 19 and 21 [appendix 3], and $\varepsilon > 0.75$ in figures 20 and 22 [appendix 3]) with an average power requirement less than 10 HP. For Bridge 2, the standard deviation of the bridge response can be reduced as much as 82% to 84% ($\varepsilon < 0.25$ in figures 23 and 25 [appendix 3], and $\varepsilon > 0.4$ in figures 24 and 26 [appendix 3]) with an average power requirement less than 20 HP. Indeed, the power requirement for the active control of the cable-stayed bridges discussed herein is very small for both the conservatively and nonconservatively designed bridges.

It should be emphasized that a 50% reduction in the standard deviation of the bridge response for Bridge 1 is probably not necessary, since it has been designed conservatively where the uncontrolled response is safe enough, i.e., $\sigma_Z(\ell/2) = 0.0274$ m. For Bridge 2, however, the 80% reduction in bridge response is necessary, since the bridge is less stiff and less conservative so that the uncontrolled response, $\sigma_Z(\ell/2) = 0.18$ m, may not be safe. Although the uncontrolled flutter speed $\bar{u}_f = 46.02$ m/sec (102.9 mph) for Bridge 2 is low, an implementation of the active control devices with 20 HP not only reduces 80% of the structural response but also raises the flutter speed up to infinity (i.e., no flutter problem). As a result, the biggest payoff of the active control devices is for application to the less stiff, more flexible and less conservatively designed cable-stayed bridges.

VIII. CONCLUSION

The dynamic analysis of typical two cable-stayed bridges implemented by active feedback control systems has been formulated. The hydraulic servomechanisms are connected to the existing four suspension cables so that under severe wind storm these cables serve also as active tendons. The control forces from each tendon (cable) acting on the bridge are regulated by the movement of the hydraulic ram which in turn is actuated by the feedback measurements of the bridge motion from the sensor.

The bridge is subjected to both buffeting and self-excited loads as well as the control forces from the tendons (cables). Both the stability condition and the statistics of bridge responses under severe storm gusts have been examined. Because of the ability of each suspension cable (tendon) to release or increase the forces acting on the bridge as regulated by the active control devices, both the torsional vibration and the flexural vibration of the bridge can be suppressed effectively and the flutter wind speed can be raised easily with a small amount of power consumption by the control devices.

The formulation has been applied to the Sitka Harbor Bridge in Alaska, as well as a hypothetical bridge

with a much smaller stiffness. Numerical results indicate that the flutter speed of both bridges can be raised up to any desirable level or infinity with a small power requirement for the control devices. Furthermore, the root mean square response of the bridge displacement can be reduced substantially (up to 80% of the uncontrolled one) with a small power requirement by the control devices. As a result, the active feedback control is feasible for practical applications to cable-stayed bridges.

Comparison of numerical results further indicates that the active feedback control is more efficient and requires smaller servomechanism capability for less stiff (more flexible) and less conservatively designed cable-stayed bridges. This is consistent with the conclusion obtained in Ref. 2 where the active tendon control is more effective for more slender and flexible structures.

The conclusions derived from this study are very encouraging. By the implementation of active feedback control systems, the conservativeness of the bridge design can be reduced significantly, while both a small level of bridge response under strong wind gusts and an extremely high flutter speed can be achieved with a small power requirement for the control devices. The potential payoff for such an active feedback control may be very significant.

LITERATURE CITED

1. Yang, J. N., "Application of Optimal Control Theory to Civil Engineering Structures," Journal of Engineering Mechanics Division, ASCE, Vol. 101, No. EM6, 1975, pp. 819-838.

2. Yang, J. N., and Giannopoulos, F., "Active Tendon Control of Slender Structures," Paper presented at the A.S.C.E. Engineering Mechanics Division Specialty Conference held in May 1977, at North Carolina State University; accepted to appear in the Journal of Engineering Mechanics Division, ASCE, 1978.

3. Yang, J. N., and Yao, J. T. P., "Formulation of Structural Control," Technical Report No. CE-STR-74-2, School of Civil Engineering, Purdue University, Sept. 1974.

4. Yao, J. T. P., "Concept of Structural Control," Journal of Structural Division, ASCE, Vol. 98, No. ST7, 1972, pp. 1567-1574.

5. Yao, J. T. P., and Tang, J. P., "Active Control of Civil Engineering Structures," Technical Report No. CE-STR-73-1, School of Civil Engineering, Purdue University, July 1973.

6. Zuk, W., "Kinetic Structures," Civil Engineering, ASCE, Vol. 38, No. 12, 1968, pp. 62-64.

7. Zuk, W., and Clark, R. H., Kinetic Architecture, Van Nostrand Reinhold Company, 1970.

8. Sae-Ung, S., and Yao, J. T. P., "Active Control of Building Structures," Technical Report No. CE-STR-76-1, School of Civil Engineering, Purdue University, 1976.

9. Sabzevari, A., and Scanlan, R. H., "Aerodynamic Instability of Suspension Bridges," Journal of the Engineering Mechanics Division, ASCE, Vol. 94, No. EM2, Proc. Paper 5889, April 1968, pp. 489-519.

10. Béliveau, J. G., Vaicaitis, R., Shinozuka, M., "Motion of Suspension Bridge Subject to Wind Loads," Journal of the Structural Division, ASCE, Vol. 103, No. ST6, Proc. Paper 12982, June 1977, pp. 1189-1205.

11. Davenport, A. G., "Buffeting of a Suspension Bridge by Storm Winds," Journal of the Structural Division, ASCE, Vol. 88, No. ST3, Proc. Paper 3181, June 1962, pp. 233-268.

12. Davenport, A. G., "The Application of Statistical Concepts to the Wind Loading of Structures," Proceedings, Institution of Civil Engineers, London, England, Vol. 19, 1961, pp. 449-472.

13. Davenport, A. G., "The Response of Slender Line-Like Structures to a Gusty Wind," Proceedings, Institution of Civil Engineers, London, England, Vol. 23, 1962, pp. 389-408.

14. Davenport, A. G., "Spectrum of Horizontal Gustiness Near the Ground in Strong Winds," Quarterly Journal, Royal Meteorological Soc., Vol. 87, April 1961, pp. 194-211.

15. Hino, M., "Spectrum of Gusty Wind," Paper I-7-2, Proceedings, Third International Conference on Wind Effects on Buildings and Structures, Tokyo, Japan, Oct., 1971.

16. Liepmann, H. W., "On the Application of Statistical Concepts to the Buffeting Problem," Journal of the Aerospace Sciences, Vol. 19, No. 12, 1952, p. 793.

17. Reinhold, T. A., Tieleman, H. W., and Maher, F. J., "Effects of Turbulence on Bridge Model Torsional Stability," Journal of the Structural Division, ASCE, Vol. 102, No. ST5, Proc. Paper 12118, May 1976, pp. 1003-1013.

18. Reinhold, T. A., Tieleman, H. W., and Maher, F. J., "Wake Study of Stiffening Truss and Box Girder," Journal of the Structural Division, ASCE, Vol. 102, No. ST9, Proc. Paper 12372, Sept. 1976, pp. 1643-1657.

19. Bleich, F., et al., The Mathematical Theory of Vibrations in Suspension Bridges, United States Government Printing Office, Washington, D.C., 1950.

20. Frazer, R. A., "Aerodynamic Oscillations of Suspension Bridges," Engineering, London, Vol. 171, No. 4440, March 1951, p. 270.

21. Sabzevari, A., and Scanlan, R. H., "Aerodynamic Investigations of Box Girder Bridges," Journal of the Structural Division, Proceedings of the American Society of Civil Engineers, ST7, July 1969, pp. 1517-1529.

22. Sabzevari, A., and Scanlan, R. H., "Some Basic Studies on the Aeroelastic Instability of Suspension Bridges," Research Report, Department of Civil and Geological Engineering, Princeton University, Princeton, N.J., May 1967.

23. Scanlan, R. H., Béliveau, J. G., and Budlong, K. S., "Indicial Aerodynamic Functions for Bridge Decks," Journal of the Engineering Mechanics Division, ASCE, Vol. 100, No. EM4, Proc. Paper 10709, Aug. 1974, pp. 657-672.

24. Scanlan, R. H., and Sabzevari, A., "Suspension Bridge Flutter Revisited," presented at the May 8-12, 1967, ASCE National Meeting on Structural Engineering, held at Seattle, Washington.

25. Scanlan, R. H., "Theory of the Wind Analysis of Long-Span Bridges Based on Data Obtainable from Section Model Tests," Proceedings, Fourth International Conference on Wind Effects, London, England, Sept. 1975.

26. Scanlan, R. H., and Tomko, J. J., "Airfoil and Bridge Flutter Derivatives," Journal of the Engineering Mechanics Division, ASCE, December 1971, pp. 1717-1737.

27. Steinman, D. B., "Design of Bridges Against Wind," Part I, Civil Engineering, ASCE, Vol. 15, 1945, pp. 469-472.

28. Steinman, D. B., "Design of Bridges Against Wind," Part II, Civil Engineering, ASCE, Vol. 15, 1945, pp. 501-504.

29. Steinman, D. B., "Design of Bridges Against Wind," Part III, Civil Engineering, ASCE, Vol. 15, 1945, pp. 558-560.

30. Steinman, D. B., "Design of Bridges Against Wind," Part IV, <u>Civil Engineering</u>, ASCE, Vol. 16, 1946, pp. 20-22.

31. Steinman, D. B., "Design of Bridges Against Wind," Part V, <u>Civil Engineering</u>, ASCE, Vol. 16, 1946, pp. 66-68.

32. Maher, F. J., Frederick, D., Estes, E. R., and Steinman, D. B., "Wind Tunnel Tests of Suspension Bridge Section Models," Virginia Polytechnic Institute, Engineering Experiment Station, Bulletin No. 69, Sept. 1948.

33. Maher, F. J., "Tests Confirm Steinman Theory of Bridge Oscillations," <u>Civil Engineering</u>, ASCE, Vol. 23, 1953, pp. 554-555.

34. Maher, F. J., Becker, L. A., and Steinman, D. B., "Dynamic Tests of Suspension Bridge Section Models," Virginia Polytechnic Institute, Engineering Experiment Station, Bulletin No. 98, April 1955.

35. Gade, R. H., and Scanlan, R. H., "Experimental Measurement and Interpretation of Aerodynamic Stability Coefficients for the Decks of Two Cable-Stayed Bridges," Report, Fairbank Highway Research Station, Department of Transportation, McLean, Virginia, 1976.

36. Sabzevari, A., and Scanlan, R. H., "Aerodynamic Instability of H-Sections," Research Report, Department of Civil and Geological Engineering, Princeton University, Princeton, N.J., April 1968.

37. Blackburn, T. R., and Vaughan, D. R., "Application of Linear Optimal Control and Filtering Theory to the Saturn V Launch Vehicle," Institute of Electrical and Electronics Engineers, Transactions on Automatic Control, Dec. 1971, pp. 799-806.

38. <u>Control of Distributed Parameter Systems</u>, American Society of Mechanical Engineers, 1969.

39. Karnopp, D. C., "Active and Passive Isolation of Random Vibration," <u>Isolation of Mechanical Vibration Impact and Noise</u>, Edited by Snowdon and Ungar, AMD, Vol. 1, ASME, 1973, pp. 64-86.

40. Love, G. G., and Lavi, A., "Evaluation of Feedback Structures," Proceedings, Joint Automatic Control Conference, 1968, University of Michigan.

41. Martin, C. R., and Soong, T. T., "Modal Control of Multistory Structures," Journal of Engineering Mechanics Division, ASCE, Vol. 102, No. EM4, 1976, pp. 613-623.

42. Murata, M., and Ito, M., "Suppression of Wind-Induced Vibration of a Suspension Bridge by Means of a Gyroscope," Proceedings, 3rd International Conference on Wind Effects on Buildings and Structures, Tokyo, Japan, 1971, pp. 1057-1066.

43. Nordell, W. J., "Active Systems for Blastic-Resistant Structures," Technical Report R-611, Naval Civil Engineering Laboratory, Port Hueneme, Calif., Feb. 1969.

44. Roorda, J., "Active Damping in Structures," Granfield Report Aero., No. 8, Granfield Institute of Technology, Granfield, U.K., 1971.

45. Roorda, J., "Tendon Control in Tall Structures," Journal of the Structural Division, ASCE, Vol. 101, No. ST3, 1975, pp. 505-521.

46. Zuk, W., Private Communication, 1977.

47. Béliveau, J. G., "Self-Excited Aeroelastic Instability of a Bridge Deck," American Society of Mechanical Engineers, presented at the American Society of Mechanical Engineers Conference, New York, Dec. 5, 1976, paper No. 76-WA/FE-25.

48. Scanlan, R. H., and Rosenbaum, R., Aircraft Vibration and Flutter, Dover Publications, Inc., New York, 1968.

49. Rocard, Y., Dynamic Instability, Frederick Ungar Publishing Co., New York, N.Y., 1957.

50. Sabzevari, A., and Scanlan, R. H., "On Dynamic Response of Bridges to Moving Vehicles," Research Report No. 67-7, Department of Civil and Geological Engineering, Princeton University, Princeton, N.J., Dec. 1967.

51. Bisplinghoff, R. L., and Ashley, H., Principles of Aeroelasticity, John Wiley and Sons, New York, 1962.

52. Fung, Y. C., _An Introduction to the Theory of Aero-elasticity_, Dover Publications, Inc., New York, 1969.

53. Béliveau, J. G., "Suspension Bridge Aeroelasticity--Nonlinear Least Squares Techniques for System Identification," Ph.D. thesis, Dept. of Civil and Geological Engineering, Princeton University, Princeton, N.J., 1973.

54. Lumley, J. L., and Panofsky, H. A., _The Structure of Atmospheric Turbulence_, John Wiley and Sons, Inc., New York, N.Y. 1964.

55. Harrison, H. L., and Bollinger, J. G., _Introduction to Automatic Controls_, International Textbook Co., Scranton, Pa., 1963.

56. Morse, A. C., _Electrohydraulic Servomechanisms_, McGraw-Hill Book Company, Inc., New York, 1963.

57. Steinman, D. B., "Modes and Natural Frequencies of Suspension Bridge Oscillations," _Annals_, New York Academy of Sciences, Vol. 79, A 74, 1959, pp. 111-142.

58. Murphy, G. J., _Control Engineering_, Boston Technical Publishers, Inc., Box 111, Cambridge 39, Mass., 1965.

59. Frazer, R. A., and Duncan, W. J., "On the Criteria for Stability of Small Motions," _Proceedings of the Royal Society_, London, Series A, Vol. 124, 1929.

60. Pipes, L. A., _Applied Mathematics for Engineers and Physicists_, McGraw-Hill Book Company, 1958.

61. Lin, Y. K., _Probabilistic Theory of Structure Dynamics_, Robert E. Krieger Publishing Company, Huntington, New York, 1976.

62. Crandall, S. H., and Mark, W. D., _Random Vibration in Mechanical Systems_, Academic Press, New York, 1963.

63. Bendat, J. S., and Piersol, A. G., _Random Data Analysis and Measurement Procedures_, John Wiley & Sons, Inc., 1971.

64. Papoulis, A., _Random Variables and Stochastic Processes_, McGraw-Hill Book Company, 1965.

APPENDIX 1

DERIVATION OF RESTORING FORCES AND MOMENTS
FROM SUSPENSION CABLES WITH ACTIVE CONTROL

Without external disturbances, such as wind gusts, each suspension cable is designed to carry the dead weight of the bridge deck, including the weight of the vehicles, denoted by T_0. Let Z_0 be the elongation of the suspension cable due to T_0. Then [see coordinate system in figure 2a]

$$T_0 = \frac{E_0 A_0}{\ell_0} Z_0 \tag{1-1}$$

Under the excitations of gust loads, the vibration of the bridge deck results in the fluctuation of tension in the suspension cable, i.e.,

$$T(t) = T_0 + \Delta T(t) \tag{1-2}$$

in which

$$\Delta T(t) = \frac{E_0 A_0}{\ell_0} \Delta Z(t) \tag{1-3}$$

where $\Delta Z(t)$ is the fluctuation of the elongation of the suspension cable from its static equilibrium value Z_0.

The fluctuation $\Delta Z(t)$ is contributed by (i) the motion of the bridge at the anchorage of the cable, and (ii) the active control devices [see figure 3]

$$\Delta Z(t) = v(t)\sin\phi + S(t) \tag{1-4}$$

in which $v(t)$ is the vertical displacement of the anchorage, ϕ is the angle between the suspension cable and the bridge deck, and $S(t)$ is the displacement of the hydraulic ram (actuator of the servomechanism).

The motion of the hydraulic ram, $S(t)$, is regulated by the feedback signal from the sensor installed at the anchorage in such a way that the vibration of the bridge can be effectively suppressed [see figure 4].[1] Since the feedback signal is proportional to the motion of the anchorage $v(t)$, $S(t)$ is related to $v(t)$ through the following equation [see equations 10, 12, and 15]

$$\dot{S}(t)+R_1 S(t) = R_1 R_{0i} L_i [v(t)] \qquad (1-5)$$

where R_1, R_{0i} and $L_i[\cdot]$ have been defined in equations 11, 12, and 15.

Therefore, the vertical restoring force $P(t)$ applied to the anchorage by the suspension cable, resulting from the bridge vibration and the control devices is [see figure 3]

$$\underset{\sim}{P}(t) = -\Delta T(t)\sin\phi = - \frac{E_0 A_0}{\ell_0}[v(t)\sin\phi+S(t)]\sin\phi \qquad (1-6)$$

It follows from equations 1-3 and 1-6 that the restoring force, $\underset{\sim}{P}(t)$, and the fluctuation of tension in the cable $\Delta T(t)$, is a linear function of the fluctuation,

---

[1]Here, in order to demonstrate the idea of active control, the control servomechanisms are assumed to be connected to the suspension cables. This may not be the case in an actual design but the principle will remain the same.

$\Delta Z(t)$, of the cable length [elongation or contraction]. Since the suspension cable cannot take compression, a necessary condition for the present analysis to be valid is that

$$Z_0 \geq |\Delta Z(t)| \qquad (1-7)$$

implying that $T_0 \geq |\Delta T(t)|$. Equation 1-7 ensures that the force in the cable is always tension [see equations 1-1 to 1-3]. In other words, the force in the suspension cable $T_0 - \Delta T(t)$ during the upward motion of the anchorage should always be positive, otherwise the problem becomes nonlinear.

Now the restoring forces from the four suspension cables at the locations $x=a$ and $x=\ell-a$ can be combined to yield the resulting restoring force and moment with respect to the cross-section of the bridge deck. The total restoring force $U(a,t)$ and Moment $Q(a,t)$ at $x=a$ are given by:

$$U(a,t) = P_\ell(a,t) + P_r(a,t) \qquad (1-8)$$

$$Q(a,t) = \frac{B}{2}[P_\ell(a,t) - P_r(a,t)] \qquad (1-9)$$

in which $P_\ell(a,t)$ and $P_r(a,t)$ are the restoring forces, respectively, from both the left and the right suspension cables at $x=a$. It follows from equation 1-6 that

$$P_\ell(a,t) = -\frac{E_0 A_0}{\ell_0}[v_\ell(a,t)\sin\phi + S_\ell(a,t)]\sin\phi$$

$$(1-10)$$

$$P_r(a,t) = -\frac{E_0 A_0}{\ell_0}[v_r(a,t)\sin\phi + S_r(a,t)]\sin\phi$$

in which $S_\ell(a,t)$ and $S_r(a,t)$ satisfy equation 1-5, i.e.

$$\dot{S}_\ell(a,t)+R_1 S_\ell(a,t) = R_1 R_{0i} L_i[v_\ell(a,t)]$$
$$\dot{S}_r(a,t)+R_1 S_r(a,t) = R_1 R_{0i} L_i[v_r(a,t)]$$
(1-11)

It is obvious from figure 2b that

$$v_\ell(a,t) = W(a,t)+\frac{B}{2}\theta(a,t)$$
$$v_r(a,t) = W(\alpha,t)-\frac{B}{2}\theta(a,t)$$
(1-12)

The displacement, $u(a,t)$, and the rotation, $v(a,t)$, of the bridge deck at $x=a$ are related to the displacements $S_\ell(a,t)$ and $S_r(a,t)$ of both hydraulic rams associated with two suspension cables as follows:

$$u(a,t) = [S_\ell(a,t)+S_r(a,t)]/2$$
(1-13)
$$v(a,t) = [S_\ell(a,t)-S_r(a,t)]/B$$

where $u(a,t)$ and $v(a,t)$ are referred to as the control displacement and rotation, respectively.

Summing and subtracting equations 1-11, one obtains

$$\dot{u}(a,t)+R_1 u(a,t) = R_1 R_{0i}[W(a,t)]$$
(1-14)
$$\dot{v}(a,t)+R_1 v(a,t) = R_1 R_{0i}[\theta(a,t)]$$

where equations 1-12 and 1-13 have been used.

Finally, by substitution of equations 1-10, 1-12, and 1-13, into equations 1-8 and 1-9 the restoring force $U(a,t)$ and moment $Q(a,t)$ at $x=a$ can be expressed as

$$U(a,t) = -\frac{2E_0 A_0}{\ell_0}[W(a,t)\sin\phi+u(a,t)]\sin\phi$$
(1-15)

$$Q(a,t) = -\frac{B^2}{2}\frac{E_0 A_0}{\ell_0}[\theta(a,t)\sin\phi+v(a,t)]\sin\phi$$
(1-16)

It is obvious from equations 1-14 to 1-16 that the restoring force U(a,t) depends on the flexural displacement W(a,t) alone, whereas the restoring moment Q(a,t) depends on the cross-sectional rotation θ(a,t).

Due to the symmetry of the two cable-stayed bridge with respect to the mid-span, the expressions for U(ℓ-a,t) and Q(ℓ-a,t) are identical to equations 1-15 and 1-16, respectively, in which the argument "a" is replaced by "ℓ-a".

APPENDIX 2

MODAL ANALYSIS

By use of the classical modal approach, the flexural displacement $W(x,t)$ and rotation $\theta(x,t)$ are expressed in terms of the normal modes as:

$$W(x,t) = \sum_k g_k(t)X_k(x)$$

$$\theta(x,t) = \sum_k f_k(t)Y_k(x) \tag{2-1}$$

where $g_k(t)$ and $f_k(t)$ are the normal coordinates in bending and torsion, and $X_k(x)$ and $Y_k(x)$ are the associated normal modes. The normal modes, $X_k(x)$ and $Y_k(x)$, should satisfy appropriate boundary conditions and the following equations:

$$EI \frac{\partial^4}{\partial x^4} X_k(x) = m \, \bar{\omega}_{g_k}^2 X_k(x)$$

$$GJ \frac{\partial^2}{\partial x^2} Y_k(x) = I_s \, \bar{\omega}_{f_k}^2 Y_k(x) \tag{2-2}$$

in which $\bar{\omega}_{g_k}$ and $\bar{\omega}_{f_k}$ are the natural frequencies of the bridge deck without the effect of the suspension cables. Substitution of equation 2-1 into equations 13 and 14 yields

$$\dot{u}(a,t)+R_1 u(a,t) = R_1 R_{0i} \sum_k L_i [g_k(t)]X_k(a)$$

$$\dot{v}(a,t)+R_1 v(a,t) = R_1 R_{0i} \sum_k L_i [f_k(t)]Y_k(a) \tag{2-3}$$

78

The functional form on the right hand side of equation 2-3 indicates that the control displacement $u(a,t)$ and rotation $v(a,t)$ can be expressed in terms of the normal modes.

$$u(a,t) = \sum_k h_k(t)X_k(a)$$

$$v(a,t) = \sum_k q_k(t)Y_k(a)$$

(2-4)

Substituting equation 2-4 into equation 2-3 and using the property of linear independence of $X_k(x)$ and $Y_k(x)$, one obtains

$$\dot{h}_k(t)+R_1 h_k(t) = R_1 R_{0i} L_i[g_k(t)]$$

$$\dot{q}_k(t)+R_1 q_k(t) = R_1 R_{0i} L_i[f_k(t)]$$

(2-5)

It can easily be shown that equations 2-3 to 2-5 hold when the position x=a is replaced by the position x=ℓ-a.

By substitution of equations 2-1 and 2-4 into equations 8 and 9, and then into equations 6 and 7, the restoring forces and moments can be expressed in terms of the normal modes and normal coordinates as follows:

$$U(x,t) = -\frac{2E_0 A_0}{\ell_0} \sin\phi \sum_k \Big\{[g_k(t)\sin\phi+h_k(t)\cdot[X_k(a)\delta(x-a)$$

$$+ X_k(\ell-a)\delta(x-\ell+a)]\Big\}$$

(2-6)

$$Q(x,t) = -\frac{B^2 E_0 A_0}{2\ell_0} \sin\phi \sum_k \left\{ [f_k(t)\sin\phi + q_k(t)] \cdot [Y_k(a)\delta(x-a) \right.$$

$$\left. + Y_k(\ell-a)\delta(x-\ell+a)] \right\} \tag{2-7}$$

By virtue of equations 5 and 2-1, the self-excited force and moment given in equations 3 and 4 can also be expressed in terms of the normal modes and normal coordinates as follows:

$$F_{s-e}(x,t) = \rho B^2 \sum_k \left\{ \omega_f^* H_1^* \dot{g}_k(t) X_k(x) + B\omega_f^*[H_2^* \dot{f}_k(t) \right.$$

$$\left. + \omega_f^* H_3^* f_k(t)]Y_k(x) \right\} \tag{2-8}$$

$$M_{s-e}(x,t) = \rho B^3 \sum_k \left\{ \omega_f^* A_1^* \dot{g}_k(t) X_k(x) + B\omega_f^*[A_2^* \dot{f}_k(t) \right.$$

$$\left. + \omega_f^* A_3^* f_k(t)]Y_k(x) \right\} \tag{2-9}$$

Finally, by use of equations 2-1, 2-2, and 2-6 through 2-9, the equations of motion, equations 1 and 2, become

$$\sum_k \left\{ [m\ddot{g}_k(t) + C_b \dot{g}_k(t) + m\bar{\omega}_{g_k}^2 g_k(t)]X_k(x) + \frac{2E_0 A_0}{\ell_0} \sin\phi \, [g_k(t)\sin\phi \right.$$

$$+ h_k(t)][X_k(a)\delta(x-a) + X_k(\ell-a)\delta(x-\ell+a)] - \rho B^2[\omega_f^* H_1^* \dot{g}_k(t)X_k(x)$$

$$\left. + B\omega_f^*(H_2^* \dot{f}_k(t) + \omega_f^* H_3^* f_k(t))Y_k(x)] \right\} = F_b(x,t) \tag{2-10}$$

$$\sum_k \left\{ [I_s \ddot{f}_k(t) + C_t \dot{f}_k(t) + I_s \bar{\omega}^2_{f_k} f_k(t)] Y_k(x) + \frac{B^2 E_0 A_0}{2\ell_0} \sin\phi \, [f_k(t)\sin\phi \right.$$

$$+ q_k(t)] \cdot [Y_k(a)\delta(x-a) + Y_k(\ell-a)\delta(x-\ell+a)] - \rho B^3 [\omega^*_f A^*_1 \dot{g}_k(t) X_k(x)$$

$$\left. + B\omega^*_f (A^*_2 \dot{f}_k(t) + \omega^*_f A^*_3 f_k(t)) Y_k(x)] \right\} = M_b(x,t) \qquad (2\text{-}11)$$

Multiplying equations 2-10 and 2-11 by $X_n(x)$ and $Y_n(x)$, respectively, and integrating over the range of x, one obtains

$$M_n \ddot{g}_n(t) + C_{bn} \dot{g}_n(t) + M_n \bar{\omega}^2_{g_n} g_n(t) - \rho B^2 \omega^*_f H^*_1 V_{g_n} \dot{g}_n(t)$$

$$+ \frac{2E_0 A_0}{\ell_0} \sin\phi \sum_k \left\{ [g_k(t)\sin\phi + h_k(t)][X_k(a)X_n(a) \right.$$

$$\left. + X_k(\ell-a)X_n(\ell-a)] \right\} - \rho B^3 \omega^*_f \sum_k \left\{ [H^*_2 \dot{f}_k(t) + \omega^*_f H^*_3 f_k(t)] G_{kn} \right\}$$

$$= \underset{\sim}{F}_n(t) \qquad (2\text{-}12)$$

$$I_n \ddot{f}_n(t) + C_{tn} \dot{f}_n(t) + I_n \bar{\omega}^2_{f_n} f_n(t) - \rho B^4 \omega^*_f [A^*_2 \dot{f}_n(t) + \omega^*_f A^*_3 f_n(t)] V_{f_n}$$

$$+ \frac{B^2 E_0 A_0}{2\ell_0} \sin\phi \sum_k \left\{ [f_k(t)\sin\phi + q_k(t)][Y_k(a)Y_n(a) \right.$$

$$\left. + Y_k(\ell-a)Y_n(\ell-a)] \right\} - \rho B^3 \omega^*_f A^*_1 \sum_k \dot{g}_k(t) G_{nk} = \underset{\sim}{M}_n(t) \qquad (2\text{-}13)$$

In which the following orthogonality conditions of the normal modes have been used,

$$\int_0^\ell X_k(x)X_n(x) = V_{g_n} \delta_{kn}$$

$$\qquad (2\text{-}14)$$

$$\int_0^\ell Y_k(x)Y_n(x) = V_{f_n} \delta_{kn}$$

where δ_{kn} is the Kronecker delta, and

$$\int_0^\ell X_k(x)Y_n(x)dx = G_{nk}$$

(2-15)

$$\int_0^\ell Y_k(x)X_n(x)dx = G_{kn}$$

$$M_n = m \, V_{g_n}$$

(2-16)

$$I_n = I_s V_{f_n}$$

$$C_{bn} = C_b V_{g_n}$$

(2-17)

$$C_{tn} = C_t V_{f_n}$$

$$\underset{\sim}{F}_n(t) = \int_0^\ell F_b(x,t)X_n(x)dx$$

(2-18)

$$\underset{\sim}{M}_n(t) = \int_0^\ell M_b(x,t)Y_n(x)dx$$

Equations 2-12 and 2-13 can be written conveniently as follows:

$$M_n \left\{ \ddot{g}_n(t)+2Jg_n\omega_{g_n}\dot{g}_n(t)+\omega_{g_n}^2 g_n(t) \right\} -\rho B^2\omega_f^* H_1^* V_{g_n}\dot{g}_n(t)$$

$$+ \frac{2E_0A_0}{\ell_0} \sin^2\phi \sum_{k\neq n} g_k(t)[X_k(a)X_n(a)+X_k(\ell-a)+X_n(\ell-a)]$$

$$+ \frac{2E_0A_0}{\ell_0} \sin\phi \sum_{k} h_k(t)[X_k(a)X_n(a)+X_k(\ell-a)X_n(\ell-a)]$$

$$- \rho B^3\omega_f^* \sum_{k} \left\{ [H_2^* \dot{f}_k(t)+\omega_f^* H_3^* f_k(t)]G_{Kn} \right\}= \underset{\sim}{F}_n(t)$$

(2-19)

$$I_n \left\{ \ddot{f}_n(t) + 2J_{f_n} \omega_{f_n} \dot{f}_n(t) + \omega_{f_n}^2 f_n(t) \right\} - \rho B^4 \omega_f^* [A_2^* \dot{f}_n(t)$$

$$+ \omega_f^* A_3^* f_n(t)] V_{f_n}$$

$$+ \frac{B^2 E_0 A_0}{2\ell_0} \sin^2\phi \sum_{k \neq n} f_k(t) [Y_k(a)Y_n(a) + Y_k(\ell-a)Y_n(\ell-a)]$$

$$+ \frac{B^2 E_0 A_0}{2\ell_0} \sin\phi \sum_k q_k(t) [Y_k(a)Y_n(a) + Y_k(\ell-a)Y_n(\ell-a)]$$

$$- \rho B^3 \omega_f^* A_1^* \sum_k \dot{g}_k(t) G_{nK} = \underset{\sim}{M}_n(t) \qquad (2-20)$$

In which it is obvious that

$$\omega_{g_n}^2 = \bar{\omega}_{g_n}^2 + \frac{2E_0 A_0}{M_n \ell_0} \sin^2\phi [X_n^2(a) + X_n^2(\ell-a)] \qquad (2-21)$$

$$\omega_{f_n}^2 = \bar{\omega}_{f_n}^2 + \frac{B^2 E_0 A_0}{2I_n \ell_0} \sin^2\phi [Y_n^2(a) + Y_n^2(\ell-a)] \qquad (2-22)$$

$$J_{g_n} = \frac{C_{bn}}{2M_n \omega_{g_n}} ; \quad J_{f_n} = \frac{C_{tn}}{2I_n \omega_{f_n}} \qquad (2-23)$$

The quantities ω_{g_n} and ω_{f_n} given in equations 2-21 and 2-22 are the natural frequencies in bending and torsion of the two cable-stayed bridge, including the effects of the suspension cables.

To further simplify the equations of motion, the normal modes $X_k(x)$ and $Y_k(x)$ for the two cable-stayed bridge are assumed to be identical with the following form [e.g., Refs. 10,57]:

$$X_k(x) = Y_k(x) = \sin \frac{k\pi x}{\ell} \qquad (2-24)$$

By use of equation 2-24, the quantities V_{g_n}, V_{f_n}, G_{nk}, and G_{kn} given in equations 2-14 and 2-15 reduce to

$$V_{g_n} = V_{f_n} = \frac{\ell}{2} \tag{2-25}$$

$$G_{kn} = G_{nk} = \frac{\ell}{2} \delta_{kn} \tag{2-26}$$

and equations 2-16 through 2-18 become

$$M = M_n = m \frac{\ell}{2} \, , \quad I = I_n = I_s \frac{\ell}{2} \tag{2-27}$$

$$C_{bn} = C_b \frac{\ell}{2} \, , \quad C_{tn} = C_t \frac{\ell}{2} \tag{2-28}$$

$$F_n(t) = \int_0^\ell F_b(x,t) \sin \frac{n\pi x}{\ell} \, dx$$

$$M_n(t) = \int_0^\ell M_b(x,t) \sin \frac{n\pi x}{\ell} \, dx \tag{2-29}$$

Furthermore, the coupling terms resulting from active control appearing in equations 2-19 and 2-20 can be written as

$$X_k(a)X_n(a) + X_k(\ell-a)X_n(\ell-a) = Y_k(a)Y_n(a) + Y_k(\ell-a)Y_n(\ell-a)$$

$$= \sin \frac{k\pi a}{\ell} \sin \frac{n\pi a}{\ell} + \sin \frac{K\pi(\ell-a)}{\ell} \sin \frac{n\pi(\ell-a)}{\ell}$$

$$= \sin \frac{k\pi a}{\ell} \sin \frac{n\pi a}{\ell} [1 + (-1)^{k+1}(-1)^{n+1}] \tag{2-30}$$

In which the identity

$$\sin k\pi(\ell-a) = (-1)^{k+1} \sin \frac{k\pi a}{\ell}$$

has been used.

Consequently, with the aid of equations 2-24 to 2-30, equations 2-19 and 2-20 can be simplified as follows:

$$\ddot{g}_n(t) + [2J_{g_n}\omega_{g_n} - H_1]\dot{g}_n + \omega_{g_n}^2 g_n(t)$$

$$+ \frac{2E_0 A_0}{M_n \ell_0} \sin^2\phi \sum_k g_k(t)\sin\frac{k\pi a}{\ell}\sin\frac{n\pi a}{\ell}\delta(k,n)$$

$$+ \frac{2E_0 A_0}{M_n \ell_0} \sin\phi \sum_k h_k(t)\sin\frac{k\pi a}{\ell}\sin\frac{n\pi a}{\ell}\delta(k,n)$$

$$- H_2\dot{f}_n(t) - H_3 f_n(t) = \underset{\sim}{F}_n(t)/M_n \qquad (2\text{-}31)$$

$$\ddot{f}_n(t) + [2J_{f_n}\omega_{f_n} - A_2]\dot{f}_n(t) + [\omega_{f_n}^2 - A_3]f_n(t)$$

$$+ \frac{B^2 E_0 A_0}{2I_n \ell_0} \sin^2\phi \sum_{k\neq n} f_k(t)\sin\frac{k\pi a}{\ell}\sin\frac{n\pi a}{\ell}\delta(k,n)$$

$$+ \frac{B^2 E_0 A_0}{2I_n \ell_0} \sin\phi \sum_k q_k(t)\sin\frac{k\pi a}{\ell}\sin\frac{n\pi a}{\ell}\delta(k,n) - A_1\dot{g}_n(t)$$

$$= \underset{\sim}{M}_n(t)/I_n \qquad (2\text{-}32)$$

in which the following notations for the aerodynamic
coefficients and $\delta(k,n)$ have been used:

$$H_1 = \frac{\rho B^2 \omega_f^* H_1^*}{m}, \qquad\qquad A_1 = \frac{\rho B^3 \omega_f^* A_1^*}{I_s}$$

$$H_2 = \frac{\rho B^3 \omega_f^* H_2^*}{m}, \qquad\qquad A_2 = \frac{\rho B^4 \omega_f^* A_2^*}{I_s} \qquad (2\text{-}33)$$

$$H_3 = \frac{\rho B^3 \omega_f^{*2} H_3^*}{m} \qquad\qquad A_3 = \frac{\rho B^4 \omega_f^{*2} A_3^*}{I_s}$$

$$\delta(k,n) = 1 + (-1)^{k+1}(-1)^{n+1}$$

For the Sitka Harbor Bridge where the suspension cables are attached to the bridge deck at

$$a = \ell/3 \qquad (2-34)$$

it is obvious that for the first three torsional and flexural modes,

$$\sin \frac{k\pi a}{\ell} \sin \frac{n\pi a}{\ell} \delta(k,n) = 2 \sin^2 \frac{n\pi}{3} \qquad (2-35)$$

Consequently, the equations of motion, equations 2-31 and 2-32, can be decoubled by virtue of equation 2-35 as follows:

$$\ddot{g}_n(t) + [2J_{g_n}\omega_{g_n} - H_1]\dot{g}_n + \omega_{g_n}^2 g_n(t) + \frac{4E_0 A_0}{M_n \ell_0} \sin\phi \sin^2 \frac{n\pi}{3} h_n(t)$$

$$- H_2 \dot{f}_n(t) - H_3 f_n(t) = \underset{\sim}{F}_n(t)/M_n \qquad (2-36)$$

$$\ddot{f}_n(t) + [2J_{f_n}\omega_{f_n} - A_2]\dot{f}_n(t) + [\omega_{f_n}^2 - A_3]f_n(t)$$

$$+ \frac{B^2 E_0 A_0}{I_n \ell_0} \sin\phi \sin^2 \frac{n\pi}{3} q_n(t) - A_1 \dot{g}_n(t) = \underset{\sim}{M}_n(t)/I_n \qquad (2-37)$$

Note that equations 2-36 and 2-37 hold only for the first three modes, i.e., $n \leq 3$.

APPENDIX 3

FIGURES
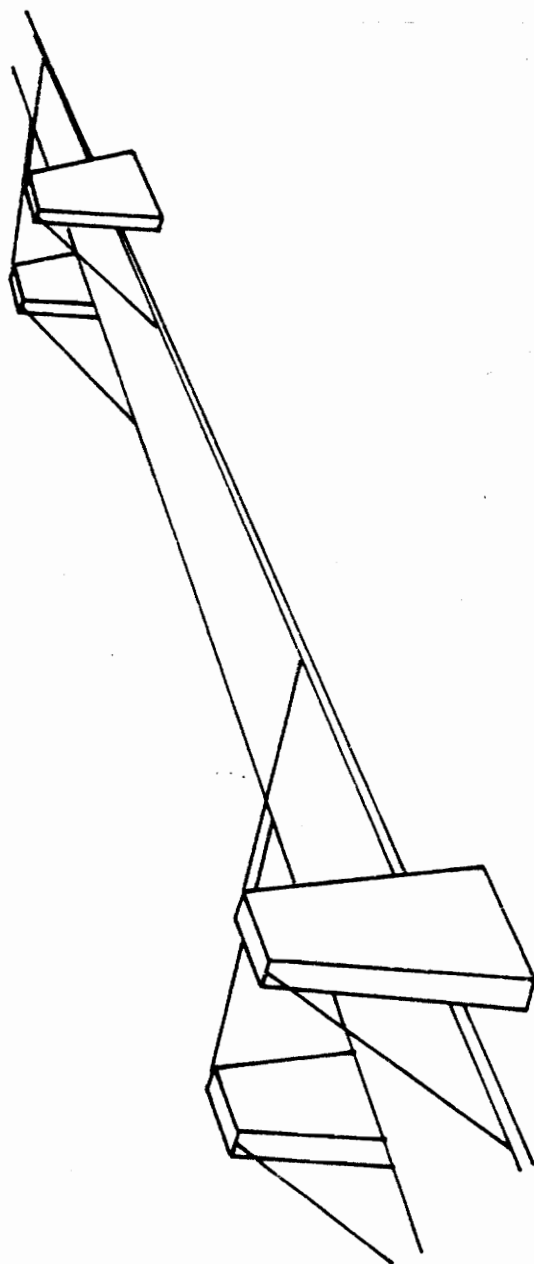
Figure 1: A Two Cable-Stayed Bridge
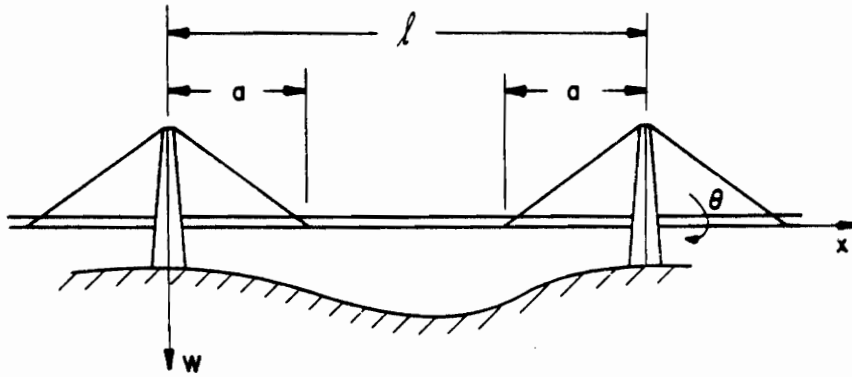
(a)
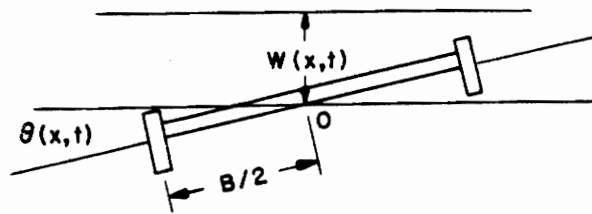
(b)

Figure 2: Structural Model: (a) Side View with Coordinate System (b) Two Degrees of Freedom Model.
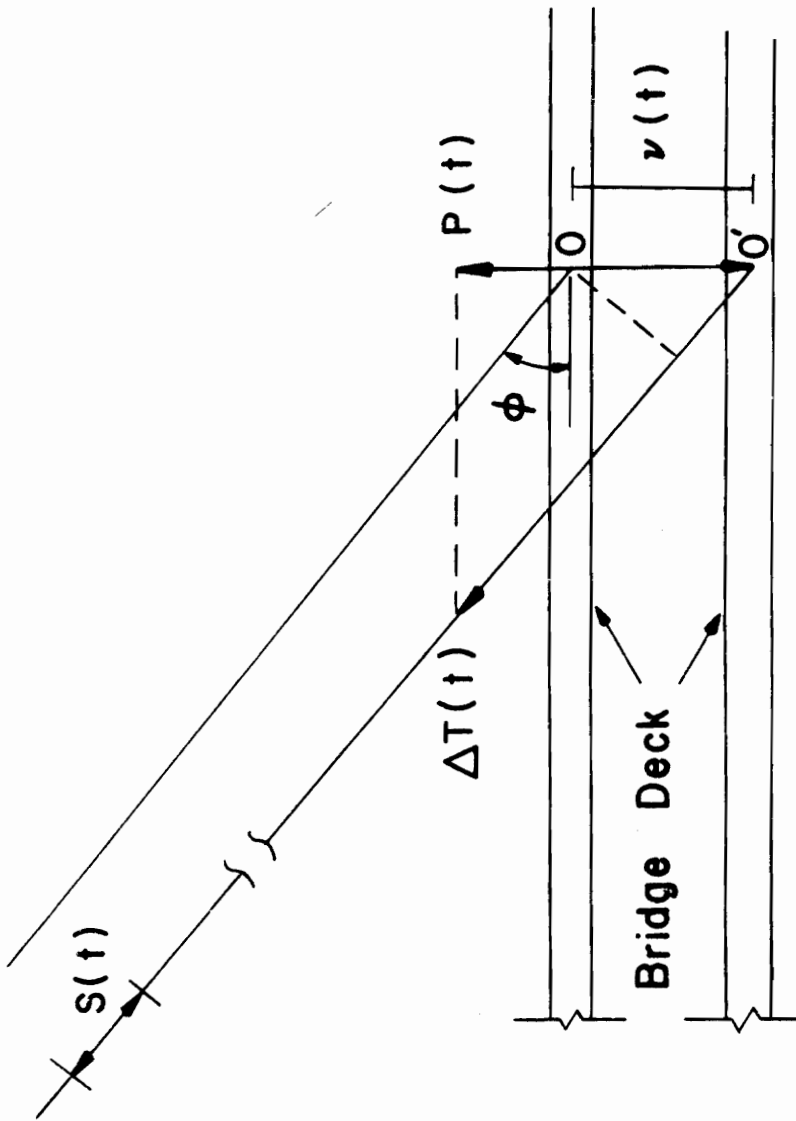
Figure 3: Restoring Forces from Suspension Cables
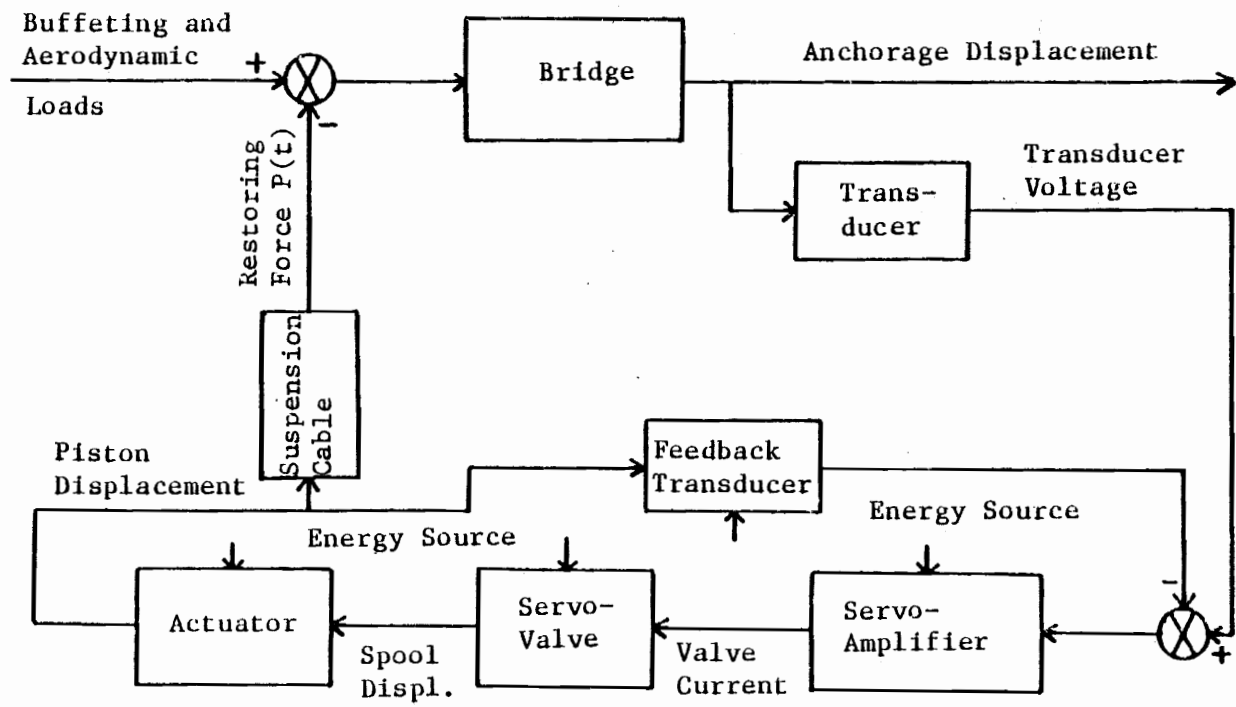
Figure 4: Block Diagram of Control Devices
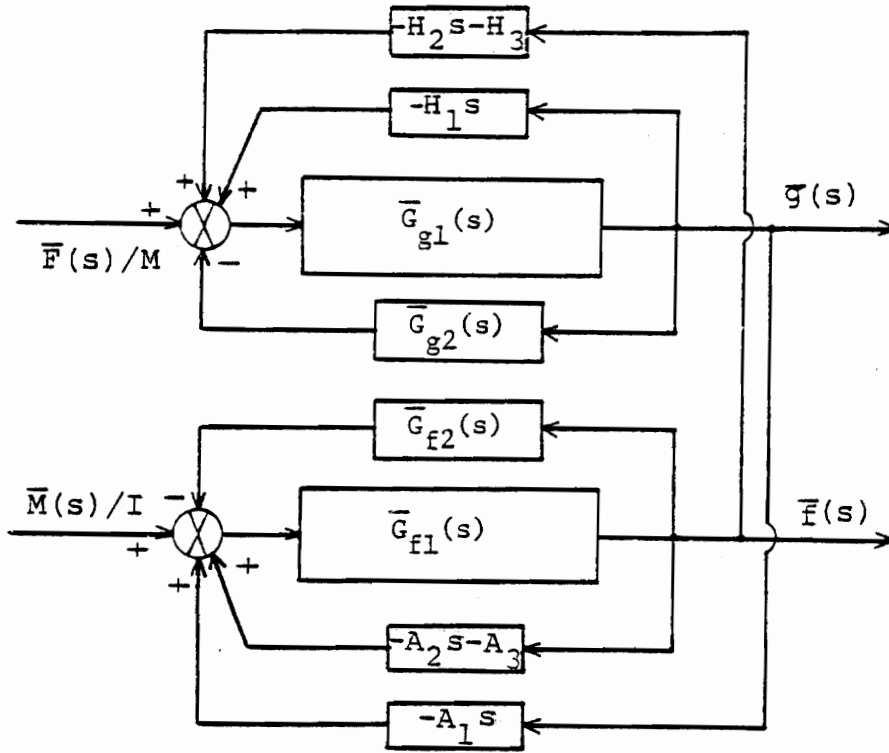
$$\overline{G}_{g1}(s) = s^2 + 2J_g\omega_g s + \omega_g^2 \qquad \overline{G}_{f1}(s) = s^2 + 2J_f\omega_f s + \omega_f^2$$

$$\overline{G}_{g2}(s) = \Gamma_g \frac{R_1 R_{0i}\overline{L}_i(s)}{R_1 + s} \qquad \overline{G}_{f2}(s) = \Gamma_f \frac{R_1 R_{0i}L_i(s)}{R_1 + s}$$

Figure 5: Block Diagram of the Coupled Dynamic System and Control Devices
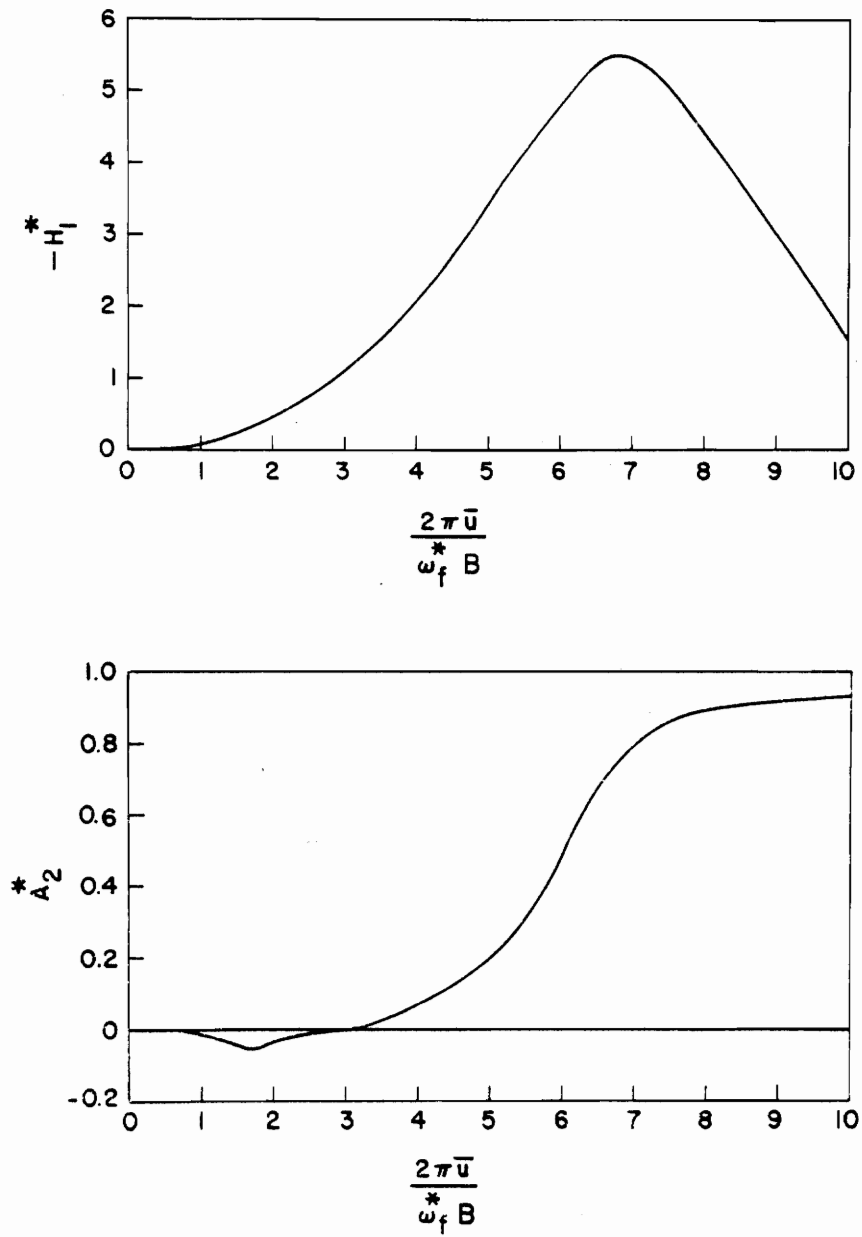
Figure 6: Aerodynamic Coefficients for the Sitka Bridge
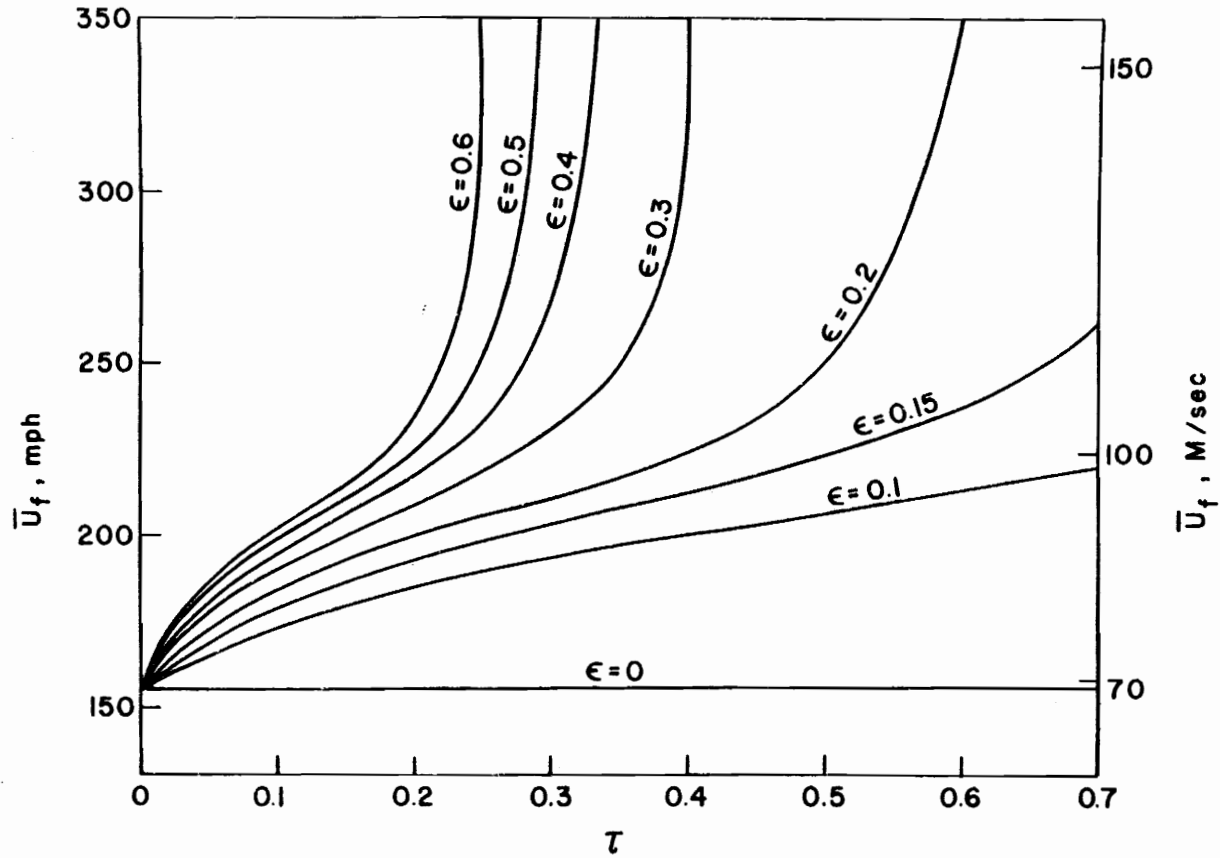
Figure 7: Critical Wind Velocities for Bridge 1 (Acceleration Sensor)
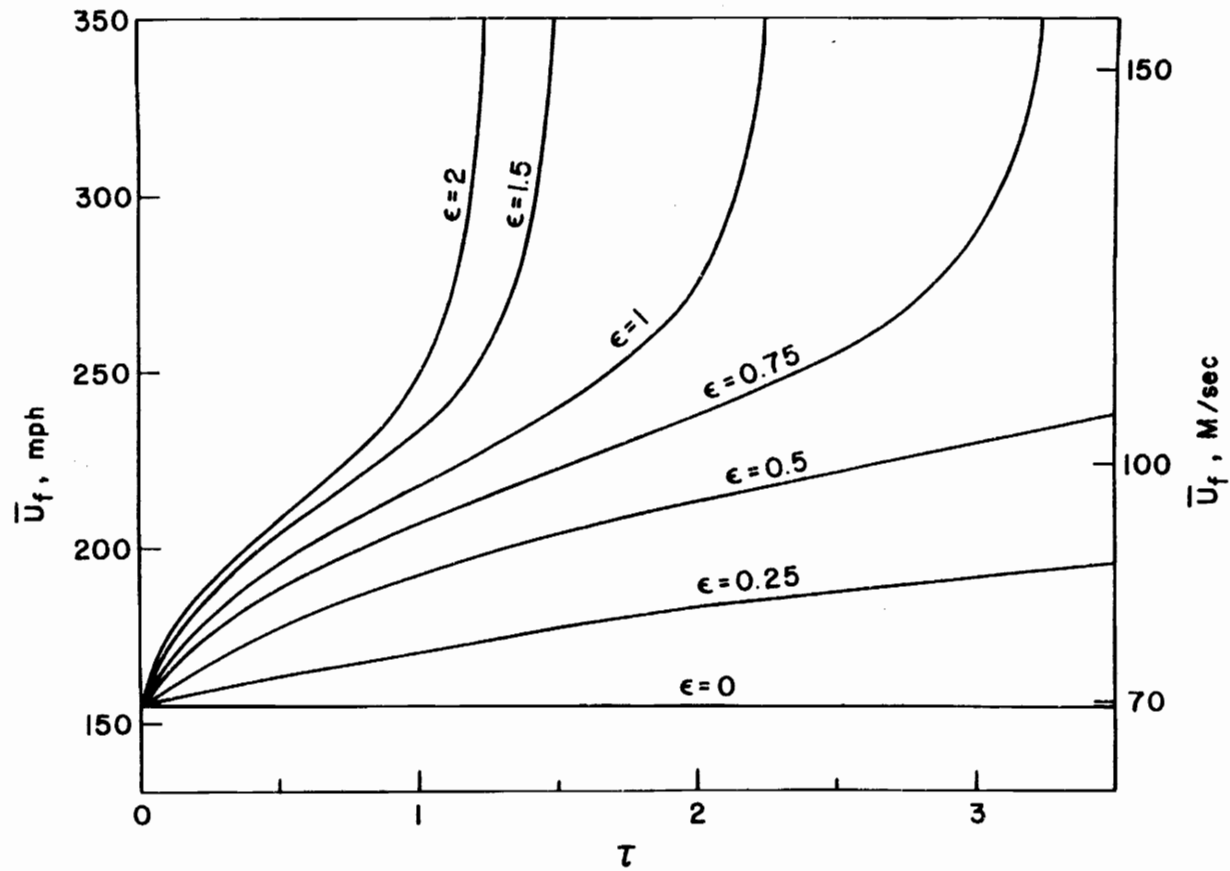
Figure 8: Critical Wind Velocities for Bridge 1 (Velocity Sensor)
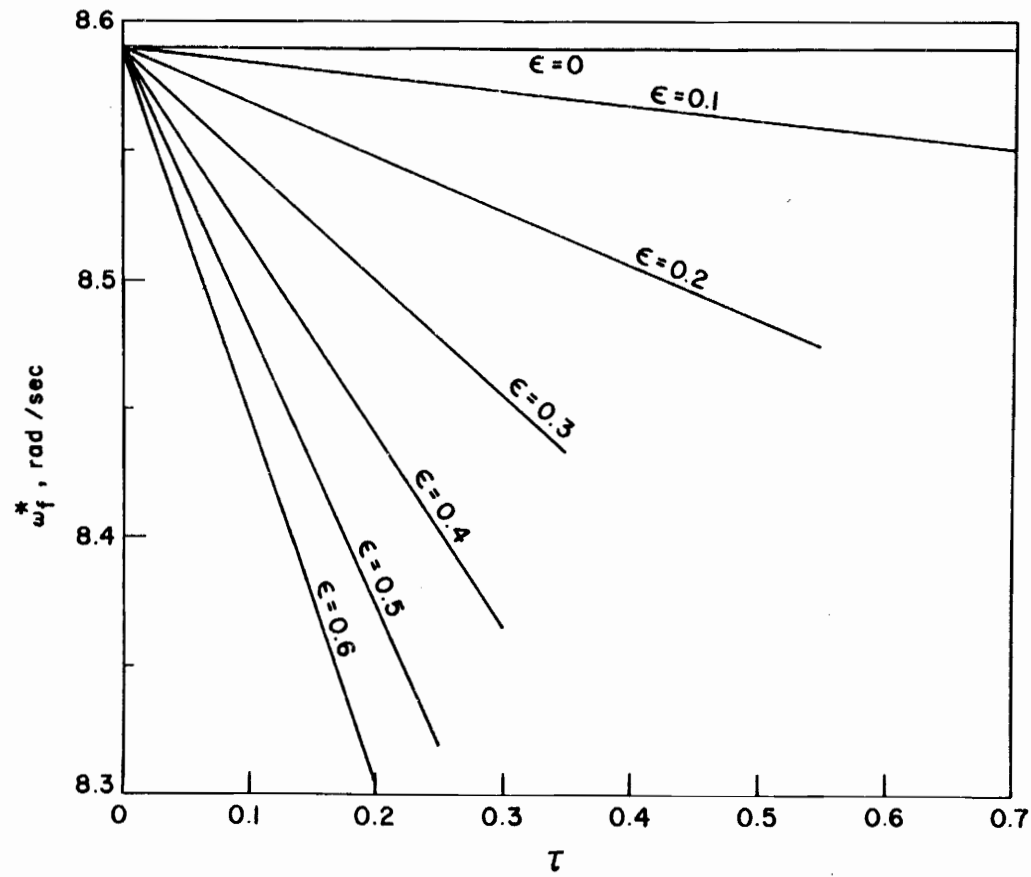
Figure 9: Flutter Frequencies for Bridge 1 (Acceleration Sensor)
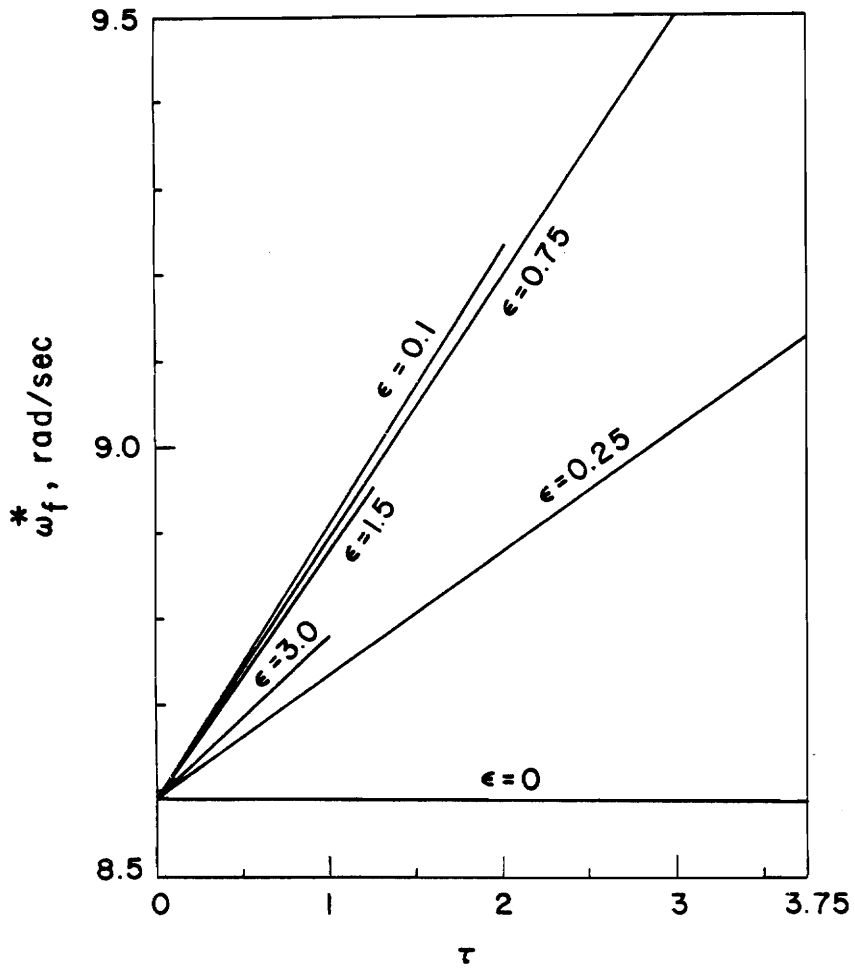
Figure 10: Flutter Frequencies for Bridge 1 (Velocity Sensor)
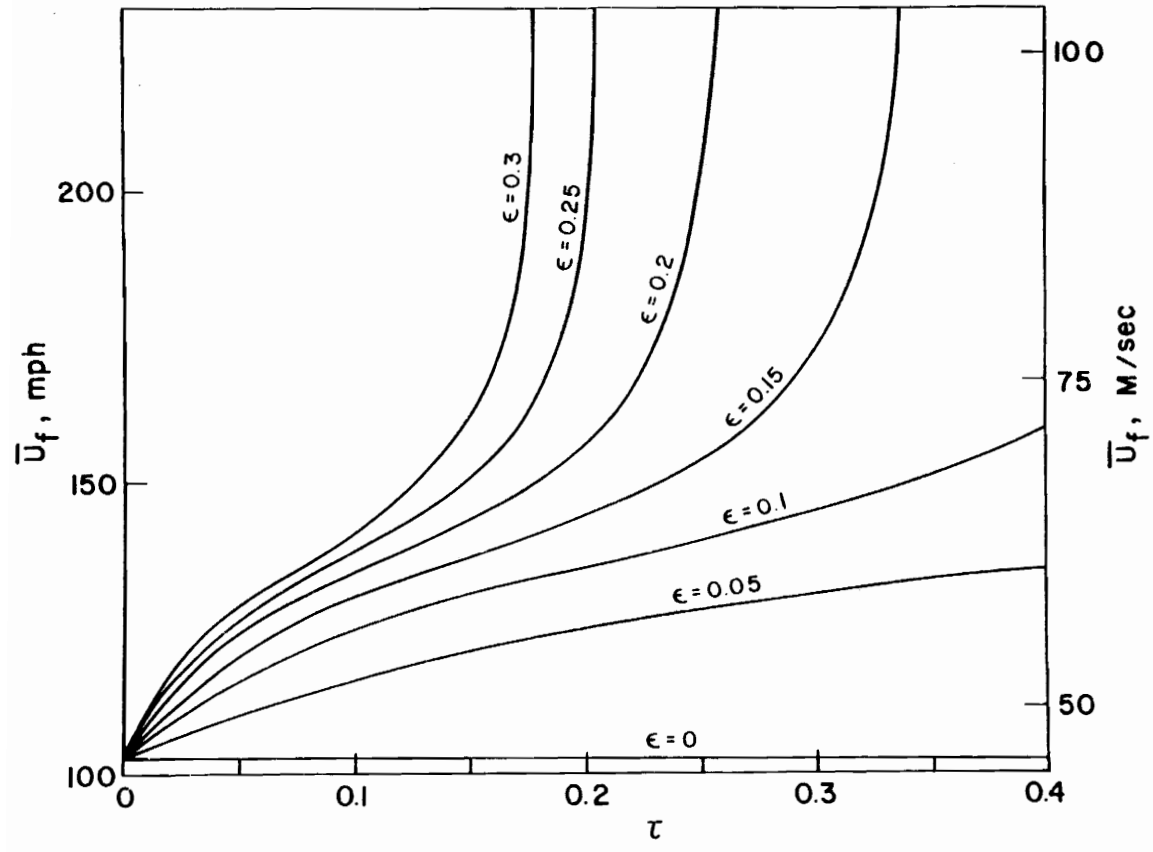
Figure 11: Critical Wind Velocities for Bridge 2
(Acceleration Sensor)
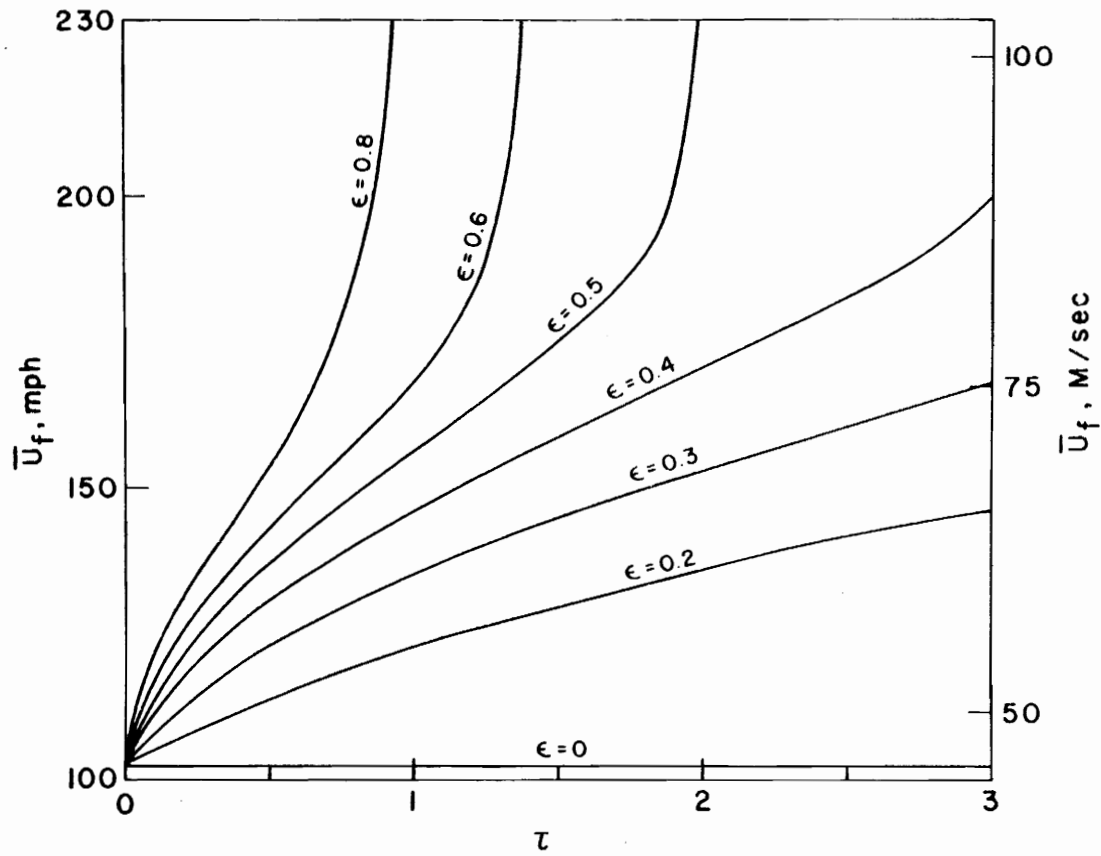
Figure 12: Critical Wind Velocites for Bridge 2
(Velocity Sensor)
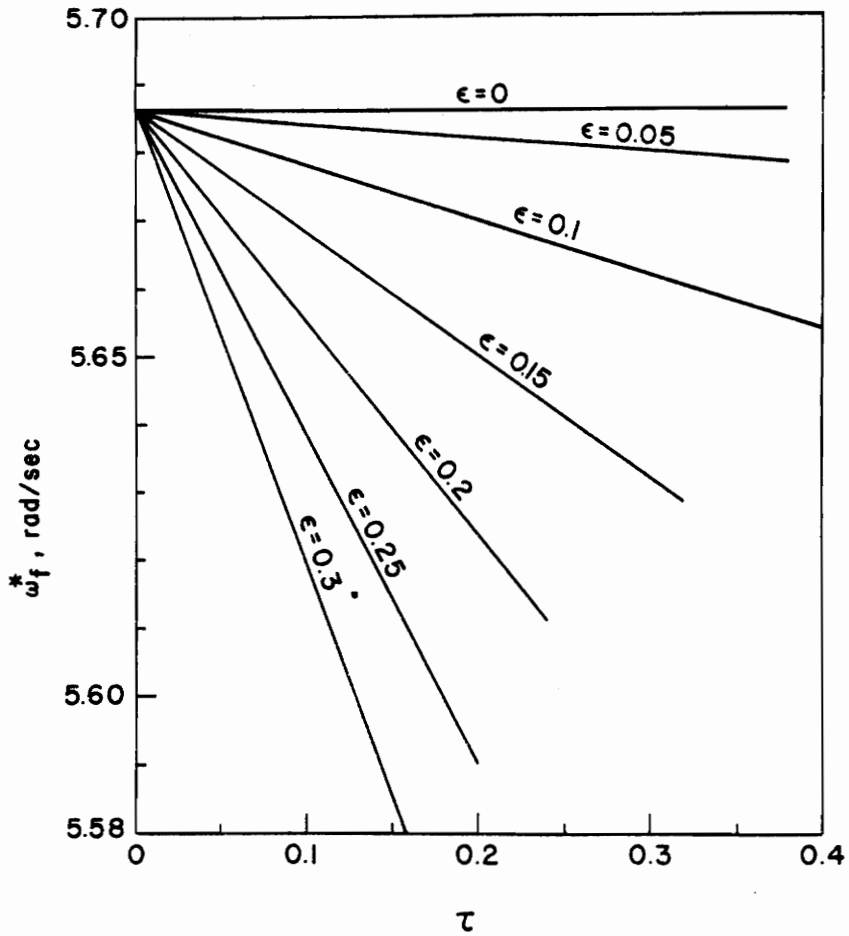
Figure 13: Flutter Frequencies for
Bridge 2 (Acceleration Sensor)
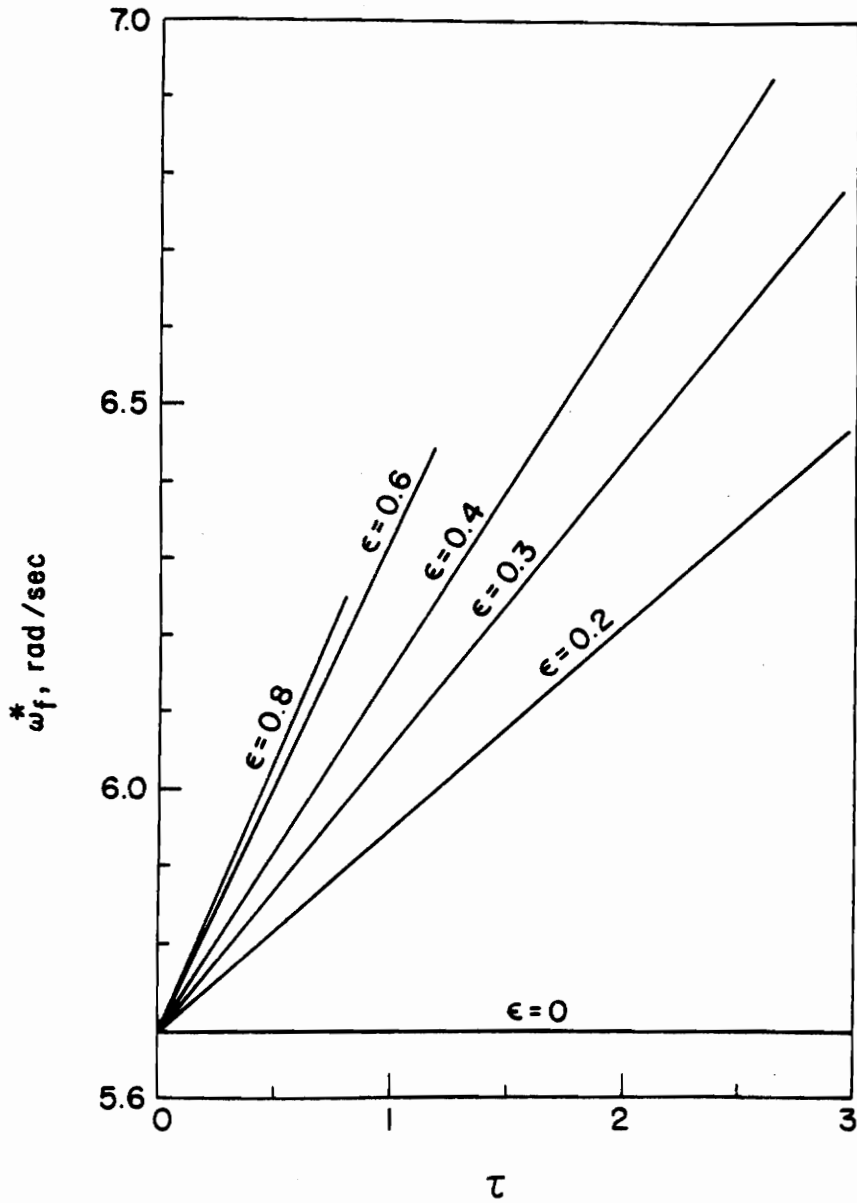
Figure 14: Flutter Frequencies for
Bridge 2 (Velocity Sensor)
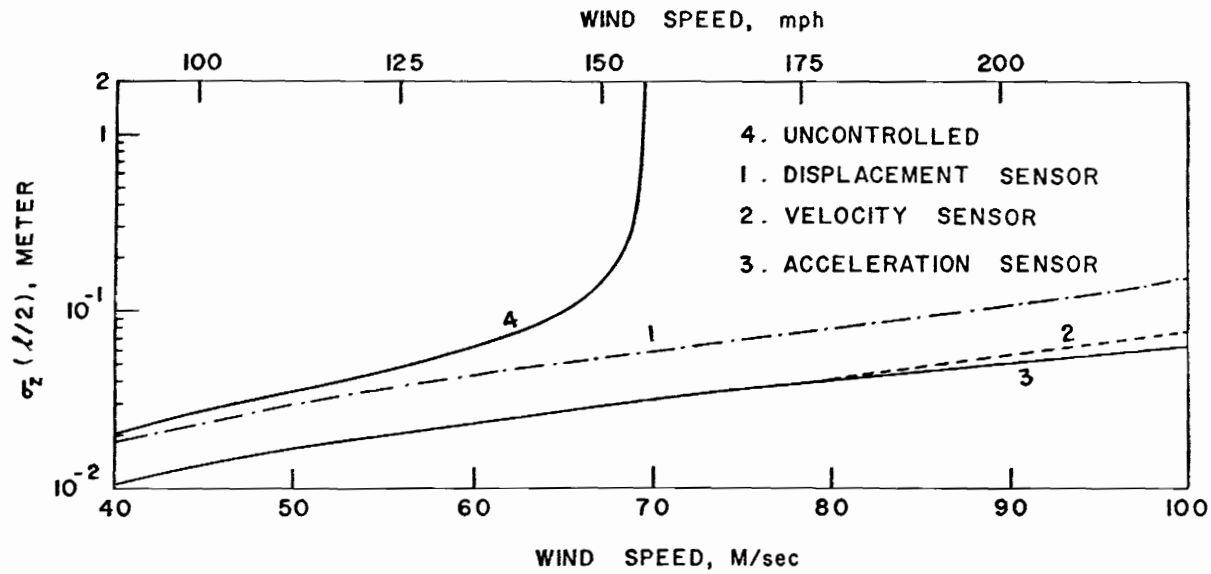
Figure 15: Standard Deviation for Bridge 1

1. ($\varepsilon = 0.1, \tau = 10$)   2. ($\varepsilon = 0.5$, $\tau = 8$)
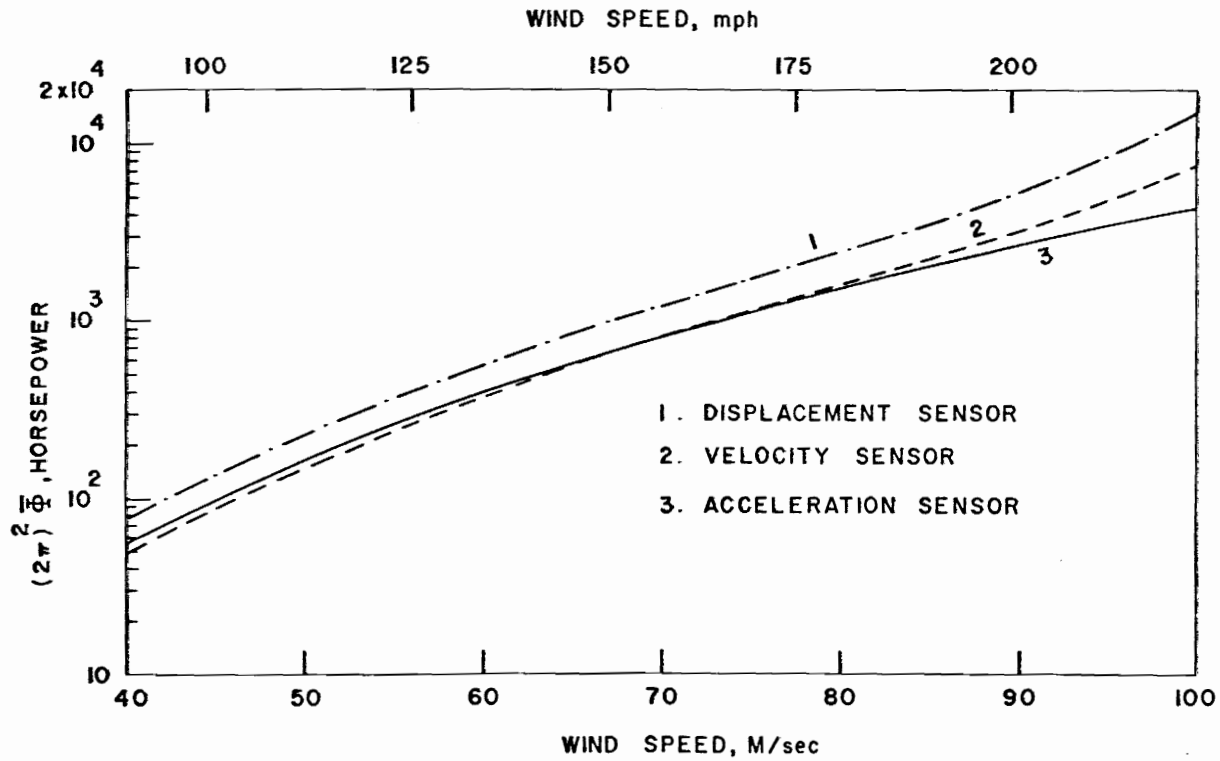
3. ($\varepsilon = 1$, $\tau = -15$)

Figure 16: Average Power Requirement for Bridge 1
1.($\varepsilon = 0.1$, $\tau = 10$)   2.($\varepsilon = 0.5$, $\tau = 8$)
3.($\varepsilon = 1$, $\tau = -15$)
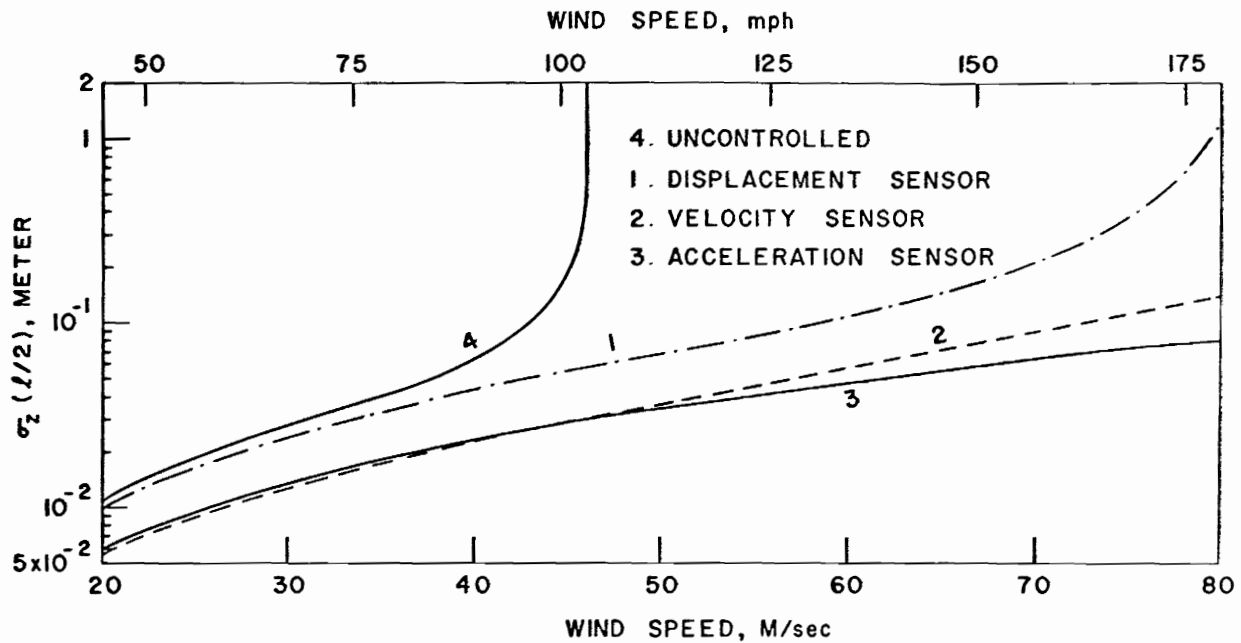
Figure 17 : Standard   Deviation   for   Bridge   2
1.($\varepsilon=0.1$, $\tau=10$)   2.($\varepsilon=0.4$, $\tau=3.64$)
3.($\varepsilon=1$, $\tau=-2.8$)
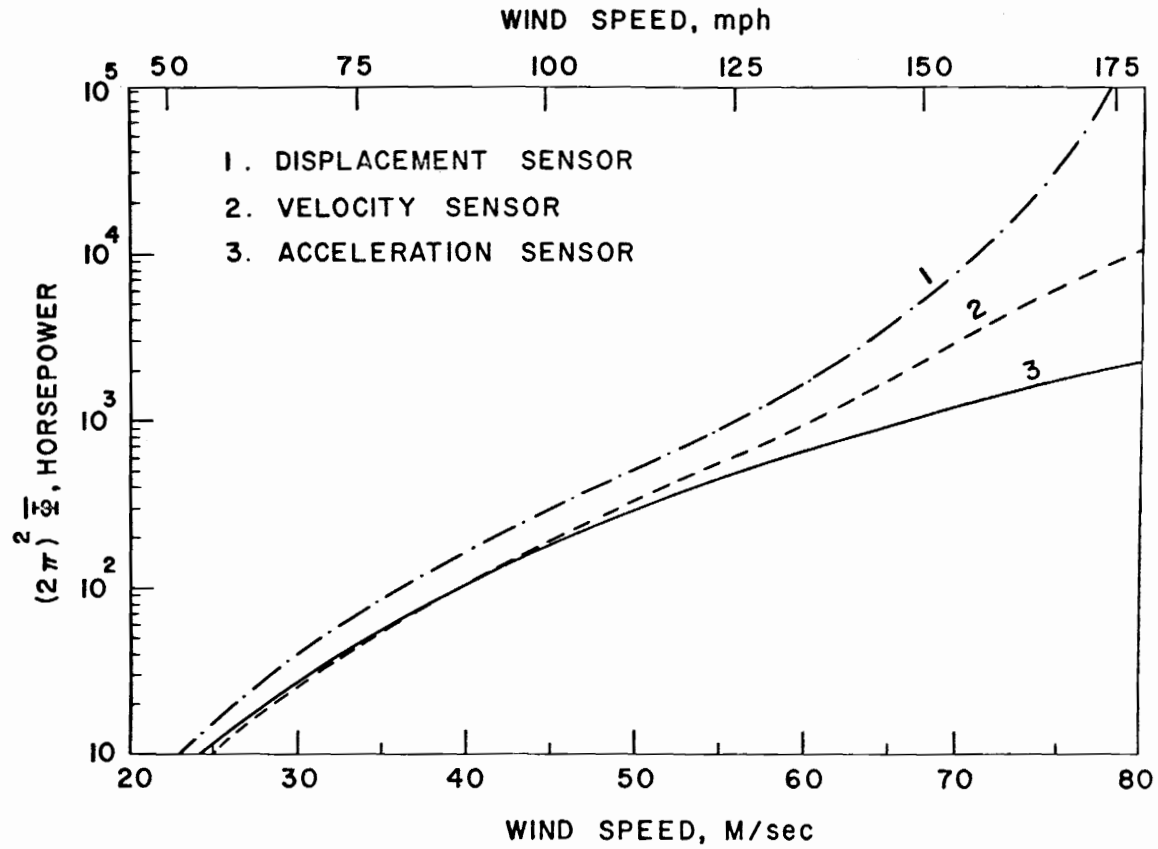
Figure 18: Average Power Requirement for Bridge 2
1. ($\varepsilon = 0.1$, $\tau = 10$)   2. ($\varepsilon = 0.4$, $\tau = 3.64$)
3. ($\varepsilon = 1$, $\tau = -2.8$)
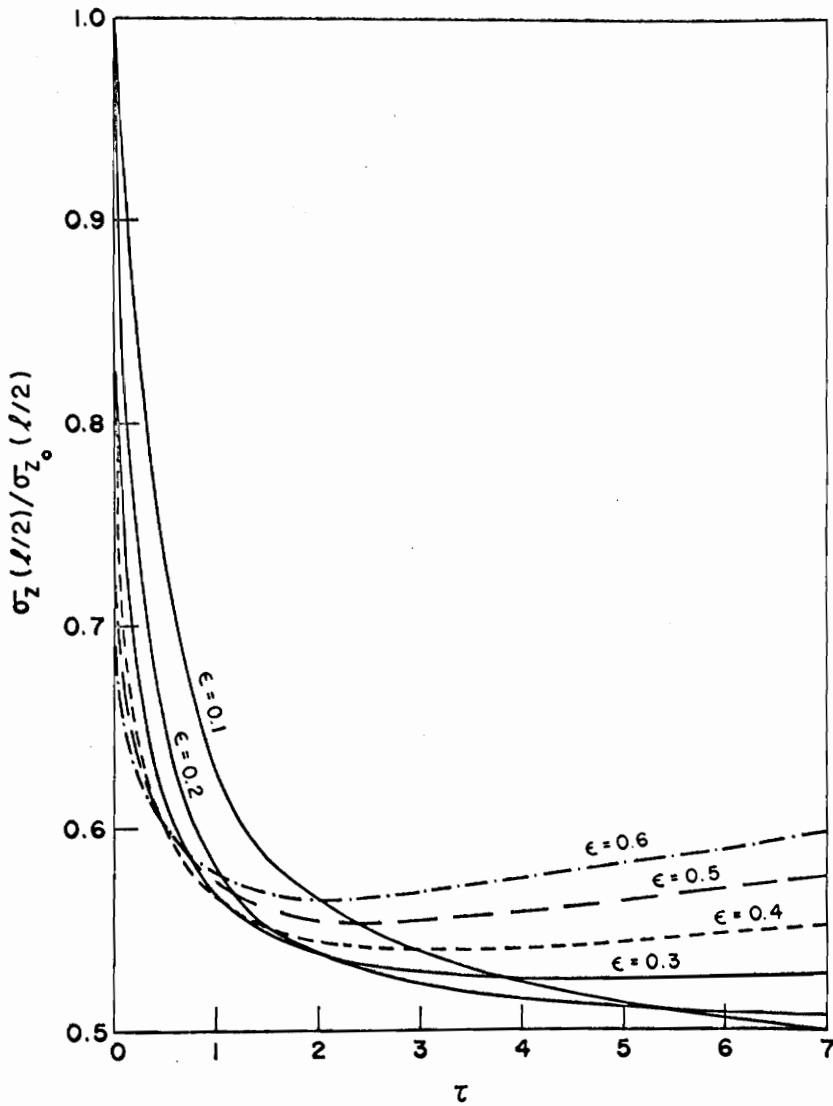
Figure 19: Standard Deviation for Bridge 1 (Acceleration Sensor)
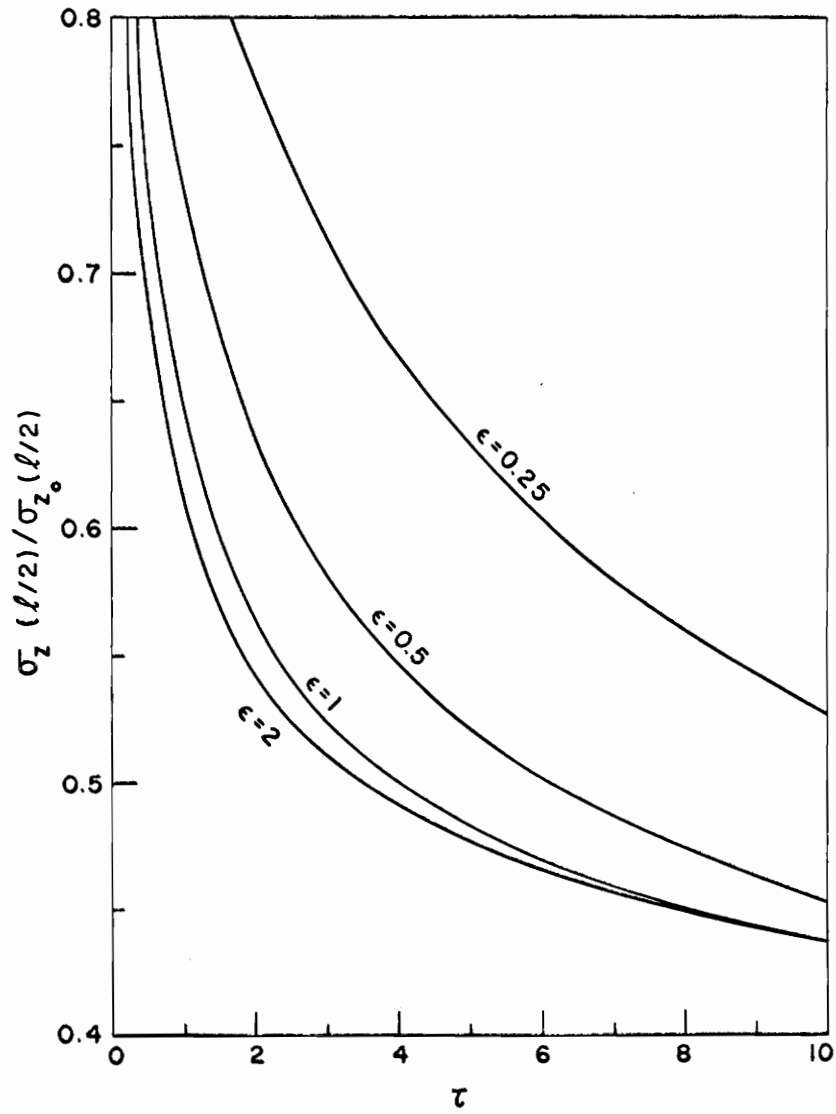
Figure 20: Standard Deviation for Bridge 1
(Velocity Sensor)
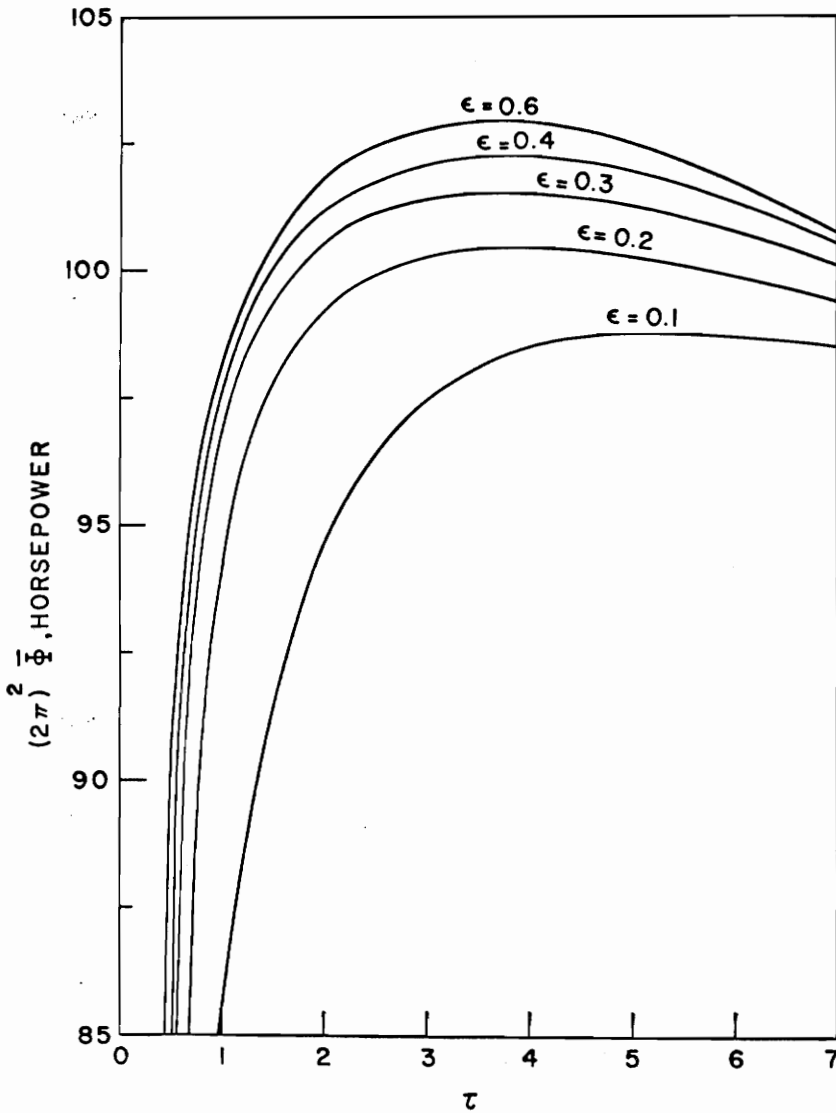
Figure 21: Average Power Requirement for Bridge 1 (Acceleration Sensor)
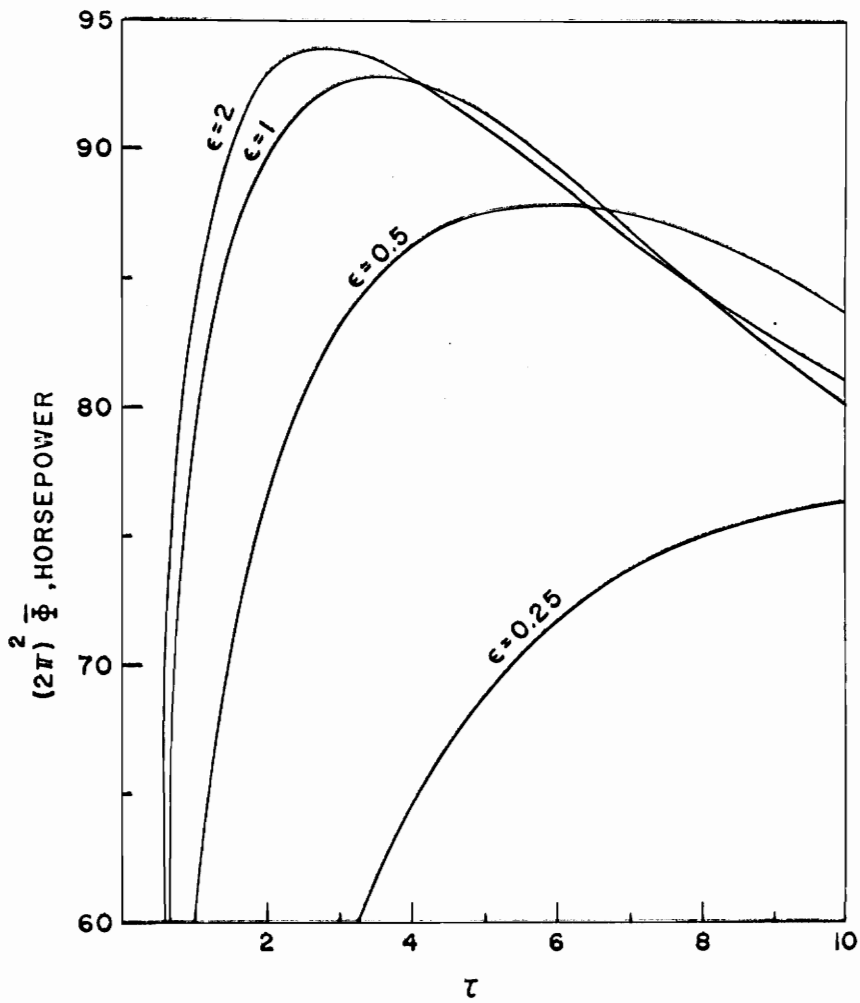
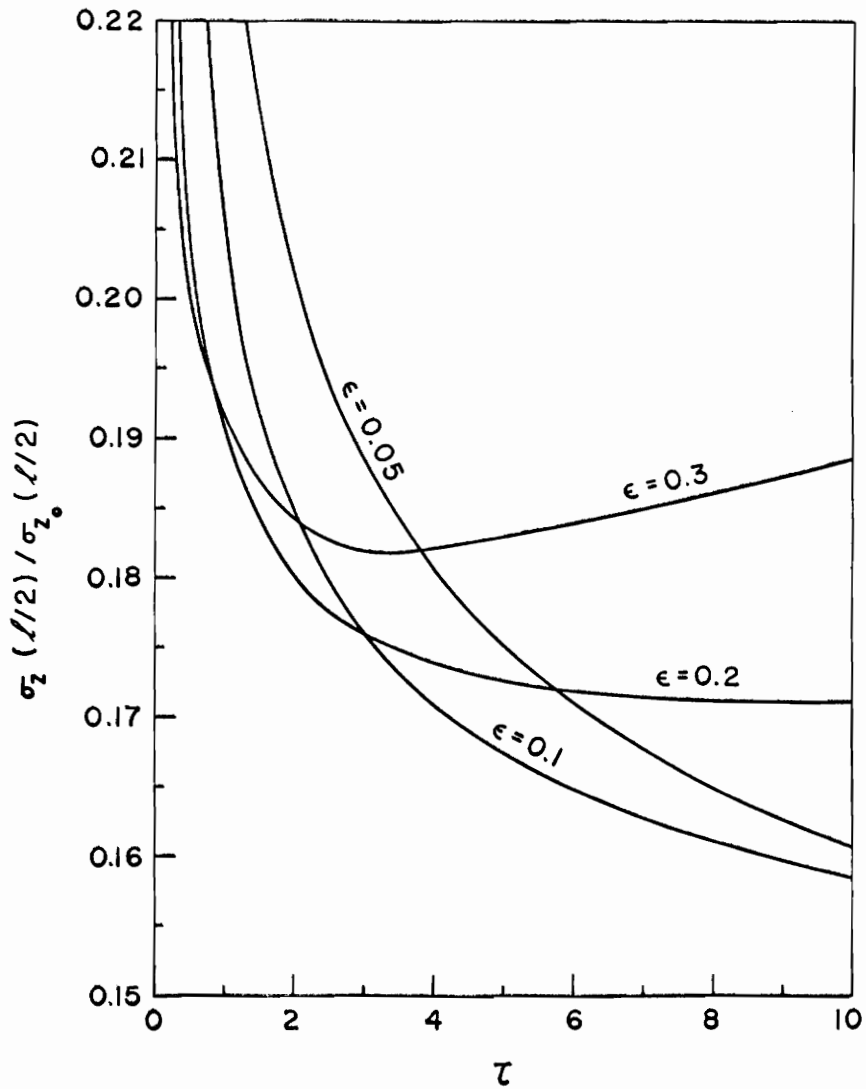Figure 22: Average Power Requirement for Bridge 1 (Velocity Sensor)

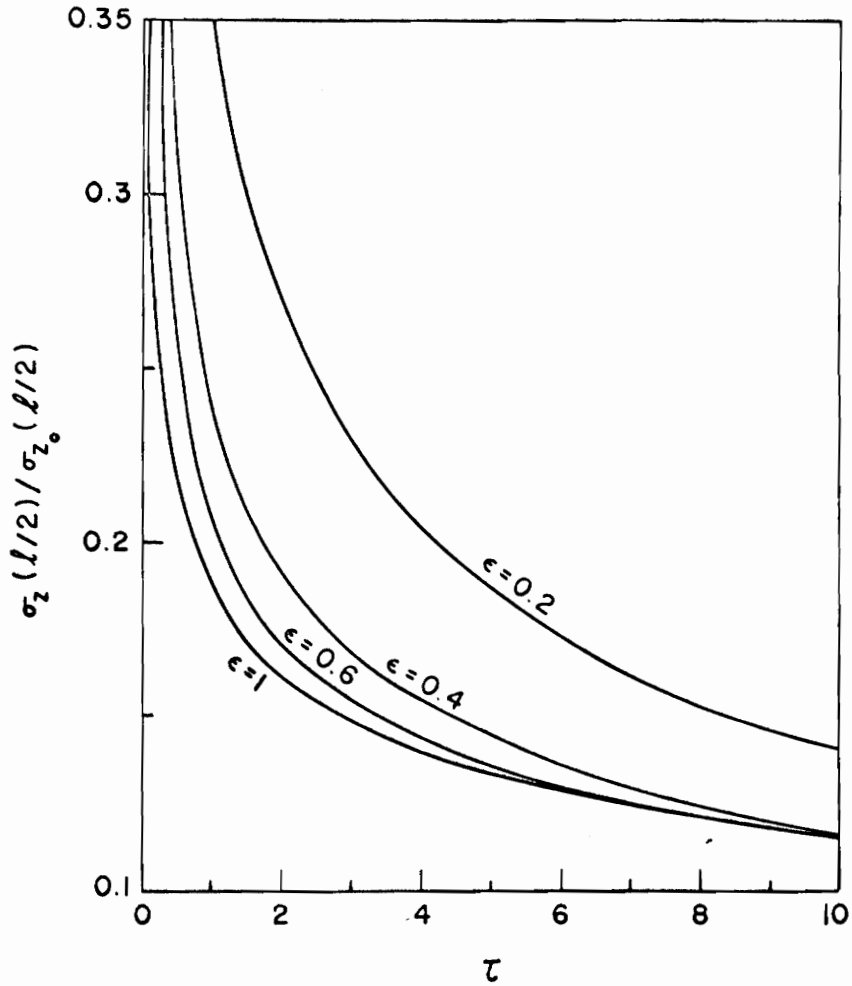Figure 23: Standard Deviation for Bridge 2 (Acceleration Sensor)

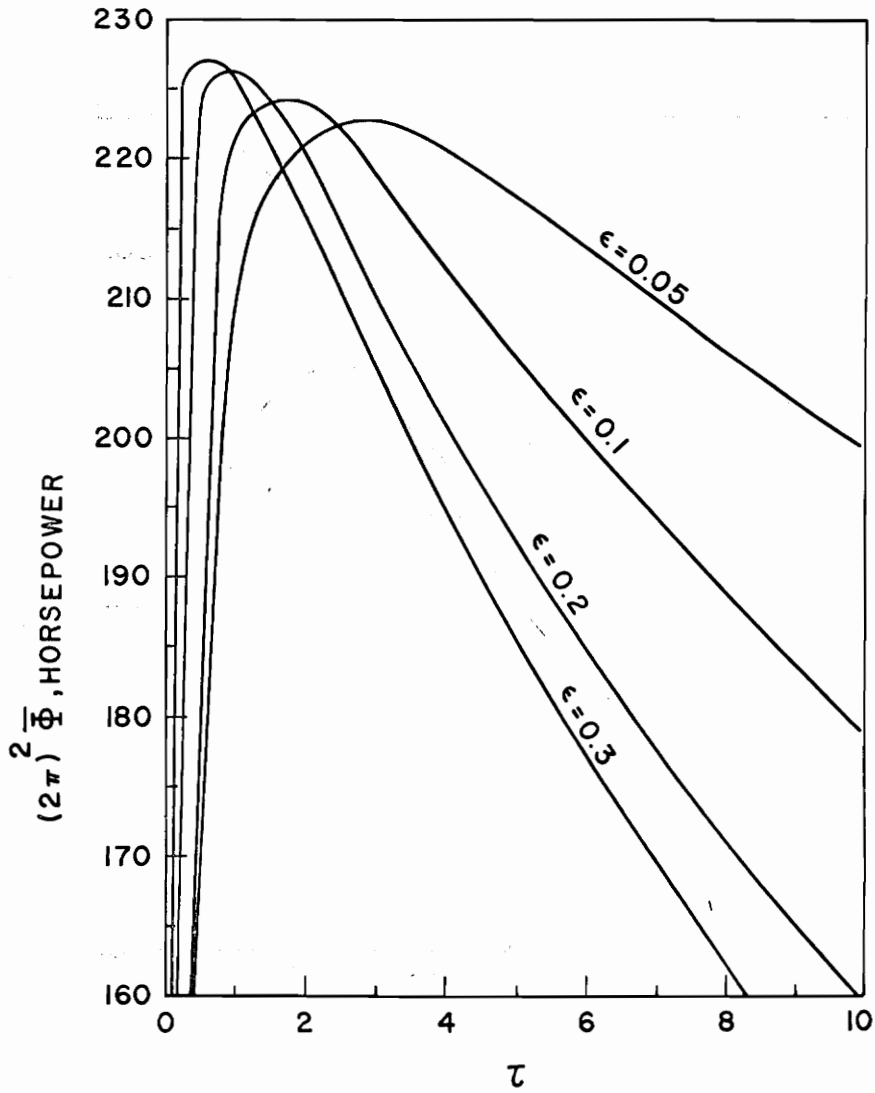Figure 24: Standard Deviation for Bridge 2 (Velocity Sensor)

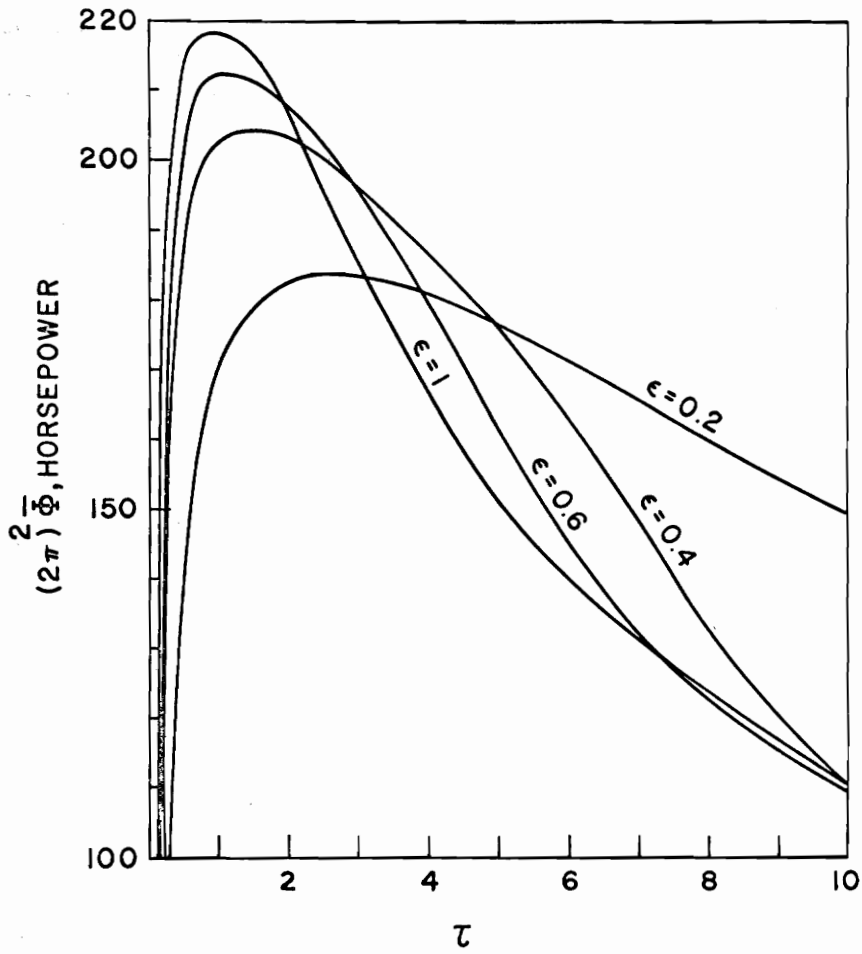Figure 25: Average Power Requirement for Bridge 2 (Acceleration Sensor)

Figure 26: Average Power Requirement for Bridge 2 (Velocity Sensor)

VITA

The author was born in Patras, Greece, on March 17, 1949. He attended the University of Patras as an undergraduate student, where he received his Bachelor's degree in Physics in 1973. He was admitted as a graduate student at the Institute of Sound and Vibration Research, University of Southampton, England, where he received his Master's degree in Sound and Vibration in 1974. He subsequently continued his graduate studies in the Department of Engineering Science and Mechanics, Virginia Polytechnic Institute and State University, where he was awarded the degree of Doctor of Philosophy in 1978.

Fanis Giannopoulos

F. Giannopoulos

DYNAMIC ANALYSIS AND ACTIVE CONTROL OF

TWO CABLE-STAYED BRIDGE

by

Fanis Giannopoulos

(ABSTRACT)

The feasibility of applying active control theory to
control both the transient and steady state response of a
two cable-stayed bridge has been investigated. The bridge
has been modelled as a two degree of freedom system in bend-
ing and torsion, excited by both buffeting and self-excited
loads. The existing suspension cables have been used as
active tendons by which the control forces are applied to
the bridge deck at the points of the anchorage. The control
force from each suspension cable is actuated through a
hydraulic-servomechanism which is regulated by the sensed
motion of the bridge deck at the anchorage of the cable.
Stability and steady state response analyses have been pre-
sented for both controlled and uncontrolled motion. The
power requirement for the control devices has been derived.
Finally, numerical examples have been worked out to demon-
strate the feasibility of the derived theory for two cable-
stayed bridges.